2007

Microstructure and tensile properties of squeeze cast magnesium-aluminum-strontium alloys

Shuping Wang
University of Windsor

Follow this and additional works at: https://scholar.uwindsor.ca/etd

Recommended Citation

Microstructure and Tensile Properties of Squeeze Cast Mg-Al-Sr Alloys

By

Shuping Wang

A Thesis

Submitted to the

Faculty of Graduate Studies

through Engineering Materials

in Partial Fulfillment of the Requirements

for the Degree of Master

of Applied Science

at the University of Windsor

Windsor, Ontario, Canada

2007

© 2007 Shuping Wang

Canada

ABSTRACT

It has been demonstrated that die cast Mg-Al-Sr alloys have enhanced high temperature properties and are capable of replacing certain existing aluminum power train components. However, due to the inherent nature of die casting, i.e. high porosity content and other defects, automotive applications of Sr-containing magnesium die casting are very limited. Squeeze casting has a super ability to eliminate porosity and other casting defects. However, there is a general lack of understanding concerning the microstructure and tensile properties of squeeze-cast Mg-Al-Sr alloys.

This thesis describes the findings of experimental investigation in obtaining an in-depth understanding on the effect of pressure levels and strontium contents on tensile properties and microstructure of squeeze cast Mg-Al-Sr alloys. The results have shown that the ultimate tensile strength (UTS), yield strength (YS) and elongation (E_f) of squeeze cast Mg-Al-Sr alloys increase with increasing applied pressures but decrease as the strontium content increases.

DEDICATION

I dedicate this thesis to my mother, my wife, my daughter and my son. Their love, support, encouragement and patience during my study at University of Windsor has given me the strength, and enabled me to go through the difficult time during the research period, and finally complete this work.

ACKNOWLEDGMENTS

I would like to appreciate my supervisor Dr. Henry. Hu, for giving me this great opportunity to study in the engineering materials program of the University of Windsor, and for his kindly suggestion, encouragement and excellent supervision of this research work.

Many thanks to Dr. Vesselin Stoilov and Dr. Murty K. Madugula for taking the time for my proposal and research presentations, as well as reviewing my thesis and giving me suggestions for this project.

I am very grateful to Mr. Andy Jenner, Mr. Steve Budinsky and other technicians of the technical support center, Mr. Patrick F. Seguin and Mr. John Robinson for their technical assistance in the experimental procedures in this research, and also to classmates in my group: A. F. Yu, L. Han, M. Masoumi and Z. Sun, for their informative and valuable discussion.

Grateful acknowledgement should also go to the Government of Ontario and the University of Windsor for financial support in the form of the University of Windsor Tuition Scholarships and the Ontario Graduate Scholarships.

Most of all I would like to express my deepest gratitude to my family: my mother, my wife, my daughter and my son for their love, understanding, encouragement and support.

v

TABLE OF CONTENTS

LIST OF FIGURES

xiii

LIST OF TABLES

CHAPTER I

INTRODUCTION

1.1 Background

Weight reduction of automobiles for increased fuel efficiency and performance has stimulated interest in using magnesium alloys for various automotive applications. The use of magnesium alloys has grown considerably since the early 1990s, and continues to rise in the automotive industry. This is mainly attributed to the lightness of magnesium--- one-third lighter than aluminium, three-fourths lighter than zinc, and four-fifth lighter than steel. Magnesium also has the highest strength-to-weight ratio of any of commonly used metals, as well as many other advantages: good castability, high die casting rates, excellent machinability and full recycle ability. Equipped with these superior characteristics, magnesium provides opportunities and impact for the automotive industry where weight reduction, fuel economy, and environmental friendliness of vehicles are increasingly demanded [1]. However, magnesium alloys face a challenge at high temperatures because of their poor creep properties plus inadequate quality of die castings in certain aspects [1, 2].

1.1.1 Magnesium and alloys

The most outstanding characteristic of magnesium is its density, 1.7 g/cm^3 (Al = 2.7 g/cm^3), which is the lowest of all structural metals; therefore, its alloys are used where lightweight is an important consideration [3, 4].

1

The conventional Mg alloy is AM (Mg-Al-Mn) and AZ (Mg-Al-Zn) alloys. Magnesium alloys exhibit excellent properties such as high specific strength at room temperature, superior die castability, a good balance of strength and ductility and good damping characteristics. AM and AZ alloys have been used extensively in the automotive industry. The current magnesium components, such as steering wheels, instrumental panels, seats, valve covers etc, are mainly manufactured by AM and AZ alloys [1]. However, the application temperature of AM and AZ alloy is generally limited to about 100 ^{0}C. It will be a rapid degradation in mechanical properties above this temperature due to the inadequate creep resistance that the conventional AM and AZ alloys inherently provide. The poor high-temperature mechanical properties of the alloys have prevented its application at elevated temperature.

In recent years, magnesium–aluminum–strontium (Mg–Al–Sr) alloy system has emerged as a potential heat-resistant Mg-alloy. Mg-Al-Sr-based alloys (AJ alloys) have shown superior creep performance at temperatures as high as 175 $^{\circ}$C with stresses up to 70 MPa [5]. The study by Argo et al. [6] shows that die cast Mg-Al-Sr-based alloys with 1.4 wt% Sr have good metal handling and melt stability properties, and superior high temperature properties, which are capable of replacing existing aluminum and steel powertrain components. However, there is a problem that limits their application: casting quality. It has been shown [6,7] that defects tend to form in castings of Mg-Al-Sr alloys compared to conventional die casting alloys AM50 and AZ91D with no addition of Sr. These defects include porosity and hot tearing, which are also present in aluminum alloys [8].

2

1.1.2 Squeeze casting

Squeeze casting is a process that involves the solidification of molten metal in a closed die under an imposed high pressure. The high applied pressure keeps entrapped gases in solution and squeezes molten metal from hot spots to incipient shrinkage pores. As a result, porosity and hot tearing in a squeeze-cast component is almost eliminated. Also due to the elimination o the air gap at the liquid-mould interface by the applied high pressure, the heat transfer across die surfaces is enhanced, which increases solidification and cooling rates. Thus, superior mechanical properties of the casting resulting from the pore-free fine microstructure are achieved in squeeze-casting processes [9]. Compared with die casting process, squeeze casting has a super ability to eliminate porosity and can produce superior mechanical properties. However, in open literature, almost all studies on Mg-Al-Sr alloys are focused on die casting processes. No detailed research reports on squeeze casting of Mg-Al-Sr alloys have been found.

It has been demonstrated [10] that the squeeze cast AM50 alloy exhibits virtually no porosity compared to the die cast counterpart. This suggests that it is essential to develop a squeeze casting process for elimination of defects present in die cast Mg-Al-Sr alloys, which could expand their application to not only temperature-related but safety-critical components as well.

3

1.2 Objectives

The objectives of this work were to determine the influence of process-oriented parameters (pressure) and alloy-related chemistry on tensile behaviour and microstructure of squeeze cast Mg-Al-Sr alloys. In order to achieve the proposed objectives, this project is divided into two parts. The first part was to investigate the effect of applied pressure levels on microstructure, mechanical properties and casting quality, including porosity and surface defects. The second part was to study the effect of strontium content on microstructure, mechanical properties and casting quality of the alloys.

1.3 Organization of the thesis

This thesis contains six chapters. Chapter I has provided a general background of magnesium alloys and the advantages of squeeze casting. Chapter II is the literature review that looks into magnesium, magnesium alloys and the development of Mg-Al-Sr alloys, as well as the process-related information of squeeze casting. The experimental procedures and the employed process used in this work are described in Chapter III. Chapter IV reports detailed results and discussion with respect to the effects of pressure level and strontium content on microstructure and tensile properties of Mg-Al-Sr alloys. The conclusions of the present study are summarized in Chapter V. Finally, chapter VI gives the recommendations for future work.

Chapter II

LITERATURE REVIEW

2.1 Magnesium and magnesium alloy

2.1.1 Magnesium

The history of elemental magnesium started in 1755, when Joseph Black, a Scottish chemist, discovered that magnesia contained a new element, magnesium [11]. Commercial magnesium production commenced in Germany in 1886 but had reached only ~10 tons worldwide by 1900. Magnesium production during the last decade has been close to 250, 000 tons/year [12], and expected the growth rate for automotive magnesium components has averaged 20% annually in next decade [1, 13]. Table 2-1 shows the major magnesium production since 1950.

Magnesium is a plentiful element comprising 2.7% of the earth's crust and magnesium ores are found in most countries. The major source of magnesium is in the oceans that contain 0~13% of this metal and therefore provide an almost inexhaustible supply [12]. Currently, the two basic processes used to produce magnesium are the electrolysis of fused anhydrous $MgCl_2$ and thermal reduction of MgO by ferrosilicon [11,12].

Magnesium is classified as an alkaline earth metal. It is found in Group 3 of the periodic table. The lattice parameters of pure magnesium estimated at room temperature are: a = 0.32092 nm and c = 0.52105 nm. The c/a ratio is 1.6236 that is close to the ideal value of 1.633. Therefore, magnesium may be considered as perfectly closed packed. Pure magnesium is soft and mechanically weak, it is mainly used as an alloying

5

element in aluminum, for steel desulphurization, production of nodular cast iron, as a reducing agent in titanium and zirconium production and as a chemical in various processes [3, 4, 11]. Table 2-2 lists some important physical properties of pure magnesium, and Table 2-3 lists important mechanical properties of pure magnesium.

Table 2-1 Major magnesium production since 1950 [11]

	Company	Location	Mg Source	Process	Type	Initial Capacity
1951	Norsk Hydro	Porsgrunn	Sea Water	Electrolytic	I.G. Farben	18,000
1959	Alabama Metallurgical	Selma, Al	Dolomite	Thermal	Pidgeon	7,500
1960	Furakawa	Japan	Dolomite	Thermal	Pidgeon	5,000
1964	Pechiney	France	Dolomite	Thermal	Magnetherm	9,000
1964	Ube Kosan	Japan	Dolomite	Thermal	Pidgeon	5,000
1965	Ust Kamenogorst	Kazakstan	Purchased MgCl₂	Electrolytic	VAMI	40,000
1965	MEL	U.K.	Dolomite	Thermal	Pidgeon	10,000
1969	Nat. Lead	Utah	Brine	Electrolytic	Modif IG	40,000
1970	Am Magnes	Texas	Brine	Electrolytic	Modif IG	25,000
1972	Dow Chem	Texas	Sea H₂O	Electrolytic	Dow Cell	25,000
1975	NoWst Alloy	Addy WA	Dolomite	Thermal	Magnetherm	30,000
1989	MagCan	Canada	Magnesite	Electrolytic	MPLC	12,500
1989	Norsk Hydro	Canada	Magnesite	Electrolytic	Norsk Hyd	45,000
2001	Noranda	Canada	Serpentine Tailings	Electrolytic	Alcan multi-polar	63,000
1996	Dead Sea Mg	Israel	Carnallite Brine	Electrolytic	VAMI/UTI	30,000
1997	AusMagCorp	Quenslnd	Magnesite	Electrolytic	Alcan multi-polar	1,500
2001	AusMagCorp	Quenslnd	Magnesite	Electrolytic	Alcan multi-polar	97,000
1987	Minhe	China	Carnallite	Electrolytic	VAMI	4,000
1990	Various	China	Dolomite	Thermal	Pidgeon	500 to 20,000

6

Table 2-2 Physical properties of pure magnesium (99.9wt%) [11]

Property	Value
Melting point	650°C ± 2
Boiling point	1107°C ± 10
Latent heat of fusion	0.37 MJ/kg
Latent heat of evaporation	5.25 MJ/kg
Heat of combustion	25.1 MJ/kg
Specific heat	
at 20°C	1030 J/(kg K)
at 600°C	1178 J/(kg K)
Electrical resistivity at 20°C	4.45 $\mu\Omega$ cm
Thermal conductivity at 25°C	155 W/(kg K)
Linear coefficient of thermal expansion at 20°C	25.2×10^{-6} K^{-1}
Density	
at 20°C	1.738 g/cm^3
at 600°C	1.622 g/cm^3
at 650°C (solid)	1.65 g/cm^3
at 650°C (liquid)	1.58 g/cm^3
Volume change during solidification	4.2%
Volume change during cooling 650–20°C	5%

Table 2-3 Mechanical properties of pure magnesium (99.9wt%) [11]

	Tensile strength MPa	Tensile yield strength MPa	Compressive yield stress MPa	Elongation % 50 mm	Brinell hardness 500 kp/10 mm
Sand cast, thickness 13 mm	90	21	21	2–6	30
Extrusion, thickness 13 mm	165–205	69–105	34–55	5–8	35
Hard rolled sheet	180–220	115–140	105–115	2–10	45–47
Annealed sheet	160–195	90–105	69–83	3–15	40–41

7

2.1.2 Conventional Magnesium alloys

Magnesium is rarely used for engineering applications without being alloyed with other metals. Aluminum, manganese, zinc, zirconium and rare earths are examples of widely differing metals that may be present in commercial alloys. The major magnesium alloys and the alloy element influence are given below [11, 12, 14-19, 21].

2.1.2.1 Classification of Magnesium alloys

A: Mg-Al Based Alloys

The most common alloys are based on the magnesium-aluminum system. Typical compositions of some Mg-Al based die casting alloys are listed in Table 2-4. The most commonly used magnesium alloy, AM and AZ alloys, belong to this category. The main alloying elements in these alloys are two or more of the elements from the following list: Al, Zn, Mn, Be, Si. Addition of Al, Zn, and Si are straightforward [11] while Mn and Be require more control. Magnesium can be melted and alloyed to produce Mg-Al based alloys using electric resistance, gas-fired and induction furnaces with mild steel crucibles. As in all magnesium alloys, Mg-Al based alloy melts must be protected against oxidation and burning during melting, alloying and casting. Fluxes (employing molten salt mixtures) or fluxless-melting techniques (using protective gas mixtures, such as SO_2, SF_6 mixed with CO_2, dry air or N_2) can be used depending on alloy compositions and processing conditions.

AZ91 is the most commonly used magnesium based alloy for pressure die casting, with excellent castability and good strength. It is typically used for automobile and

8

computer parts, mobile telephones, sporting goods, housings and covers, brackets, chain saw housings, handheld tools, and household equipment, etc.

AM60 and AM50 are alloys with outstanding ductility and energy absorbing properties combined with good strength and castability. Typical uses are automotive seat frames, steering wheels, instrument panels, brackets, and fans, etc. AM20 is an alloy recognized for its ductility and impact strength. Typical uses are automotive safety parts where the highest possible ductility is required.

AS41, AS21 and AE42 are alloys with good creep properties up to about 150^0C. Decreased aluminium content in AS21 compared to AS41 results in increased creep resistance and ductility, and in some decrease in tensile strength and castability. All three alloys offer good mechanical properties at room temperature.

Table 2-4 Typical composition of Mg-Al based die casting alloys [11]

Alloy	Al	Zn	Mn	Si	RE [a]
AZ91, MgAl9Zn1	9	0.7	0.3		
AM60, MgAl6Mn	6		0.4		
AM50, MgAl5Mn	5		0.4		
AM20, MgAl2Mn	2		0.4		
AS41, MgAl4Si	4		0.4	1	
AS21, MgAl2Si	2		0.4	1	
AE42, MgAl4RE2	4				2.5

[a] Rare earth. All values are given in weight percent.

B: Mg-Al + (Rare-Earth) Alloys

Rare earths are used when enhanced high temperature properties are required.

9

Rare-earth elements, which include elements such as Ce, Nd, Pr, are added to Al-containing alloys of magnesium for improved creep resistance. The most economical route is to use mischmetal, which has a naturally occurring combination of rare earth elements and is available in the form of lumps of various sizes. The additive can oxidize readily in moist atmosphere and reacts violently with water. It should always be stored under a coating of a non-corrosive wax or oil. Mischmetal usually contains 85-90% total rare earth content.

C: Mg-Al + (Alkaline Earth) Alloys

Mg-Al based alloys containing alkaline earth elements Ca and/or Sr have emerged in the 1990s. Ca and Sr are added for improved creep resistance. Some of these alloys also contain rare earth elements or contain Zn, Si, Mn, and the addition techniques are the same as in the previous description. It is preferable to add the other alloying elements first and then to introduce the alkaline earth elements though it is also possible to add these elements simultaneously with the others. The addition of calcium and strontium can be carried out in the form of master alloys as well as pure metal. Master alloy additives are usually easier to handle and store.

D: Mg-Li Alloys

Lithium is the only alloying element that decreases the density of magnesium. Lithium with a relative density of $0.53 g/cm^3$ is the lightest of all metals and has extensive solid solubility in magnesium. The benefits of lithium additions to a magnesium alloy are lower density (~ 1.5 g/cm^3) and improved cold rollability and formability. The application of lithium in magnesium alloys extends the properties of these regarding smaller density

10

and clearly increased ductility. Hereby can be met to demands even on the part of the automobile industry for damage-tolerant, better ductile magnesium components. Investigations of hexagonal magnesium lithium alloys show promising results, which contain not only more balanced mechanical properties but also an improved corrosion behavior.

2.1.2.2 Alloying elements and their influence

Pure magnesium is hardly used as a construction material. Alloying elements are used to influence a wide variety of properties, both to increase the manufacturability and the product properties. Below is a summary of the effect of some alloying elements and their effect on the metallurgical behavior of magnesium [10, 11, 20,]. The most used alloying elements are: aluminum, manganese, zinc, zirconium and rare earths.

Aluminium:

Aluminum is one of the most important alloying elements in magnesium. Several systems contain Al up to 10 mass %, e.g., AZ, AE, AM and AS alloy. Al is one of the few metals that dissolve easily in magnesium. Al has a maximum solubility of 12.7wt% at the eutectic temperature. It confers strength and refines the cast structure of magnesium, particularly in conjunction with superheating.

Manganese:

Manganese is an important major addition for many magnesium alloys. More recently it has become important in the development of high performance creep-resistant alloys. Manganese is added to the alloys mainly for corrosion resistance, and also provides greater ductility and fracture toughness. In addition, Mn has a function for

11

reducing the soluble iron content in the alloy melt. In Mg-Al alloys, manganese combines with the detrimental impurity iron and precipitates it to the bottom of the melt as a Fe-Mn-Al intermetallic. In the alloy melt, the manganese addition also passivates the residual iron that remains in solution provided the content is less than a critical limit for the alloy, referred to as the critical Fe/Mn ratio. Mn has a solubility of 2.2wt% at the peritectic temperature. It forms the basis for the well-established medium strength Mg-Mn wrought alloys and the Mg-Al-Mn pressure die casting alloys (AM series). Mn is added to AM alloys in small quantities (0.4 wt%) mainly to improve the corrosion resistance of the alloys.

Zinc:

Zinc is an important alloying element but rarely serves as the major alloying element. Zn is often used in combination Al to produce improvement in room temperature strength. Zn has a maximum solubility of 6.2 wt% at the eutectic temperature. It causes grain refinement and increases strength in Mg. Alloys containing Zn are heat treatable but are somewhat brittle and prone to hot shortness unless Zr is added to further refine the grain size.

Zirconium

Zirconium is a very effective grain refiner for magnesium and can be used with all alloys except those containing aluminum or manganese. The solubility of zirconium in magnesium is 3.8 wt % at the melting temperature and decreases to 0.2 wt % at room temperature.

12

Rare earth metals

RE are added to Mg alloy to increase the strength of Mg alloys at elevated temperature. They also reduce weld cracking and porosity in casting.

Beryllium

Beryllium is added to magnesium die cast alloys at trace levels of 5-30 ppm for improved oxidation resistance of the molten metal. Its incorporation into the melt surface oxide is through the formation of a mixed BeO-MgO layer.

Silicon

Silicon can be introduced into molten magnesium as elemental metallic silicon. The addition of Si to Mg alloys has been found to increase fluidity of the metal in the molten state. In the presence of iron it will reduce the corrosion resistance. It is employed in very few alloys (AS21 and AS41).

However, these elements, such as Iron and Nickel, are harmful impurities in Mg alloys since they greatly reduces the corrosion resistance if present in even small amounts. Usually 0.005% is specified as the upper limit for Fe and Ni content.

2.1.2.3 Effect of alloy elements on physical and mechanical properties

Alloying elements have a strong influence on physical properties [11].

Density: Figure 2.1 shows the influence of alloying elements on the density of magnesium with addition of binary elements. The common alloying elements increase the density of the alloys. However, only lithium addition dramatically reduces the density of magnesium.

13
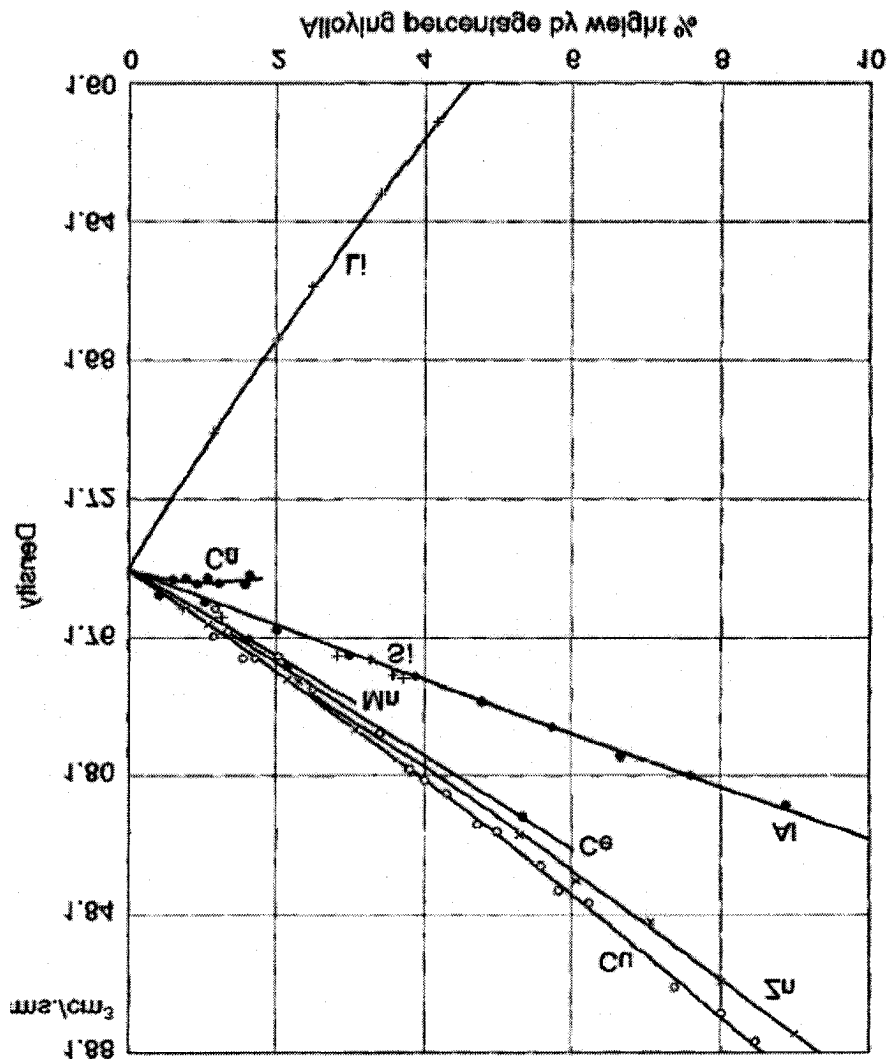
Figure 2.1 Influence of alloying elements on the density of magnesium at room

temperature [11].

Electrical resistivity and thermal conductivity: The electrical resistivity increases with

alloying element additions, but a corresponding decrease in the thermal conductivity.

Damping capacity: The damping capacity decreases rapidly with additions of alloying

elements that increase the hardness of the material. This includes aluminum and

14

manganese. Zirconium in small amounts does not significantly influence the damping capacity.

Mechanical properties: the strength of cast magnesium alloys is obtained by one or more of the well known hardening mechanisms such as solid solution hardening, grain size hardening, and age hardening. The influence of alloying elements on hardness is shown in Fig. 2.2 These diagrams illustrate that the hardening effect is far from linear. This is to be expected since the elements have a wide variation in solid solubility. Hence the alloying elements are partly present in solid solution, partly as intermetallic constituents.

The most common hardening elements are aluminium, zinc, silicon, rare earth elements, silver and yttrium. Aluminium, zinc, silver and yttrium exhibit a high solid solubility, and the solid solubility decreases with falling temperature. Some of the alloying elements form high density, stable dispersions of precipitates, capable of stabilizing the structure under load at elevated temperature. Such elements include Ce, Nd, Pr, Y, Ca, Sr, Si and heavy rare earth elements such as Gd and Tb. While some of these elements have a low liquid solubility, forming precipitates during solidification, elements like Y, Gd and Tb have extensive liquid solubility and also considerable solid solubility. The solid solubility is reduced on decreasing the temperature.

15
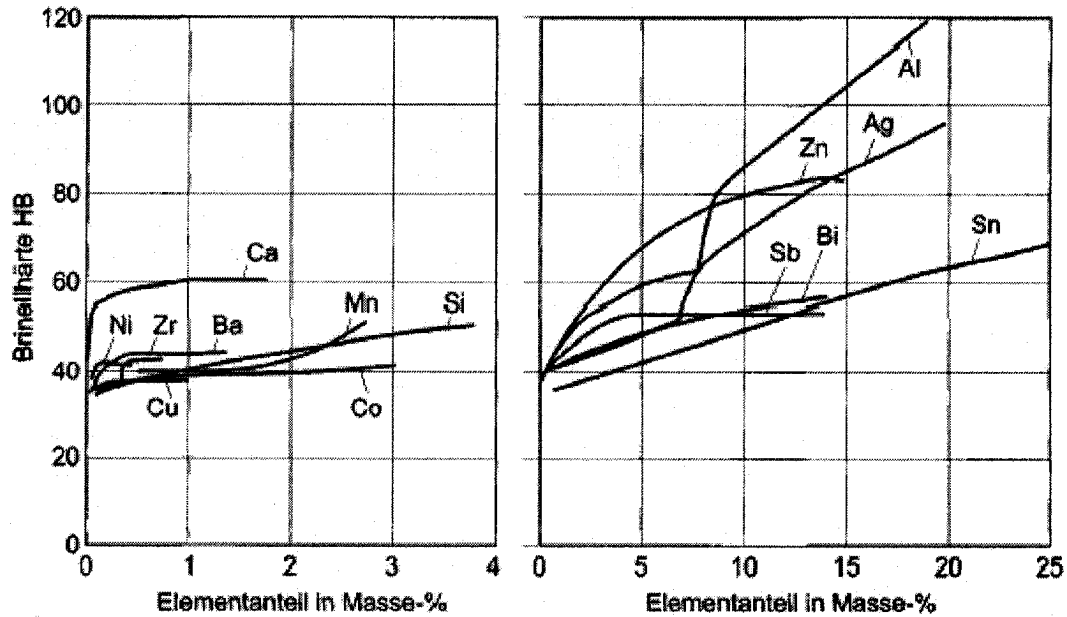
Figure 2.2 Influence of alloying elements on hardness of magnesium [11].

2.1.2.4 Effect of alloy elements on grain refining

Magnesium alloys, except for some special Li-containing alloys, all exhibit a hexagonal crystal structure. This means that at ambient temperatures, the number of operating slip systems limits the formability of the metal. This is due to localized slip and build-up of stresses at the grain boundaries in locations where the localized deformation occurs. The larger the grain size, the larger the buildup of stresses. The result is that coarse-grained alloys show only limited formability at ambient temperatures. Also the yield strength is low due to the extremely high stress concentration factors resulting from localization of slip.

Grain refining can be achieved by different methods, superheating, trace element additions, peritectic additions, constitutional grain refining. It is well known that a certain grain refining effect is obtained by adding alloying elements. This kind of grain refining

16

is due to a slow-down of the growth rate because of solute build-up. Even if the nucleation rate is not influenced, this leads to the formation of a fine grain structure. In the binary Mg-Al-system it has been shown that the effect is considerable [11].

It has also been reported that addition of Sr to Mg-Al alloys, causes a significant grain refining effect [7, 22]. In Mg-Al alloys the eutectic consists of α-Mg and $Mg_{17}Al_{12}$. The $Mg_{17}Al_{12}$ phase is brittle. This means that alloys with high amounts of aluminium tend to become brittle, and the maximum Al-content in commercial alloys is limited to about 10 wt%. The improvement in the properties arises from a better distribution of the $Mg_{17}Al_{12}$, and the reduction in the amount on the boundary due to the effect of strontium.

2.1.3 Advantages and disadvantages of conventional magnesium alloys

Magnesium alloys exhibit excellent properties such as high specific strength at room temperature, good damping characteristics and castability. AM and AZ alloys have been used extensively in the automotive industry since they exhibit superior die castability and a good balance of strength and ductility. Magnesium alloys combine low component weight with cost competitive manufacturing. Thin walls, net shapes, high casting rates and long die life are typical advantages to be gained from using magnesium die castings. Other advantages include excellent machinability, good damping capacity and electromagnetic interference (EMI) and radio frequency interference (RFI) shielding properties.

However, the application temperature of AM and AZ alloy is generally limited to about 100 °C. There could be a rapid degradation in mechanical properties above this temperature due to the presence of $Mg_{17}Al_{12}$ with a lower melting temperature. The poor

17

high-temperature mechanical properties of the alloy have prevented its application at elevated temperature.

2.2 Mg-Al-Sr Alloy

Within the ternary Mg–Al–Sr system, there is a huge amount of possibilities to select alloy compositions [23, 24]. Introduction of the high-ductility, energy absorbing alloys in the AM-series is a major driving force behind the expansion of the automotive use of magnesium die castings. Engine parts exposed to temperatures exceeding 120 ^{0}C represent a potentially large market for magnesium die castings. Major efforts are undertaken to improve the creep resistance of magnesium die casting alloys to allow for operating temperatures exceeding 150 ^{0}C [5].

2.2.1 Introduction

Strontium, an alkaline earth metal, is a soft silver-white or yellowish metallic element that is highly reactive chemically. The metal turns yellow when exposed to air, it is a face-centered cubic structure; malleable, ductile, and somewhat softer than calcium; density 2.64 g/cm3; melts at 777 °C; vaporizes at 1,382 °C. It should be kept under kerosene to prevent oxidation. Freshly cut strontium has a silvery appearance, but rapidly turns to an yellowish color with the formation of the oxide. The finely divided metal ignites spontaneously in air. Volatile strontium salts impart a beautiful crimson color to flames, and these salts are used in pyrotechnics and in the production of flares [25, 26, 27]. Pure Sr can also be used as an additive. However, the tenacious white oxide that

18

forms on the metal can reduce recovery. To minimize the oxidation, pure Sr needs to be stored under argon and dipped in oil during manipulation before addition.

2.2.2 Effect of Sr on Mg alloy

2.2.2.1 Positive effect on Mg alloys

The most significant application for strontium metal is the modification of aluminum-silicon casting alloys. Modification refers to the change in morphology of the eutectic silicon particles from a coarse acicular shape to one that is fine and fibrous. Strontium modified castings exhibit many advantages, including improved ductility, impact strength as well as improved machinability and electrical and thermal conductivity. Strontium has also been shown to distribute micro-shrinkage uniformly during solidification. As a result, strontium modified castings have expanded into a wide range of industries, including the automotive industry where manifolds, engine blocks, wheels and cylinder heads are manufactured from strontium modified aluminum castings. Most recently, significant benefits have been reported with strontium addition to high pressure die castings of aluminum-silicon alloys, and with aluminum wrought alloys [28, 29].

Recent studies [5, 23, 30-40] have shown that strontium addition to magnesium alloys significantly improves their creep resistance as well as mechanical properties at both room and elevated temperatures.

Baril et al. [5] studied Mg-Al-Sr alloys (AJ alloys) and pointed out that AJ alloys have superior creep performance at temperatures as high as 175 ^{0}C with stresses up to

19

70 MPa. They also found that an increase in strontium level from 1.4 wt.% to 2.4 wt.% enhanced their creep resistance, but decreased the tensile strength and ductility. This hinted that decreasing Sr levels reduced porosity content, which increased the tensile strength, but unfortunately decreased the creep resistance.

Grain refinement, often combined with fine and uniform distribution of intermetallic phases, can improve the mechanical properties. Gruzleski and Aliravci [33] reported that adding 0.005 to 0.03 wt.% Sr to AZ91 alloy significantly reduced its grain size from 225 to 75 ~150 μm and also reduced its microporosity. Wang et al. [34] indicated that Sr had a significant grain-refinement effect in wrought magnesium alloy AZ31. The study by Zeng et al. [30] showed that small additions of Sr can effectively decrease the grain size of the AZ31 magnesium alloy, but the effect was sensitive to cooling rate. For a given composition, the grain size decreased with increasing cooling rate; for a given cooling rate, the grain size first decreased, then increased, and finally it decreased again with increasing Sr content in the range of 0.5 wt.% to 1.0 wt.%. Zhao et al. [22] reported that small additions of Sr could refine the as-cast microstructure and improve the mechanical properties. They found that most of strontium atoms dissolved into β particles, refining the as-cast microstructure, especially the second phase, but did not cause the formation of new phases in the microstructure. The strength at room and high temperatures as well as creep resistance was remarkably increased after the 0.1 wt.% strontium addition because of the modification and thermal stability improvement of $Mg_{17}Al_{12}$ phases. When strontium addition became greater than 0.4 wt.%, a lamellar Al_4Sr phase was formed in the as-cast microstructure, which is related to the

20

improvement of yield strength and creep resistance of the alloy at elevated temperature. Strengthening precipitates, such as Al_4Sr phase, would influence the creep behavior at high temperature. Addition of 1.0 wt.% strontium decreased the tensile strength and elongation despite an improvement in the yield strength at room temperature. Creep strength of the alloy increased with the strontium content.

Hirai et al. [31] developed a cast AZ91-based magnesium alloy by adding the elements of Ca and Sr, which exhibited excellent mechanical properties, such as high temperature strength and enhanced creep resistance. From the microstructural observations, the optimal concentration of elements, Ca and Sr, were 1.0 and 0.5 wt.%, respectively. The room-temperature tensile strength and elongation of the developed AZ91-based Sr and Ca containing magnesium alloy with a fine grain size of 20 mm were 250 MPa and 3.5%, respectively, which are higher than those of conventional AZ91 alloy. At an elevated temperature of 448 K, the strength of the developed alloy was also significantly higher than AZ91D alloy.

It has also been indicated [30-34] that Sr addition tends to reduce micro-shrinkage porosity and modifies its distribution in both cast magnesium and aluminum alloys. The applied Sr content in the alloys may vary from 0.02 to 2 wt.%.

It has been reported by Li et al. [35] that when rare earths and strontium were compositely added into AM60, strontium can counteract the grain coarsening effect caused by rare earths addition and reduce the adverse influence of grain coarsening on the mechanical properties and hot cracking resistant property. As a consequence, it improved the yield strength at elevated temperature and eliminated the decline of hot cracking

21

resistant property caused by rare earths addition.

2.2.2.2 Negative effect on Mg alloys

Emadi et al. [8] indicated that strontium aggravates porosity in Al-Si castings. Also strontium modification is known to alter the amount, characteristics, and distribution of porosity in Al-Si castings [32].

2.2.2.3 Sr-containing master alloys

Sr can be introduced into magnesium as Sr-Al master alloys. The master alloys may contain either low amount of Sr (10%) or high amount of Sr (90%). 90%Sr-10%Al master alloy is often used to introduce Sr to magnesium alloys since low aluminum content of the master alloy minimizes chemistry change of magnesium alloy (Table 2-5). This master alloy comes in the form of waffles or packed in aluminum tubes to avoid excessive oxidation (brittle dark gray) of the additive. The preferred alloying temperature is around 675-700 ^{0}C and results in 85-95% recovery. The low Sr master alloys (e.g., 10-90 Sr/Al and 15-85 Sr/Al) is usually used to add Sr to aluminum alloys. High melt temperature of 725-775 °C is required for high alloying efficiency.

Table 2-5 Chemical composition of typical strontium additives [11]

Additive	Element %										Others
	Sr	Al	Ca	Fe	Cu	Ni	Mn	Si	Ba	Zn	
90Mg-10Sr	balance	8-12	0.1 max	≪0.2	0.0035	0.0033	0.0052	0.02 max	0.5 max	0.004	Mg: 0.2 max
Pure Sr	balance	<0.01	0.01	0.01	<0.01	–	–	<0.001	0.1	–	Mg: 0.01
10Sr-90Al	9-11	balance	0.03	0.3	–	–		0.2	0.1	–	0.05 max*
15Sr-85Al	14-16	balance	0.05	0.3	–	–		0.2	0.1	–	0.05 max*

* Total 0.15%.

22

2.2.3 Mg-Al-Sr alloys

The development of Mg-Al-Sr alloy was aimed at replacing RE additions to magnesium with alkaliearth elements due to the grain coarsening effect caused by RE elements. Several Mg-Al-Sr alloys have been developed and exhibited superior creep performance and tensile strength at high temperature. An alloy family based on the Mg-Al-Sr system -- AJ alloys [5] have been developed by Noranda, which have excellent high temperature creep resistance and excellent high temperature tensile properties. The first generation alloy formulation Mg-5Al-2Sr (AJ52x) has shown improved creep resistance, and high high-temperature properties. A new alloy formulation with Mg-6Al-2Sr (AJ62x) offers further advantages: superior creep performance, high ductility, enhanced die castability and hot-tear resistance, as well as corrosion resistance.

Argo et al. [36] studied the AJ alloys systematically, and indicated that the AJ alloy family possesses unique physical properties, which influence their castability, especially a higher thermal conductivity than the typical Mg die casting alloys.

Although a number of studies with regard to the Mg-Al-Sr alloys show their superior creep performance and tensile strength at high temperatures, the alloys were primarily designed for die casting processes. Since die casting processes have its inherent disadvantages – entrapping gases in product and high tendency to form hot tearing, and also Sr addition promotes porosity entrapment, die castings of Mg-Al-Sr alloys could not be suitable for safety-critical applications.

Argo et al. [6, 36] studied process parameters and die castability of Mg-Al-Sr alloys by die casting valve cover. Their results indicated that the metal handling and melt

23

stability properties of the alloys are as good as conventional die casting magnesium alloys. However, die casting of the Sr-alloyed Mg-Al alloys required a high die temperature of 30 ^{0}C to 50 ^{0}C, and a high melt temperature of 40 ^{0}C to 70 ^{0}C. Examination of casting quality manifests that hot tears and cold shuts occurred in die castings of the alloys. High die and melt temperatures tend to result in a short die life. Despite that the alloy was die castable in a production environment with the optimized die design and process parameters, acknowledgement was made [36] that, it was difficult to die cast the Mg-Al-Sr alloy in thin wall applications. Their comparison study showed that the AJ alloys were rated poorer than AZ91 and AM50 in turn of a castability index as illustrated in Table 2-6, where the lower number gives better castability.

Table 2-6 Castability Index of Selected Mg Diecasting Alloys [36]

ALLOY	Castability Index, Ic		
	Thin-walled castings	Medium-walled castings	Thick-walled castings
AZ91	20	20	20
AM50	25	24	35
AS21	39	38	49
AE42	50	50	60
AJ52x	32	24	35
AJ51x	38	32	42
AJ50x	42	37	45

Although applied pressures are capable of eliminating porosity, no detailed investigation has been carried on understanding effect of pressure levels on microstructure and tensile properties of Mg-Al-Sr alloys in squeeze cast process. Also, no

24

studies have been reported on the influence of Sr addition on microstructure and engineering performance of the alloys. To further expand the applications of Mg-Al-Sr alloy, it is essential to develop an understanding of these process and chemistry-related aspects of the alloys.

2.3 Squeeze casting

Squeeze casting is a process that involves the solidification of molten metal in a closed die under an imposed high pressure. The high applied pressures, which are several orders of magnitude greater than the melt pressure developed in normal casting processes, keeps entrapped gases in solution and squeezes molten metal from hot spots to incipient shrinkage pores. As a result, the porosity in a squeeze cast component is almost eliminated. Furthermore, due to the elimination of the air gap at the liquid-mould interface by the applied high pressure, the heat transfer across die surfaces is enhanced, which increases solidification and cooling rates. Thus, superior mechanical properties of the casting resulting from the pore-free fine microstructure are achieved in squeeze-casting processes [9].

2.3.1 Definition of squeeze casting

Squeeze casting is a forming process that combines gravity die casting with closed die forging in a single operation. Other terms used to describe the same process are: extrusion casting, liquid pressing, liquid metal stamping, pressure crystallization and squeeze forming [37]. The main purpose of using squeeze casting is to produce reliable, high integrity castings by reducing the gas volume present in the product, which

minimizes porosity. Squeeze casting (slow gate speed, high cavity pressure) is presently a

leading cost-effective technology for high quality casting in the casting industry [38].

2.3.2 Squeeze casting process

Squeeze casting is a single step which transformation of molten metal into dense

pore-free components. It can be produced in a single process from molten metal to solid

components within re-usable dies. Figure 2.3 shows the schematic diagram of a squeeze

casting process [37, 41].

Step 1: a suitable die set is installed on the bed of a hydraulic press; the die set is

usually sprayed with a commercial graphite lubricant; then the dieset is preheated

to the required working temperature.

Step 2: a metered quantity of molten metal is poured into an open female die

cavity located on the bed of a hydraulic press; initial cooling of the metal may

occur before the application of pressure.

Step 3: the upper die or punch (male) is lowered, coming into contact with the

liquid metal and sealing the metal within the die, and continues to travel until the

applied pressure has reached the desired level; the pressure is maintained until all

the molten metal has solidified; during this period the metal is forced into intimate

contact with the die surfaces.

Step 4: the upper punch returns to its original position and the casting is ejected.

26

STEP 1: Preheat, Lubricating tooling.   STEP 2: Transfer melt into die cavity.

STEP 3: Solidify melt under pressure.   STEP 4: Eject casting.
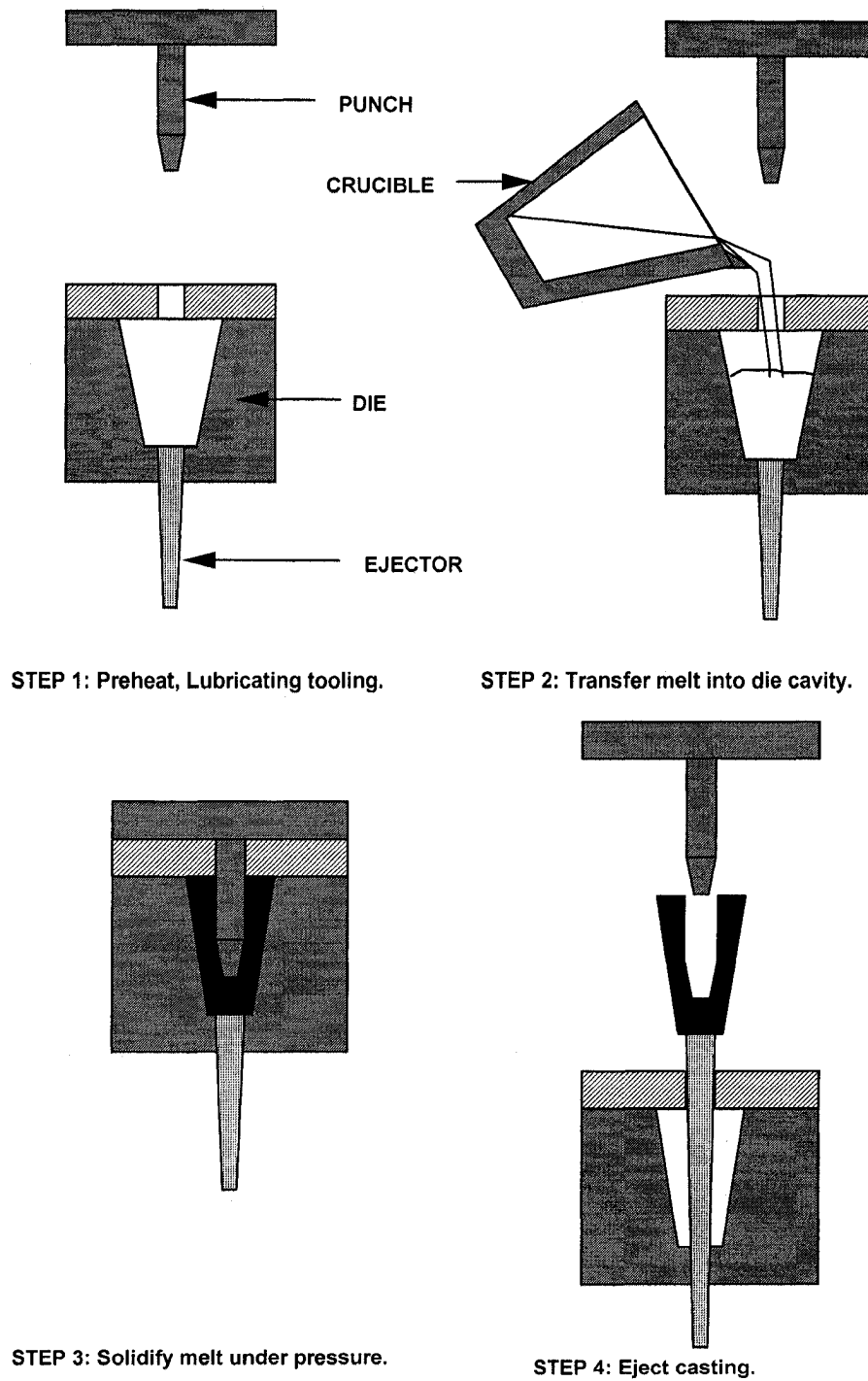
Figure 2.3 Schematic diagram of squeeze casting process [41].

27

2.3.3 Advantages

Squeeze casting, combination of casting and forging, provides many advantages. Compared to die casting, superior mechanical properties can be obtained from squeeze casting. It is possible to completely eliminate shrinkage and /or gas porosity. Zhou et al. [10] compared the squeeze cast AM50 alloy with high-pressure die cast AM50 and showed that the squeeze cast AM50 alloy exhibits virtually no porosity. Figure 2.4 shows no porosity in squeeze cast AM50 alloy, while Figure 2.5 illustrates the presence of porosity in the die cast same alloy. The porosity levels between the squeeze cast and die cast are compared in Figure 2.6.
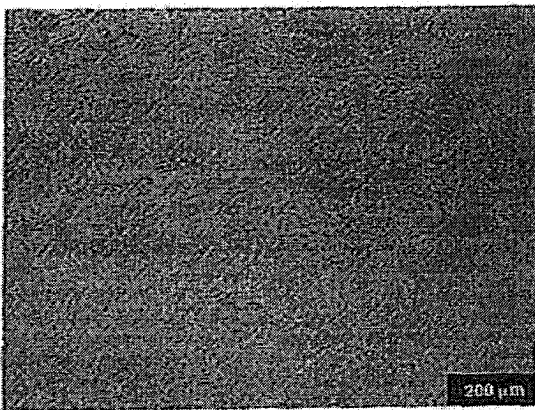
Figure 2.4 Optical micrograph showing almost porosity-free squeeze cast AM50 alloy with a section thickness of 10 mm [10].
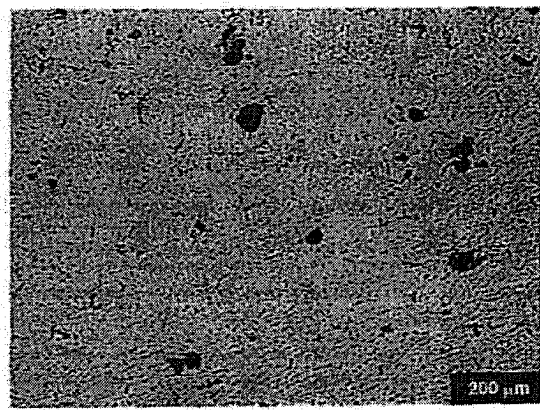
Figure 2.5 Optical micrograph showing porosity in die cast AM50 alloy with a section thickness of 10 mm [10].

28
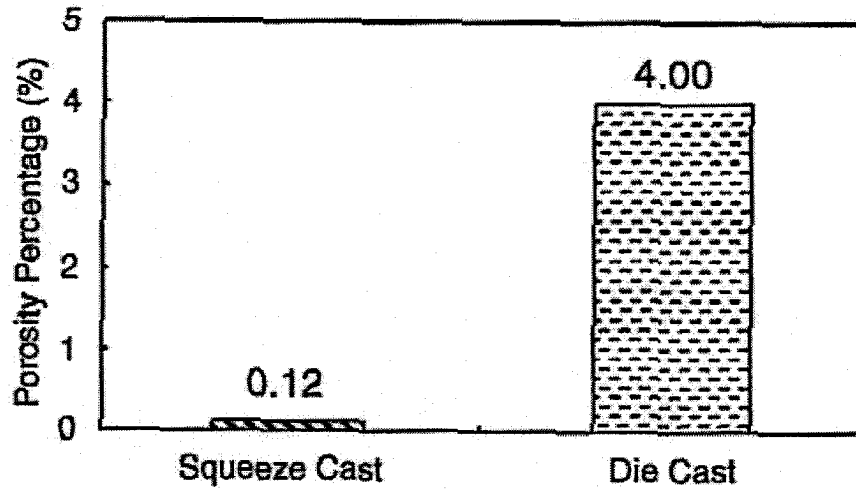
Figure 2.6 Porosity levels of squeeze cast and die cast AM50 with a section

thickness of 10 mm [10].

Table 2-7 lists the tensile properties of both the squeeze cast and die cast AM50

alloy with 10mm section thickness. Figure 2.7 shows a representative true stress versus

strain curve for squeeze cast and die cast AM50 alloys.

Table 2-7 Tensile properties of AM50 alloy with 10 mm section thickness at room

Temperature [10].

Casting condition	0.2% YS, MPa	UTS, MPa	Elongation %
Squeeze cast	75	175	8.0
Die cast	80	100	2.1

29
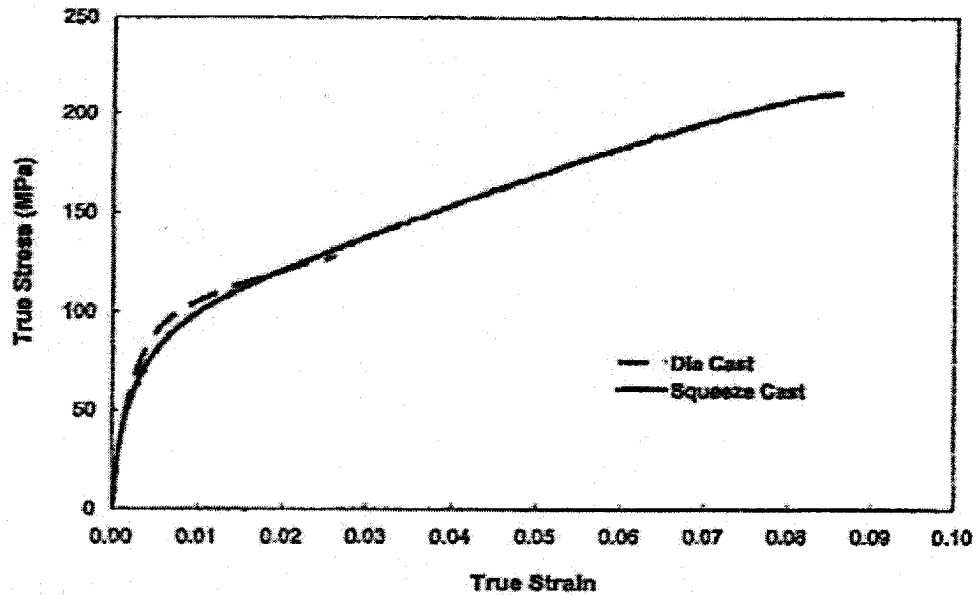
Figure 2.7 Representative true stress versus strain curves for squeeze cast and die cast

AM50 alloys [10].

Luo et al. [42] compared the squeeze cast and die cast AZ91D alloy components

and pointed that there was a significant improvement in ductility for the squeeze casting

samples over the conventional die cast parts.

In the absence of a running or feeding system, a high metal yield can be achieved,

and almost all the metal poured into the die is used to form the components. Moreover,

excellent surface finish becomes achievable. Squeeze castings are heat treatable due to

their low or no porosity content. In conjunction with high quality re-usable dies and thin

die coatings, squeeze castings have good dimensional reproducibility [37].

2.3.4 Comparison of squeeze casting with die-casting

Squeeze casting differs from other die casting processes in two major aspects [38,

43]:

30

First, the slow gate speed used in squeeze casting allows metal to flow into a die in a smooth and even manner, which greatly reduces the amount of gas and thus blow holes entrapped in the metal. As a result, the molten metal being cast enters the die cavity without turbulence. In addition, the molten metal is subjected to an applied pressure and the pressure is maintained until the liquid to solid transformation is complete. Therefore, squeeze casting can eliminate almost all porosity in final product.

Compared to squeeze casting, die casting has itself advantages, such as high production rate, dimensional accuracy and stability, and simplified assembly. But, due to high cavity filling velocities, the presence of porosity in die castings is inevitable. There are four main causes of porosity in die casting: [41]

1. Shrinkage porosity due to differences in specific volumes of the molten metal at the liquidus temperature and the solidified metal at the solidus temperatures;

2. Release of dissolved hydrogen during the solidification and its subsequent entrapment;

3. Porosity due to vaporization of die lubricant and die spray; and

4. Trapped air arising in the die casting process.

2.4 Summary

The poor high-temperature mechanical properties of the AM and AZ alloys have prevented their applications at elevated temperatures. Sr is a suitable addition to Mg alloys to improve their mechanical properties at elevated temperatures. From the literature review, it can be seen that the addition of Sr has a significant effect on

31

microstructure and mechanical properties of die cast Mg alloy. Up to now, most work on Mg-Al-Sr alloys has been focused primarily on die casting processes. Die castings of the Sr-containing magnesium alloys have a high tendency of forming defects such as porosity and hot tearing. Also, information on the effect of Sr content on tensile properties and microstructure of Mg-Al-Sr alloys is limited in the open literature. Squeeze casting is capable of eliminating porosity and suppressing hot tearing. To apply Mg-Al-Sr alloys to safety-critical components for which both high cyclic thermal and mechanical loadings are required, fundamental studies on squeeze casting of Mg-Al-Sr alloys need to be carried out with consideration of applying different levels of external pressures. Effect of Sr content on microstructure and tensile properties should also be investigated.

CHAPTER III

EXPERIMENTAL PROCEDURE

3.1 Methodology

3.1.1 Alloy and casting preparation

3.1.1.1 AM60 and Sr master alloy

The magnesium alloy selected for this study was the conventional magnesium alloy AM60B, of which chemical composition is listed in Table 3-1. Ingots of AM60B provided by Hydro Magnesium were cut into cubes (100 mm x 100 mm x 50 mm), so that it can be easily loaded into a crucible. AlSr90 master alloy supplied by Timminco was used as Sr addition with chemical composition listed in Table 3-2, Figures 3.1 (a) and (b) show sectioned AM60B cubes and AlSr90 alloys.
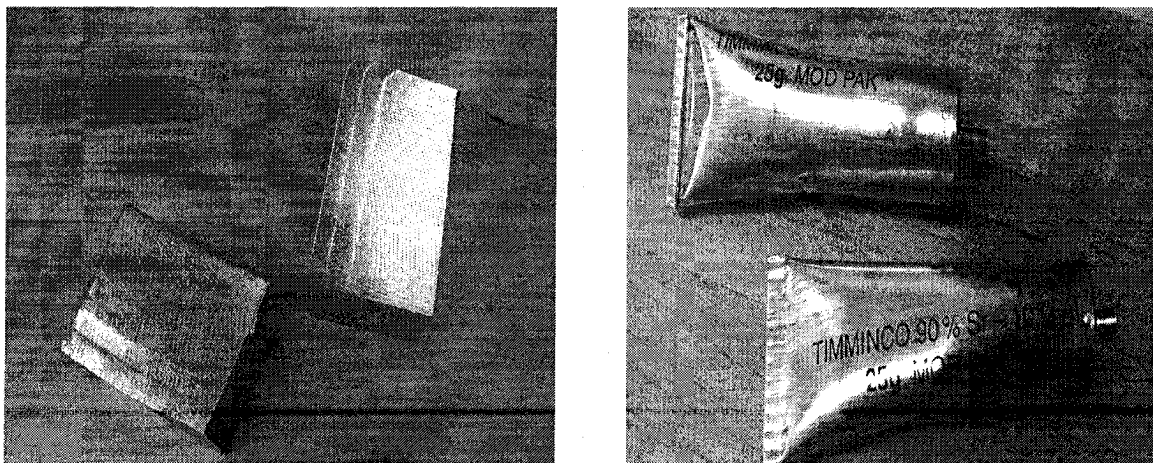
Figure 3.1 (a) Sectioned AM60B ingot and (b) AlSr90 master alloys.

Table 3-1 Chemical composition of AM60B

Alloy	Al	Zn	Mn	Si	Cu	Fe	Ni	Others
AM60	6%	<0.22%	>0.25%	<0.1%	<0.01%	<0.005%	<0.002%	<0.003%

Table 3-2 Chemical composition of AlSr90

Alloy	Sr	Al	Fe	Ca	Si	Ba	Mg	Others
AlSr90	Reminder	10	<0.15%	<0.017%	<0.08%	<0.023%	<0.014%	<0.1%

3.1.1.2 Protective gas

Melting pure magnesium or magnesium alloys requires the use of a protective gas mixture in order to protect the melt from oxidation and burning. The gas mixture employed in this study was the Sulfur Hexafluoride SF_6 0.5% (CO_2) plus carbon dioxide in balance. SF_6 is one of the most popular insulating gases. It has a number of nice properties: it's not flammable, it's non-toxic, it's moderately inexpensive and it's a good insulator (being an electronegative gas) with a breakdown strength of about 3 times that of air. Since SF_6 density is far higher than air and oxygen (see Table 3-3), it can cover on the top of the melt and separate it from air to prevent oxidizing. The flow rate of SF_6 mixed gas was controlled between 0.8 and 1.0 liter per minute with the outlet pressure of 20 to 25 psi during melting of magnesium alloys [44].

Table 3-3 Densities of different gases

Gas	Carbon monoxide	Air	Oxygen	Argon	Carbon dioxide	SF_6
Density of Gas (kg/m^3)	1.25	1.29	1.31	1.784	1.80	**6.27**

3.1.2 Squeeze casting machine and melting unit

A 75-ton, vertical hydraulic press as shown in Figure 3.2 was employed for squeeze casting of prepared Mg-Al-Sr alloys. The melting was performed in an electrical resistance furnace. Figure 3.2 shows a squeeze die-casting machine and Figure 3.3 shows the electrical furnace with a control unit and protective gas system.
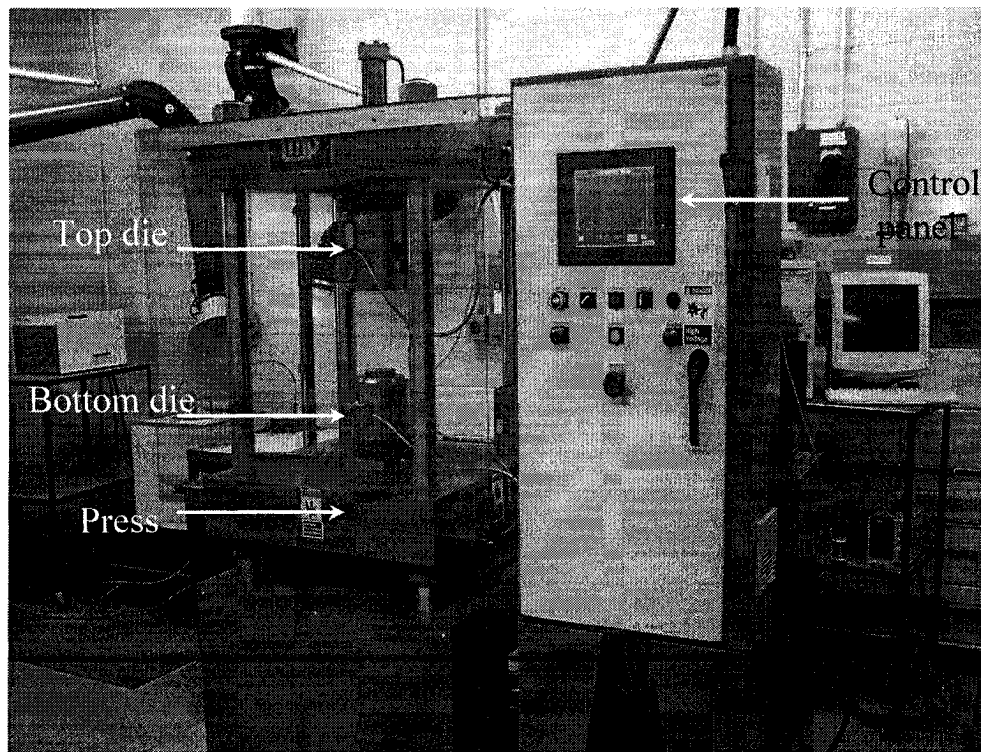
Figure 3.2 Squeeze casting machine.

35
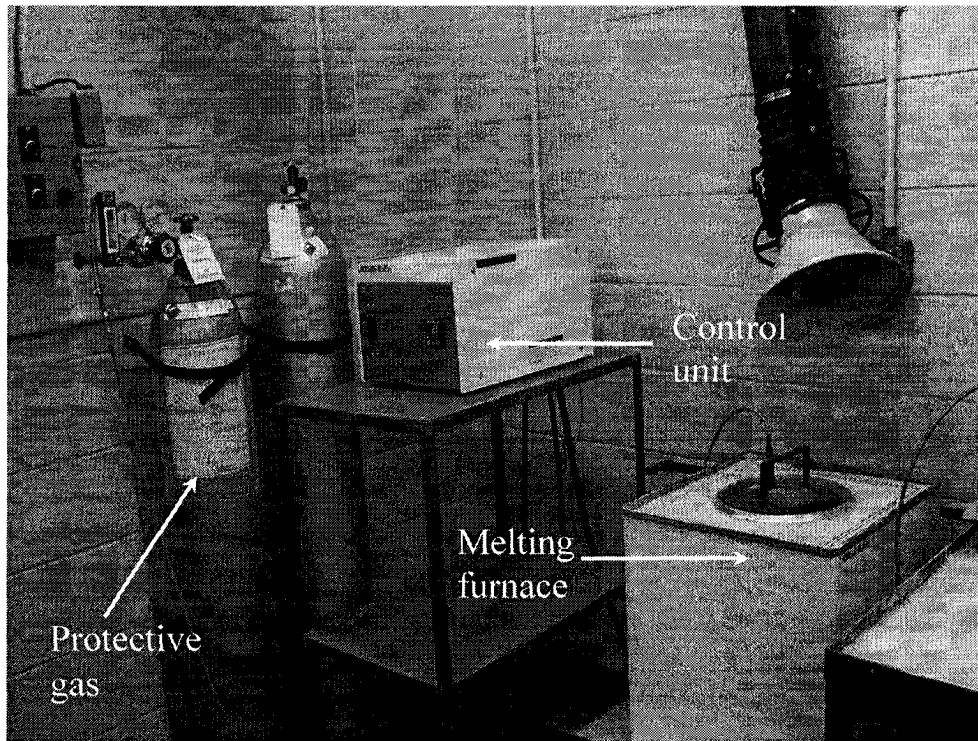
Figure 3.3 SF$_6$ protective gas system and melting furnace.

3.1.3 Melt Preparation and Squeeze casting

When running a squeeze casting experiment, the list of safety procedures and sequence must be followed at all times:

1. Do not use water when running an experiment;

2. Ventilation System is ON;

3. Protection Gas is ON;

4. Safety hard hat with a full face shield, safety shoes, lab coat and leather gloves should be worn all time;

5. Moulds and tools need to be preheated to approximately 150 °Celsius;

6. Fire extinguisher can be quickly and easily accessed; and

36

7. There are at least two students in the lab when running an experiment.

3.1.3.1 Melt Preparation

3.1.3.1.1 Tool Preheating

One very important point that needs to be stressed is always preheat the tools, such as skimming rods, stirring rods, ingot pieces, permanent moulds and ingot moulds prior to immersing those tools into liquid magnesium or to cast ingots or any other type of test specimens. Tools and moulds need to be preheated and should always be free of moisture in order to avoid a violent reaction with the molten magnesium contacting water. Tools were preheated around 150 °C on top of the furnace for at least 20 minutes prior to use.

3.1.3.1.2 Melting Process

Melting of magnesium alloy AM60B was carried out in a 2.6 kw, 50/60 HZ electrical furnace with a maximum temperature of 1200 ^{0}C. The furnace temperature was usually set up at 850 ^{0}C when running the experiment to ensure the temperature of the inside crucible (melt) is kept around 760 ~780 ^{0}C. Both the control panel of the furnace and a handhold digital thermometer closely monitored the temperature of the melt. The set furnace temperature was decided according to the AM60B and Sr-containing master alloy melting temperatures, as well as the factor that the heat lost in skimming and transferring process. AM60B melting temperature is 651 $^{\circ}$C (1202 $^{\circ}$F), Sr melting point is 777 $^{\circ}$C (1431 $^{\circ}$F), and AlSr90 melting point is 764 $^{\circ}$C (1390 $^{\circ}$F).

Small pieces of AM60B were put on the top of the furnace cover to preheat as the furnace temperature increased. Once the control panel showed that the furnace

temperature reached 850 ^{0}C with a crucible inside the furnace, 2.5 kg magnesium alloy AM60B cubes were fed into the crucible. The protective gas mixture should then be fed into the furnace chamber at this stage in order to make sure that the magnesium pieces were not oxidized as the metal temperature increased. Meanwhile, the ventilation was turned on for adequate air circulation. Small pieces of strontium master alloy covered by aluminum foil were put at the top of the furnace cover for preheating. Then, in the melt stage, magnesium pieces will change from solid stage to liquid stage in approximately one hour (depending on the number of pieces). When handhold digital thermometer monitored the temperature of the melt is 760 ^{0}C to 770 ^{0}C, AlSr90 pieces was put into furnace to melt together with AM60B under SF_6/CO_2/air atmosphere. Sr alloy stays in furnace at least 15 minutes and the melt temperature around 760 ~ 780 ^{0}C to ensure that the AM60B and Sr melt thoroughly. Allow proper time to melt the charge and furnace to reach the targeted temperature. Open the furnace cover and skim the melt surface by using the mild steel tool available for this operation.

Once the surface of the charge has been skimmed and cleaned, make additions to the charge and stir the melt. Allow sufficient time for the additions to dissolve, and then stir the melt thoroughly. When the melt composition has been adjusted according to the test plan and the melt temperature has reached the desired set point, then the crucible is removed from the furnace chamber in order to cast test specimens.

3.1.3.2 Squeeze Casting

Before transferring the melt from the crucible to the casting die as shown in Figure 3.2, the die cavity of the mould was purged with the CO_2/SF_6-0.5% protective gas

38

mixture to avoid oxidizing the magnesium during casting and solidification. The mould

was preheated to the pre-set temperature of 400 ^{0}C of the band heater. The preheating of

the mould ensured the temperature of the die inside reached 275 ^{0}C that was monitored

by a handhold digital thermometer. A desired applied pressure level was set through

control panel. In this experiment, the employed pressures were 0 MPa, 30 MPa, 60 MPa,

or 90 MPa according to the experimental requirement.

Squeeze casting experiments started with the transfer of a metered quantity of

prepared molten Mg-Al-Sr alloys into the bottom half of the preheated die set mounted in

the hydraulic press. The dies were then closed by lowering the top half (punch) into the

bottom die. The pressure exerted by the punch on the molten metal steadily increased to a

predetermined pressure level and maintained until the entire casting solidified.

3.1.4 Squeeze cast coupon

Squeeze casting coupons had a cylindrical geometry with a diameter of 100 mm

and a thickness of 25 mm (Figure 3.4). Casting coupons were cut for density

measurement, porosity evaluation, tensile testing and microstructure analysis. The test

samples were taken from the center of coupon (Figures 3.5 - 3.7).

39

Figure 3.4 Squeeze cast cylindrical coupons with dimensions of approximately 100 mm

in diameter and 25 mm in thickness.
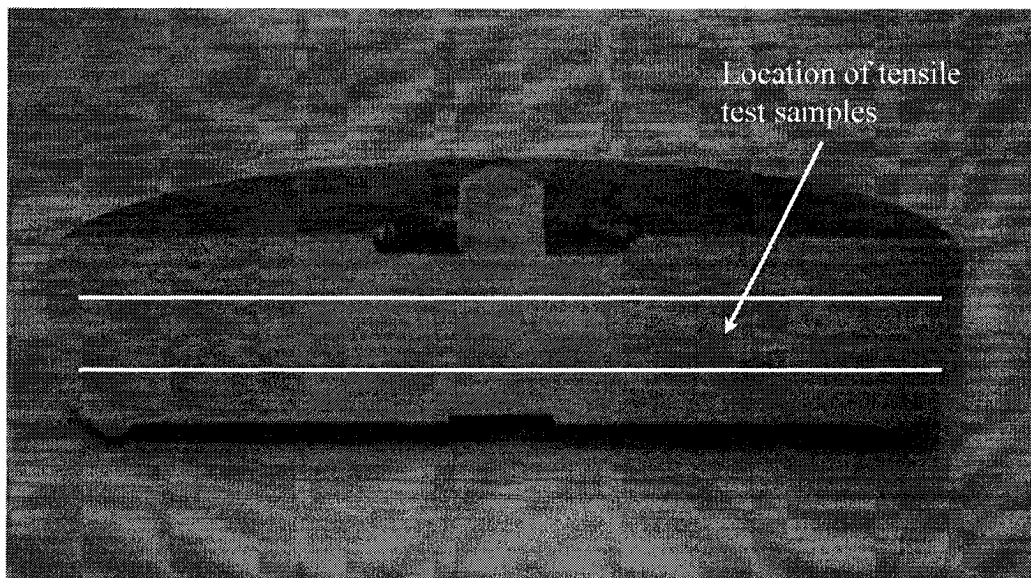
Figure 3.5 Photograph showing the location of the coupon from which samples were

taken for tensile testing.

40
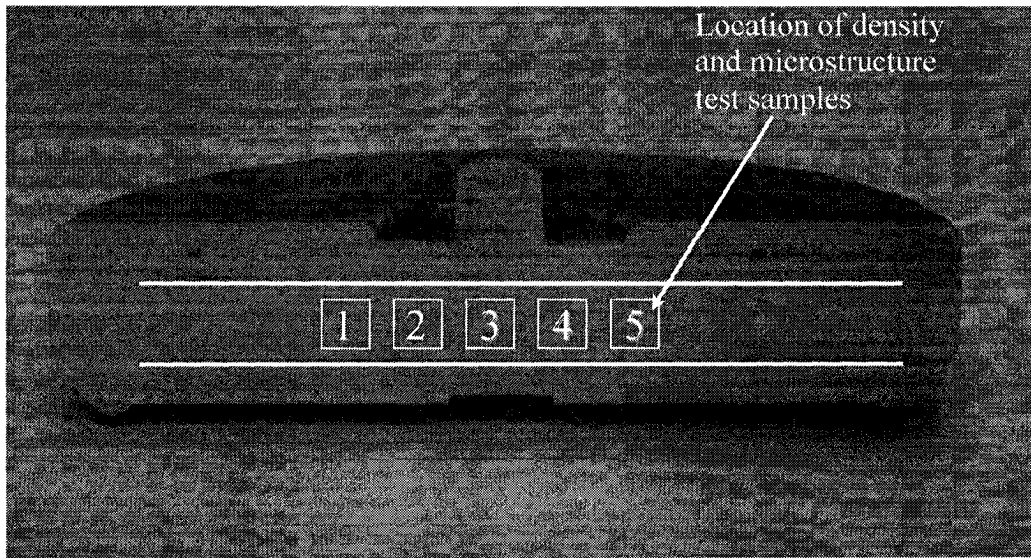
Figure 3.6 Photograph showing the location of the coupon from which samples were taken for porosity and microstructure analyses.
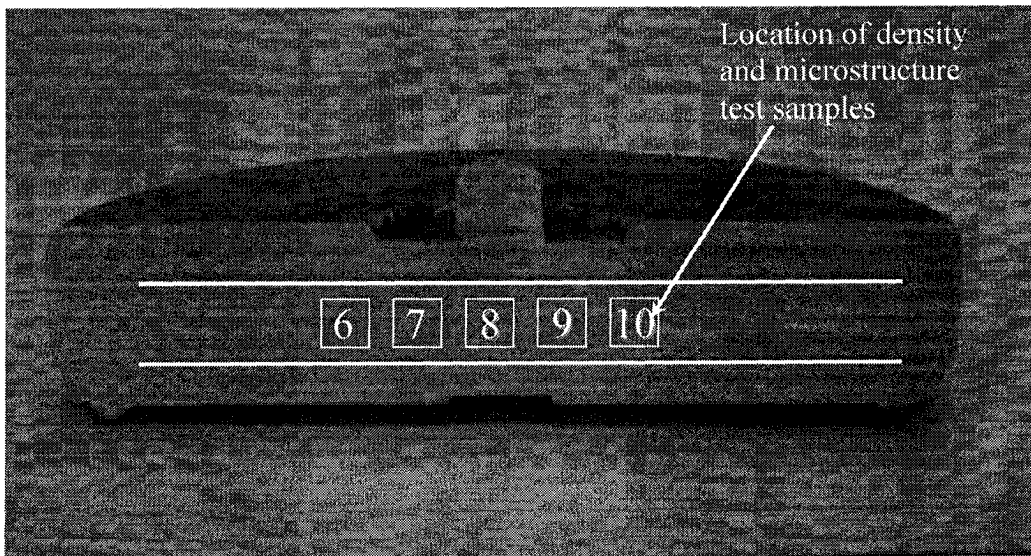
Figure 3.7 Photograph showing the location of the coupon from which samples were taken for porosity and microstructure analyses.

3.2 Porosity Evaluation

Porosity of squeeze cast coupons was evaluated via density measurement. Following the measurement of specimen weight in the air and distilled water, the actual density (D_a) of each sample with the dimensions of 10x10x10 mm was determined using the Archimedes' principle based on ASTM Standard D3800 [44].

$$D_a = W_a D_w / (W_a - W_w)$$

where W_a and W_w are the weight of the specimen in the air and in the water, respectively, and D_w is the density of water.

The porosity of each specimen was calculated by the following equation (ASTM Standard C948) [45]

$$\% \ Porosity = [\ D_t - D_a / D_t] \times 100\%$$

where D_t is the theoretical density of the alloys, which was assumed to be ones squeeze cast at the highest pressure level (90 MPa) in this study because the standard densities of Mg-Al-Sr alloys are not available in the literature. Figure 3.8 show the experimental samples of a density test, and Figure 3.9 show the density measurement setup.
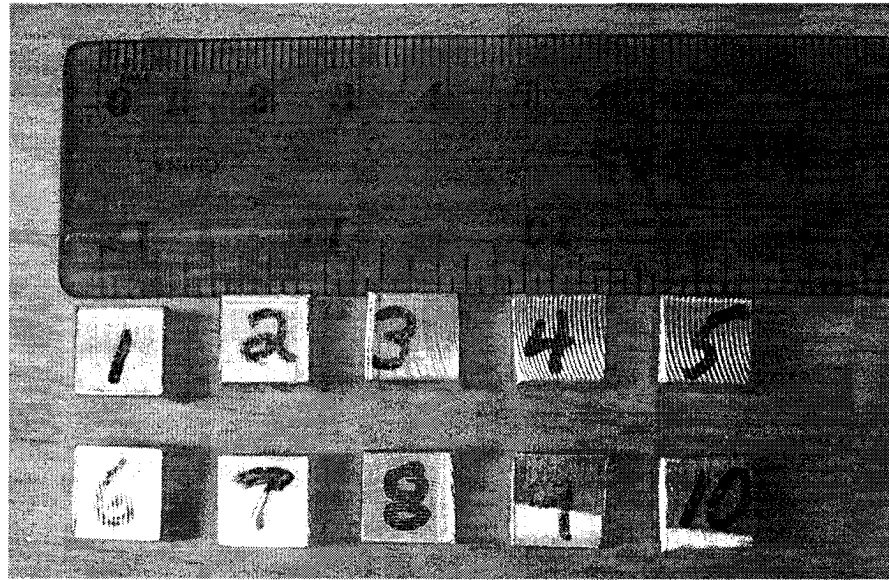
Figure 3.8 Samples for density measurement.
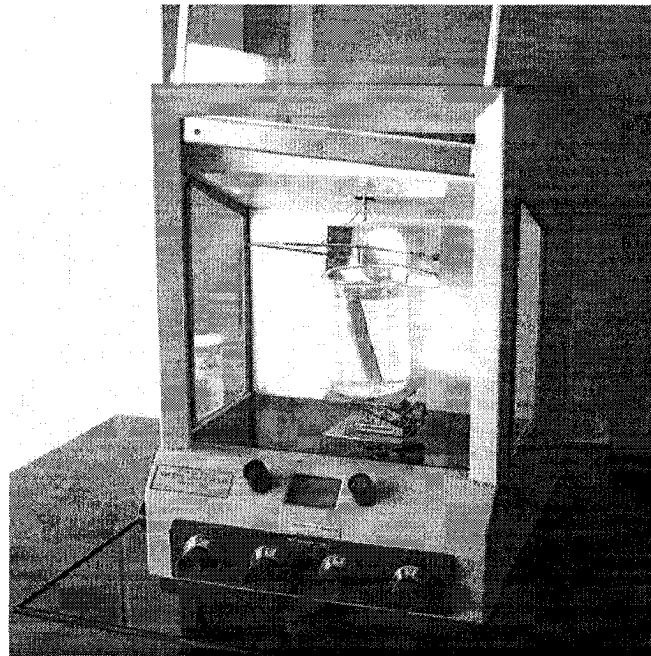
Figure 3.9 Experimental setup for density measurement.

43

3.3 Tensile Testing

The mechanical properties of the squeeze cast Mg-Al-Sr alloys were evaluated by tensile testing, which was performed at room temperature on an Instron (Grove City, PA) machine equipped with a data acquisition system. Following ASMT B557 [46], subsize flat tensile specimens (25 mm in gage length, 6 mm in width, and 5 mm in thickness) were machined from the squeeze cast discs. The tensile properties, including ultimate tensile strength (UTS), 0.2% yield strength (YS), and elongation to failure (E_f) were obtained based on the average of four tests. Figures 3.10 – 3.12 show the dimensions of a tensile specimen, the samples of machined tensile test bars, and the tensile test machine, respectively.
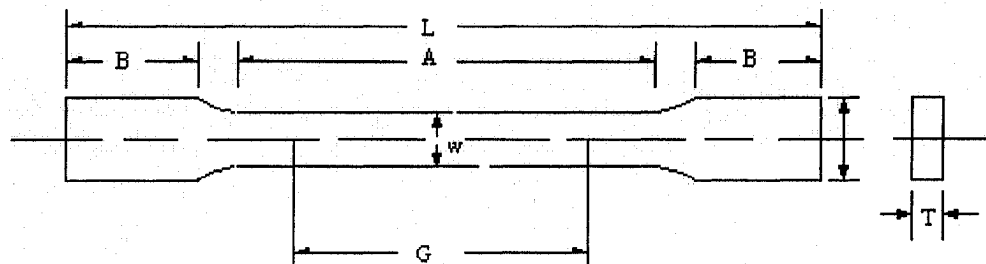
Figure 3.10 Schematically illustration of Tensile Test Specimen (subsize).

G – Gage length: 25.4 ± 0.1 mm   W – Width: 6 ± 0.1 mm

T – Thickness: 5 mm ± 0.1 mm   R – Radius of fillet, min: 6 mm

L – Overall length, min: 100 mm   A – Length of reduced section: 32 mm

B – Length of grip section, min: 30 mm   C – Width of grip section: 10 mm

44
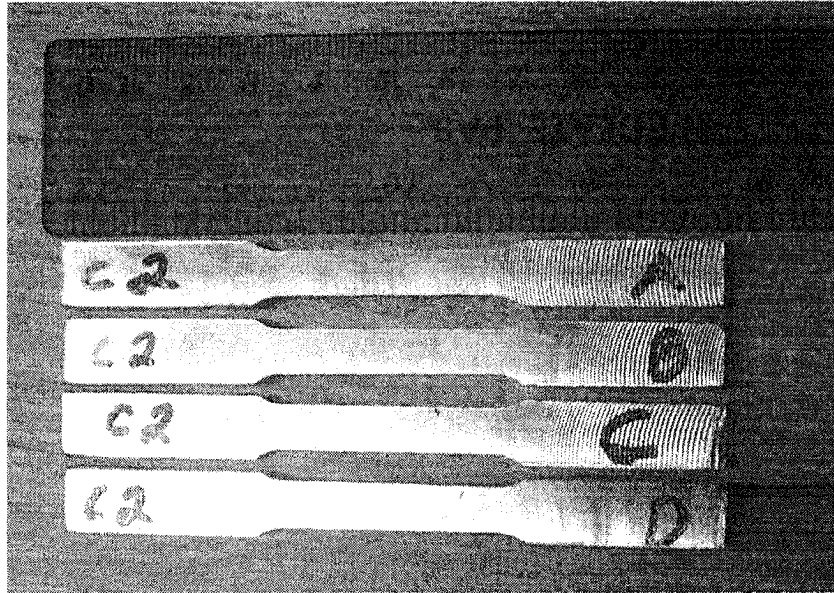
Figure 3.11 Machined tensile testing specimens.
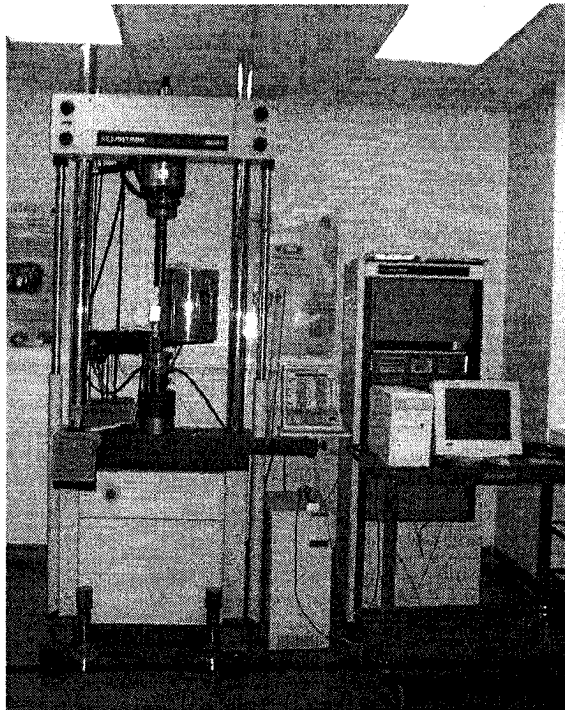
Figure 3.12 Instron Tensile Test Machine (Model 8562).

45

3.4 Microstructure Analysis

3.4.1 Specimen preparation

For the microstructure analysis, specimens were chosen from the center of the coupons (Figure 3.6 and 3.7). The procedure of specimen preparation included: sectioning, mounting, grinding, polishing and etching.

A. Sectioning

Specimens were cut from the center of coupons in the form of cubes with the dimensions of 10x10x10 mm.

B. Mounting

Specimens were mounted by Buehler simplimet3 mount machine. The mount materials are one of the common plastic mounting materials, cold mounting material – epoxy. Then the mounted samples were ground down on the 180 grit by using a belt grinder to smooth the edge of the samples.

C. Grinding

The roughly ground mounted samples went through a wet grinding process by using the series of SiC papers in the sequence procedures: 240, 320, 400, and 600 grit.

D. Polishing

Mechanical polishing was performed in two stages by using polishing machine and DP-PAN polishing cloth with 3 μm Al_2O_3 suspension, and 0.05 μm Al_2O_3 suspension. Rough polishing (stage one) removed the major part of the disturbed metal remaining after the final grinding step. Finish polishing (stage two) removed the superficial scratches that remain after rough polishing. Then using cold water, liquid soap and ethyl alcohol cleaned the polished specimens, and dried with a hair dryer using cold air.

46

E. Etching

Etch the samples for 20 to 30 seconds with 2~3 % Nital (3 ml HNO_3 + 100 ml ethanol). Etching was performed by submerging specimens into the etchant for 20 ~ 30 seconds. Then specimen surfaces were rinsed with running water and etchant, and dried with cold air. Etched specimens were covered by a plastic cap to prevent surface damage prior to standard metallographic analyses.

3.4.2 Optical and scanning electron microscopy

A Buehler optical image analyzer 2002 system was used to determine primary characteristics of the specimens. Measurement of grain size was carried out by using average line length measured in microns in grain diameter method through the Buehler optical image analyzer. Figure 3.13 shows the Buehler optical image analyzer 2002 system. The detailed features of the microstructure were also characterized at high magnifications by A JSM-5800LV scanning electron microscope (SEM) with a maximum resolution of 100 nm in a backscattered mode/1μm in X-Ray diffraction mapping mode, and maximum useful magnification of 30,000. Figure 3.14 shows Scanning Electron Microscope (Jeol Model JSM-5800LV). In order to maximize composition reading of the Energy Dispersive Spectroscopy (EDS) data, etchant was applied to the specimens for microscopy examination. The SEM to ascertain the nature of fracture mechanisms also analyzed fractured surfaces of tensile specimens. The longitudinal section of tensile tested specimens passing through the fractured surface were also polished and examined in an effort to understand the extent of damage beneath the fractured surface.

47
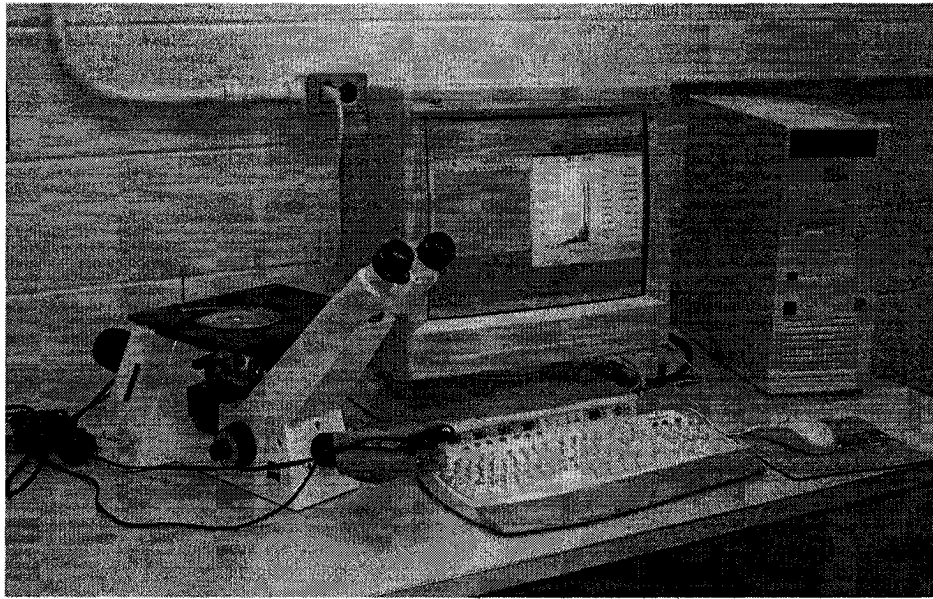
Figure 3.13 Buehler Optical Image Analyzer Model 2002.
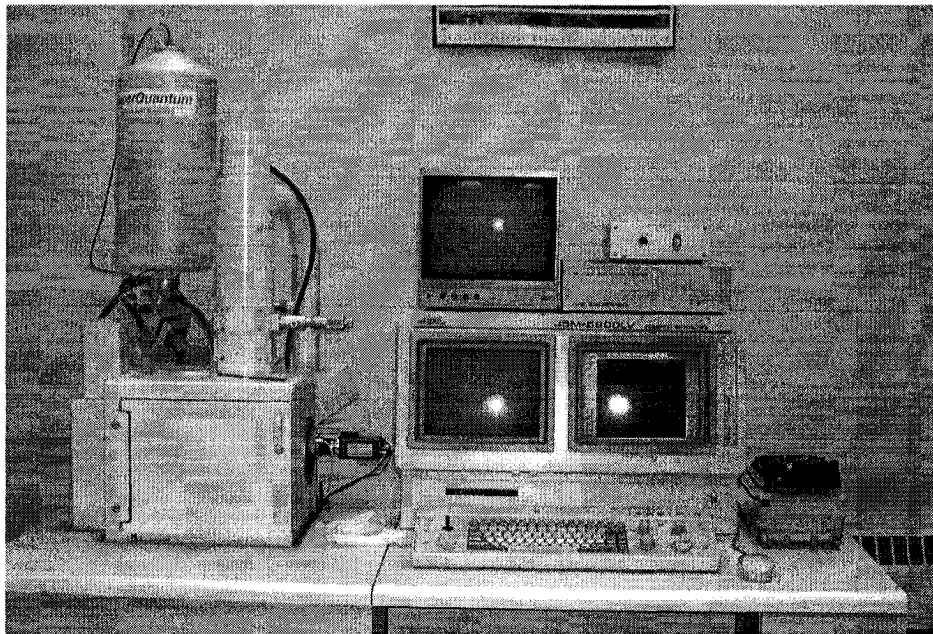
Figure 3.14 Scanning Electron Microscope (Jeol Model JSM-5800LV).

48

3.4.3 TEM

Thin flakes for the analysis of transmission electron microscopy (TEM) were ground with CARBIMET abrasive papers to thin foils with thickness of ~20 μm. The thin foils were further thinned by ion beam milling with an incidence angle of 3 ~ 5° for about 1 hour. TEM investigations were undertaken with a JEOL 2010 transmission electron microscope (TEM) equipped with an energy dispersive X-ray spectrometer (EDX) at an operating volt of 200 keV, as shown in Fig. 3.15. Two-beam conditions were used to observe the contrast caused by the coherent strain at the interfaces between precipitates and matrix. Selected area electron diffraction (SAED) combined with centered dark field imaging was usually used to identify various phases.
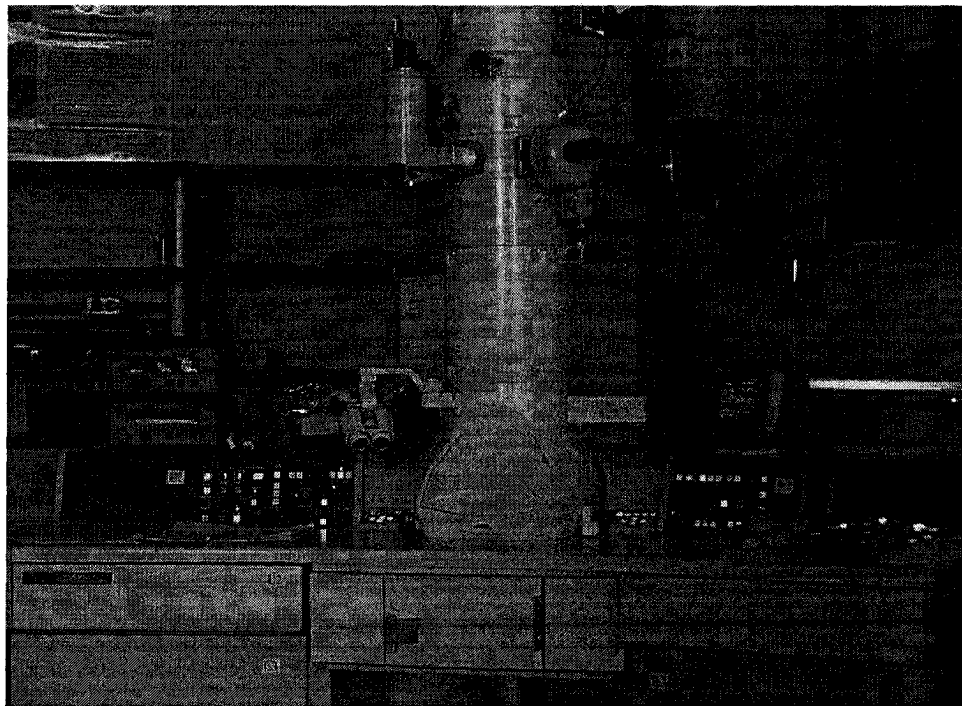
Figure 3.15 JEOL 2010 Transmission Electron Microscope with an Energy Dispersive X-ray Spectrometer (EDX)

49

CHAPTER IV
RESULTS AND DISCUSSION

4.1 Introduction

In this chapter, the details of microstructural analysis and tensile properties of squeeze cast Mg-Al-Sr alloy are presented. The influences of pressure levels and strontium contents on tensile properties are discussed.

The results in this chapter will be presented in the following sequence:

1. Casting surface cracking,

2. Material densification, including density and porosity evaluation, as well as microstructural images showing porosity,

3. Microstructure analysis including grain size measurement, optical microstructure and SEM phase characterization,

4. Tensile properties and behavior,

5. Fracture behaviour, and

6. Summary.

4.2 Effect of Pressure Levels on Tensile Properties and Microstructure of Squeeze Cast Mg-Al-Sr Alloys

To investigate the effect of applied pressures on microstructure and mechanical properties of squeeze cast Mg-Al-Sr alloys, four different levels of applied pressures, 0, 30, 60, and 90 MPa, were employed while the strontium content of the alloys was kept constant at 0.5 wt%.

50

4.2.1 Symbolization of squeeze cast Mg-Al-Sr alloys

To ease the presentation of experimental results and facilitate the discussion, all the tested Mg-Al-Sr alloys are labeled. The designed symbols are listed in Table 4-1 by taking into consideration both the involvement of applied pressure levels and Sr content in the alloys. The symbolization system considers "S" as "Sr", uses "05", "15", "20", "30" representing the Sr content of "0.5%", "1.5%", "2.0%", "3.0%", and "A", "B", "C", and "D" representing "0", "30", "60" and "90" MPa, respectively. The results of chemical analysis of the alloy samples taken from the squeeze cast coupons with different levels of strontium content are summarized in Table 4-2.

Table 4-1 Symbols of squeeze cast Mg-Al-Sr alloys

| | | Sr (wt.%) | | | | | Series |
		0	0.5	1.5	2.0	3.0	
Presure Level (MPa)	0	AMS600A	AMS605A	AMS615A	AMS620A	AMS630A	AMS-A
	30	AMS600B	AMS605B	AMS615B	AMS620B	AMS630B	AMS-B
	60	AMS600C	AMS605C	AMS615C	AMS620C	AMS630C	AMS-C
	90	AMS600D	AMS605D	AMS615D	AMS620D	AMS630D	AMS-D

Table 4-2 Chemical composition of squeeze cast Mg-Al-Sr alloys

Alloy Symbol	Al (wt.%)	Sr (wt.%)	Mn (wt.%)	Zn (wt.%)	Ni (wt.%)
AMS605	5.89	0.49	0.335	0.0068	0.0004
AMS615	5.87	1.71	0.315	0.0115	0.0008
AMS620	5.83	2.22	0.318	0.0111	0.0007
AMS630	5.71	3.04	0.302	0.0104	0.0006

4.2.2 Surface cracking of Mg-Al-Sr alloys

As discussed in the Chapter II, Sr has a negative affection on Mg alloys [8, 31]. There is possible that strontium aggravates porosity in Mg alloys and Sr addition enables Mg alloys to easily form surface cracks due possibly to hot tearing. To understand the effect of pressure levels on the formation of surface cracks, direct observations on the surfaces of cast Mg-Al-Sr alloys with different applied pressure and Sr content levels were made.

Figure 4.1 shows obviously that there are shallow V shape and line cracks formed in the top middle of AMS630A alloy. No apparent cracks were observed on the surfaces of AMS630B, AMS630C, AMS605A and AMS620A alloys as illustrated in Figures 4.2-4.5. The observation indicates that not only Sr addition, but also the levels of the external pressure influence the formation of the surface crack of the alloys. With relatively low content of strontium alloy, less than 3 wt%, no surface cracks were found in the alloys as illustrated in Figures 4.4 and 4.5. However when strontium content increased to 3 wt%, cracks were formed in the central area of the top face of the alloy, where the last solidification took place during cooling. However, the application of external pressure

52

suppresses evidently the formation of surface cracks. It is clear that surface cracks appeared in the top face of alloy AMS630A when no external pressure was present. But, an exertion of applied pressure (30 MPa) eliminated the occurrence of surface cracking in the alloy (Figure 4.2).

Figure 4.1 Alloy AMS630A: crack formation in the middle of the sample solidified under

no applied pressure.

Figure 4.2 Alloy AMS630B, no crack formation in the sample solidified under 30 MPa

applied pressure.

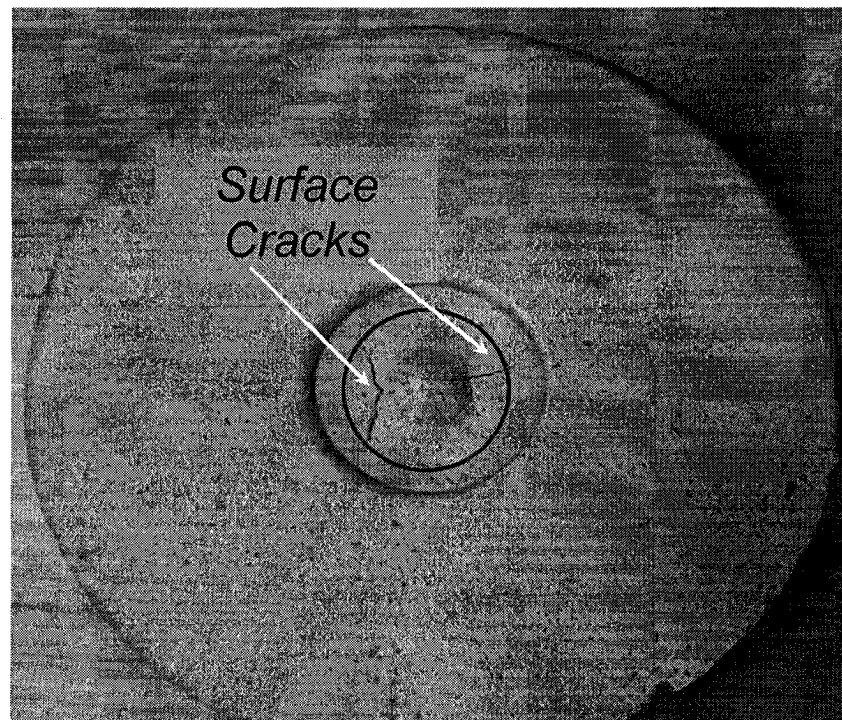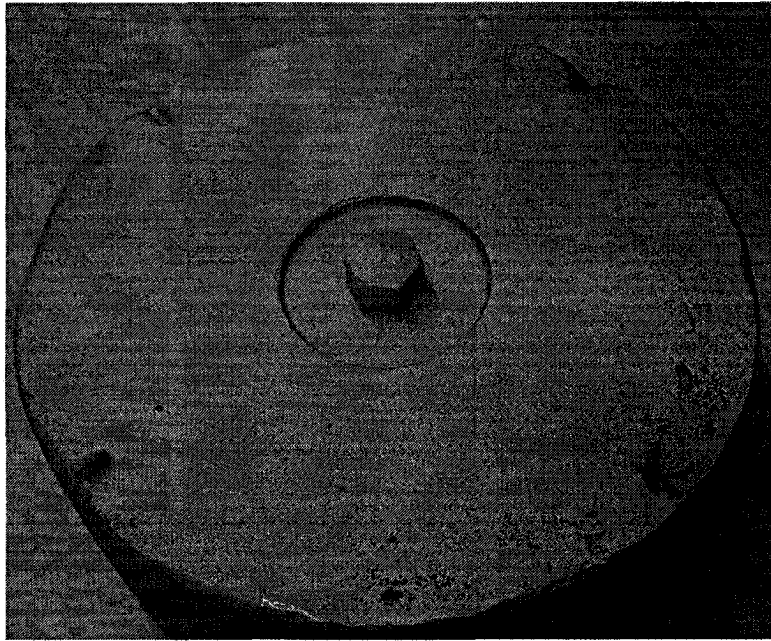Figure 4.3 Alloy AMS630C, no crack formation in the sample solidified under 60 MPa
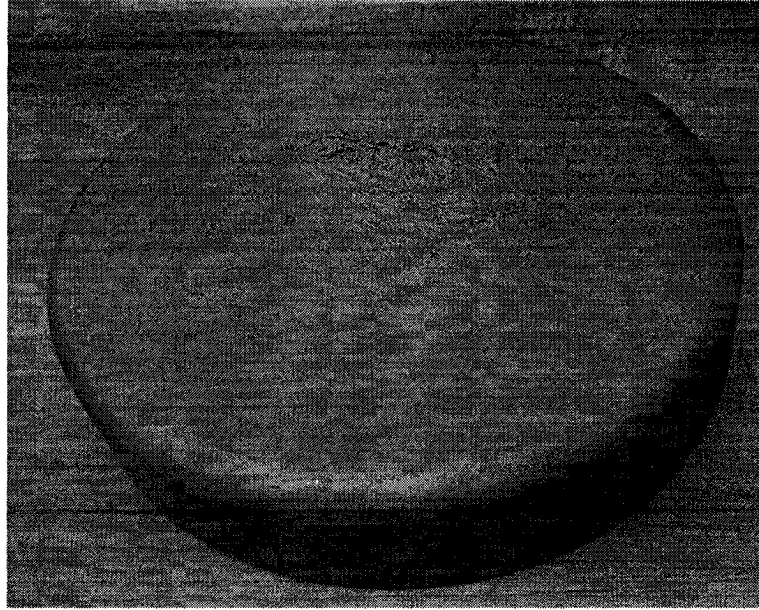
applied pressure.

54

Figure 4.4 Alloy AMS605A, no crack formation in the sample solidified under no applied pressure.

Figure 4.5 Alloy AMS620A, no crack formation in the sample solidified under no applied pressure.

55

4.2.3 Material densification

Figures 4.6 and 4.7 present the density and porosity measurements of AMS605 series of the alloys squeeze cast under different pressure levels of 0 (AMS605A), 30 (AMS605B), 60 (AMS605C) and 90 (AMS605D) MPa, respectively. It is evident from Figures 4.6 and 4.7 that the density of squeeze cast AMS605-series alloy samples increases and its porosity decreases with an increase in applied pressure.

Figures 4.8 and 4.9 show the preliminary microstructural results of AMS615 alloys with Sr 1.5 wt% squeeze cast without applied pressure (0 MPa) and with an applied pressure of 60 MPa, respectively. It can be seen that when no pressure is applied, porosity tends to form in the AMS615 alloy. However, porosity is eliminated with the application of an applied pressure of 60 MPa.

An optical micrograph given in Figure 4.10 shows the presence of porosity in AMS605A. Figure 4.11 depicts porosity-free microstructure of AMS605D alloy. Figures 4.12, 4.13 and 4.14 present the microstrucutre results of SEM analyses for the AMS605 alloys solidified under the applied pressures of 0, 30 and 60 MPa, respectively. The SEM results given in Figures 4.12, 4.13 and 4.14 further validate the porosity measurement. At 0 MPa applied pressure, the solidification process with no help of external applied pressure was incapable of eliminating porosity as given in Figure 4.12. However, as the applied pressure increased to and beyond 30 MPa, no porosity was observed in the squeeze cast alloys (Figures 4.13 and 4.14).

The densification and porosity reduction of squeeze cast AMS605-series alloys should be attributed to the fact that the applied pressure capable of deforming the solidifying metal suppresses gas nucleation and also enables the melt to feed the

microshrinkage forming in the last solidifying region of casting. As a result, the alloy

becomes highly densified with considerably small amount of porosity.

4.2.3.1 Density vs Pressure level
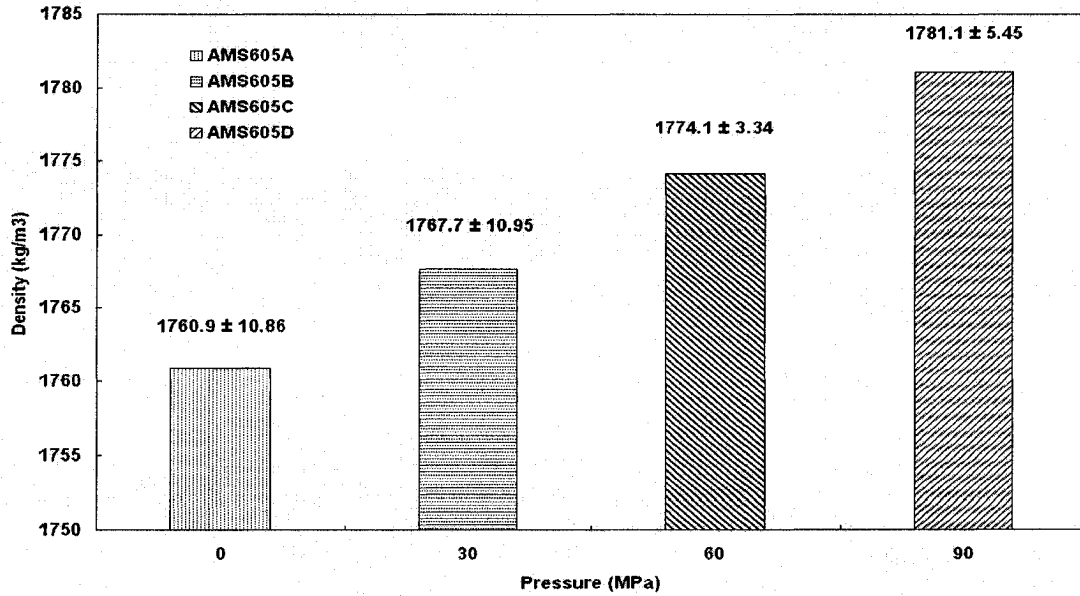
Figure 4.6 Effect of applied pressure levels on density of alloy AMS605.

4.2.3.2 Porosity vs Pressure level
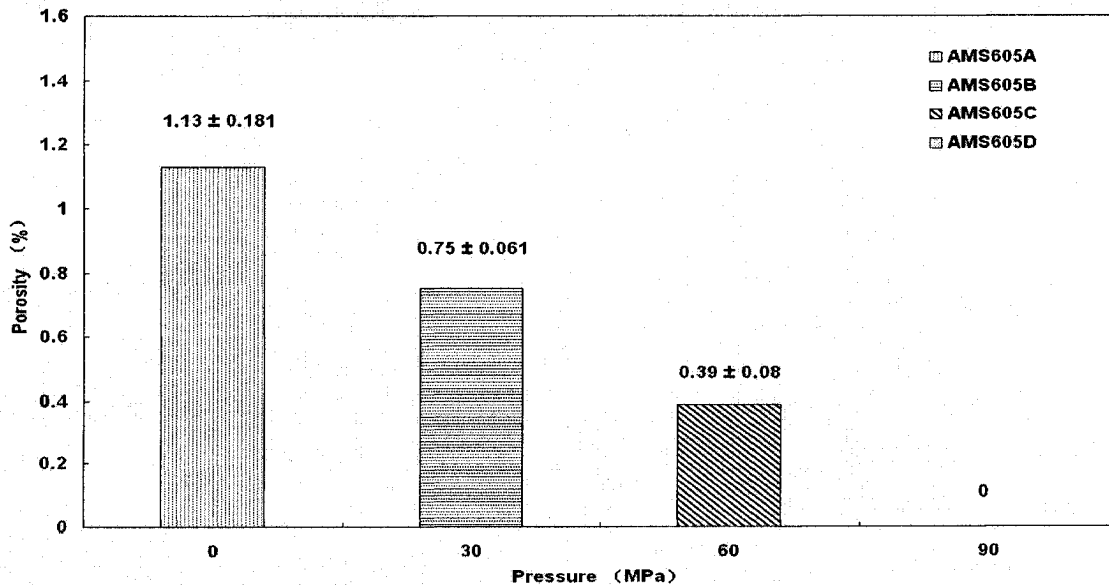
Figure 4.7 Effect of applied pressure levels on porosity of alloy AMS605.

57

4.2.3.3 Porosity observation
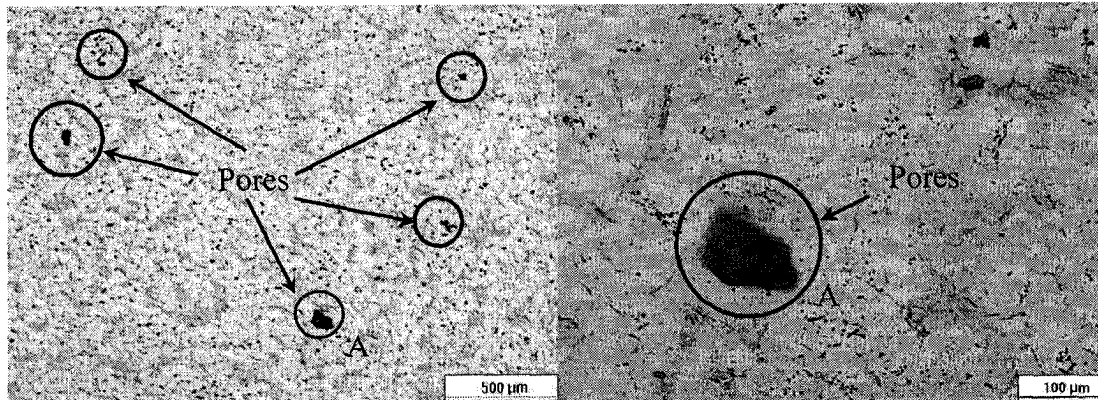
a) low magnifications   b) high magnifications

Figure 4.8 Optical micrograph showing porosity in AMS615A alloy cast under 0 MPa.

Label A shows the porosity in the same position in different magnification.
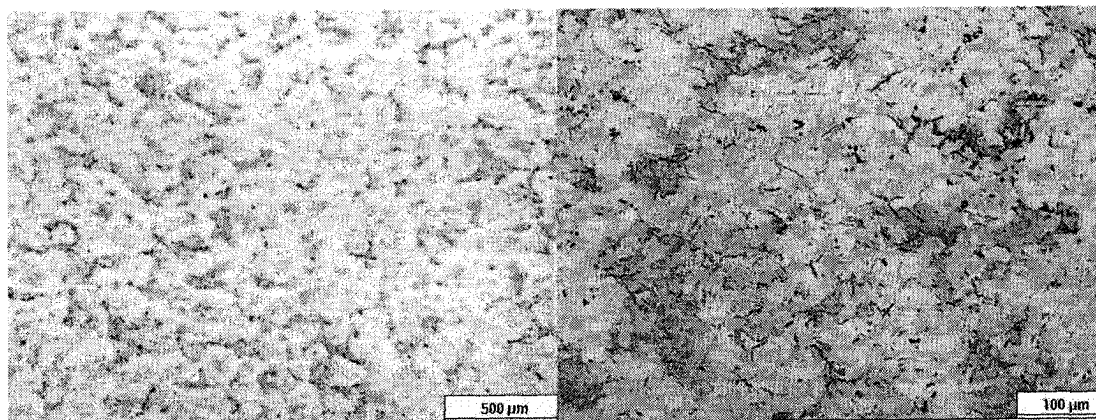
a) low magnifications   b) high magnifications

Figure 4.9 Optical micrograph showing porosity-free microstructure of AMS615C cast

under an applied pressure of 60 MPa.

58

Figure 4.10 Optical micrograph showing porosity in AMS605A alloy.
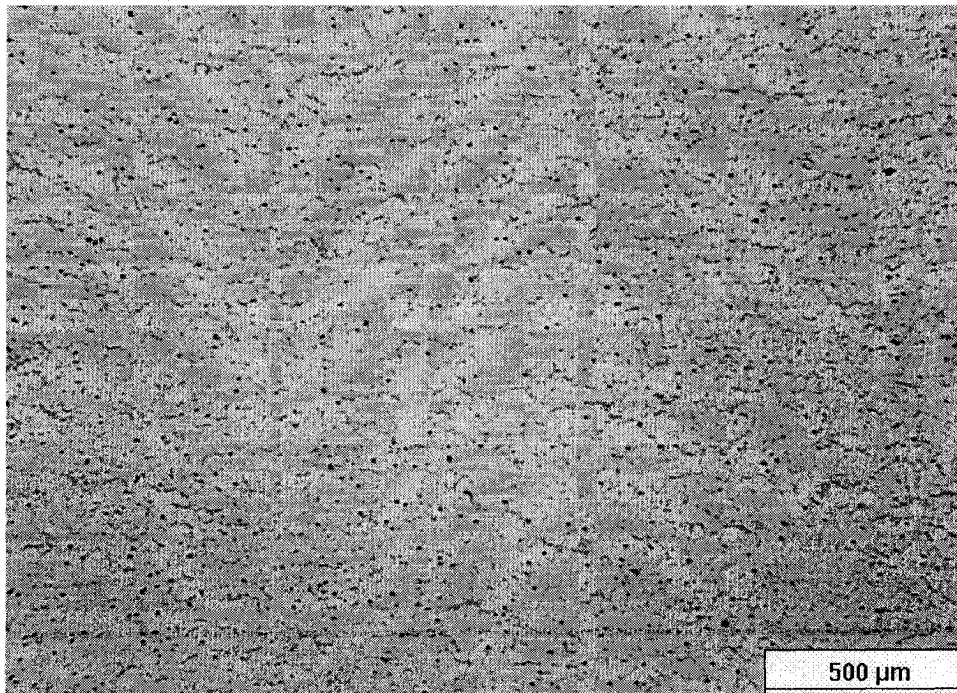
Figure 4.11 Optical micrograph showing porosity-free microstructure of AMS605D alloy.

59
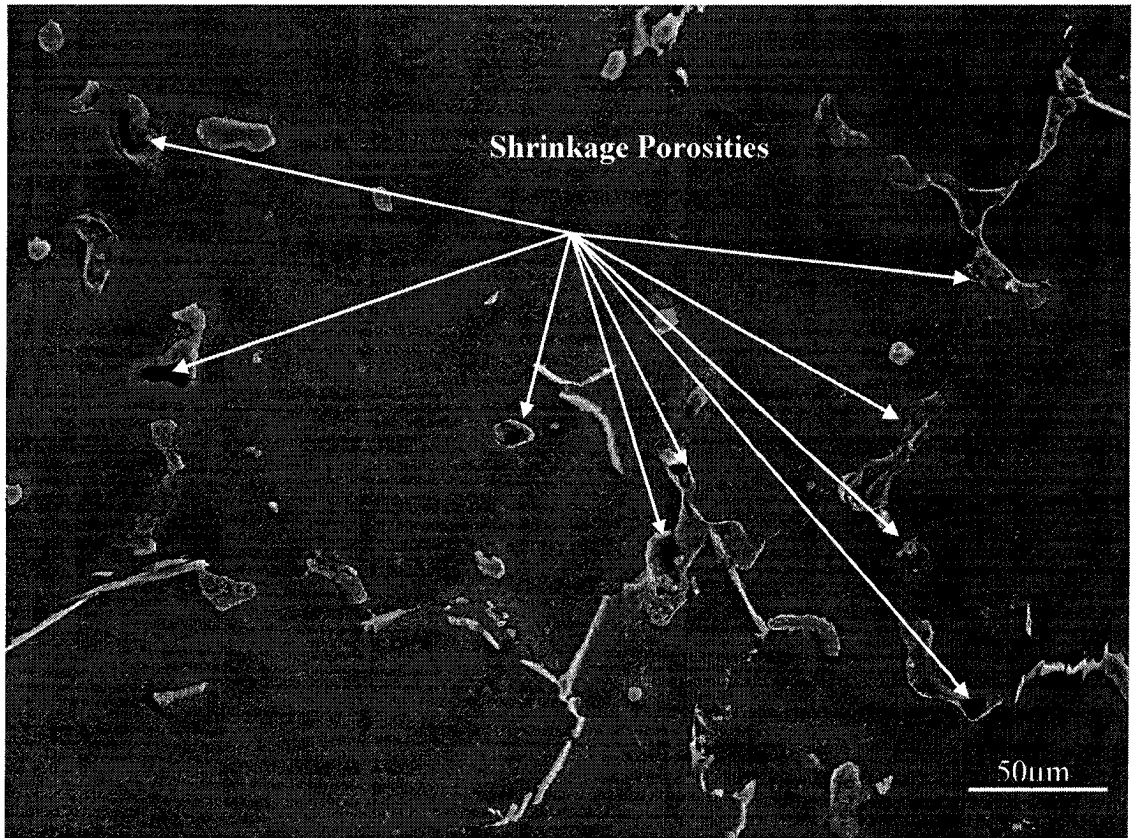
Figure 4.12 Shrinkage porosities in AMS605A.

60
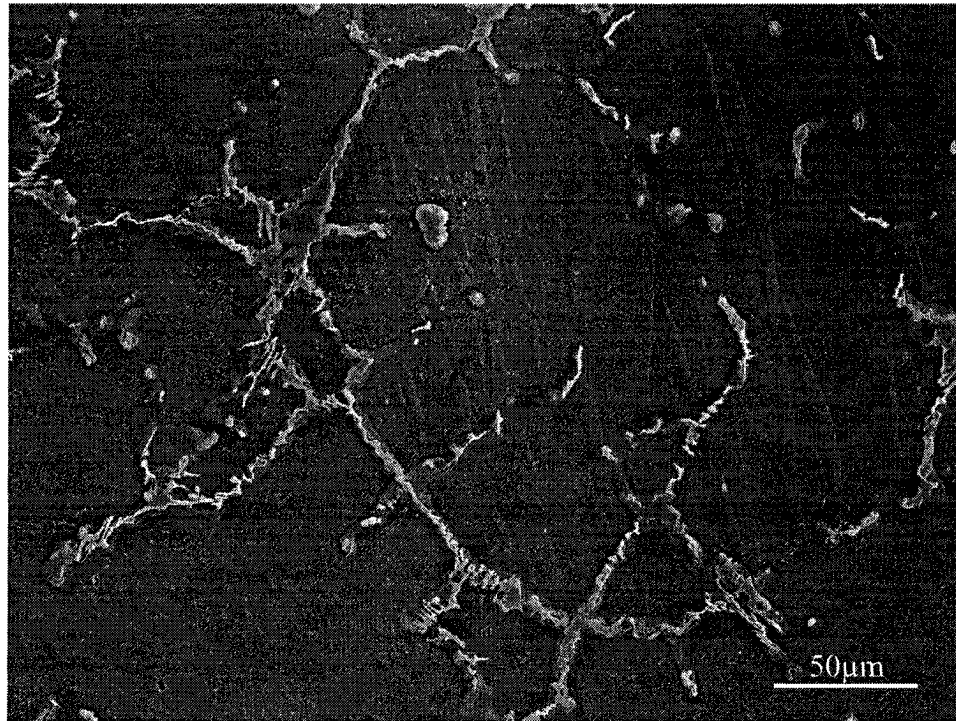
Figure 4.13 No shrinkage porosities in AMS605B.
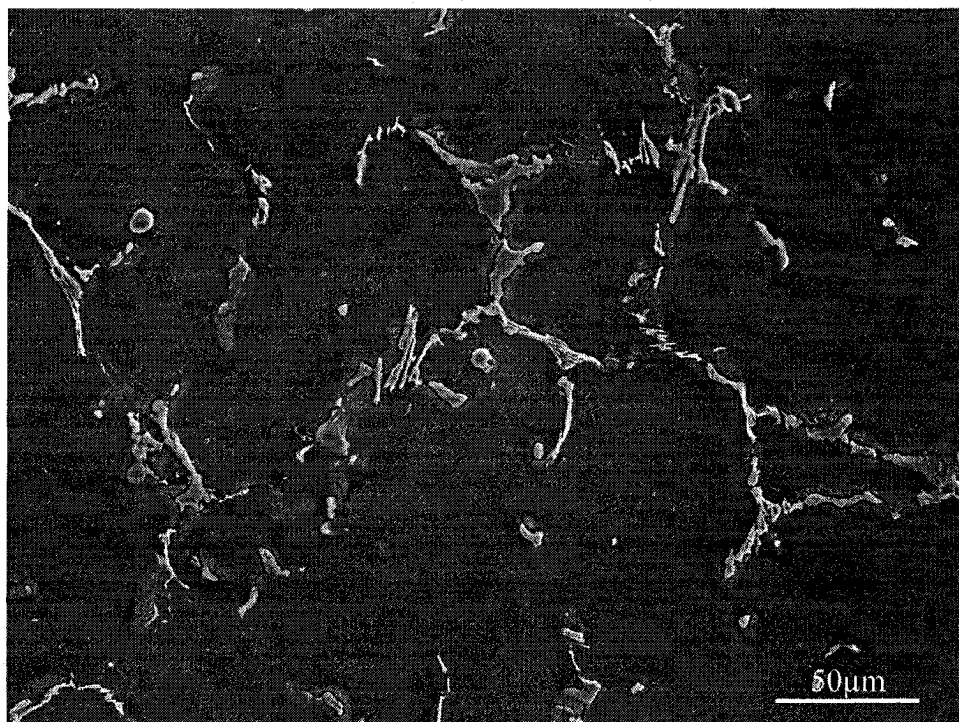
Figure 4.14 No shrinkage porosities in AMS605C.

61

4.2.4 Microstructure analysis

4.2.4.1 Variation of grain size with applied pressure levels

Figure 4.15 show the measured grain size varying in AMS605 alloys with applied pressure levels. There is an obvious decrease in grain size to 33.9 µm from 92.4 µm when the pressure increases from 0 to 90 MPa. This experimental observation indicates that an increase in applied pressure leads to a significant reduction in the grain size of the alloy (Figures 4.16-4.19).
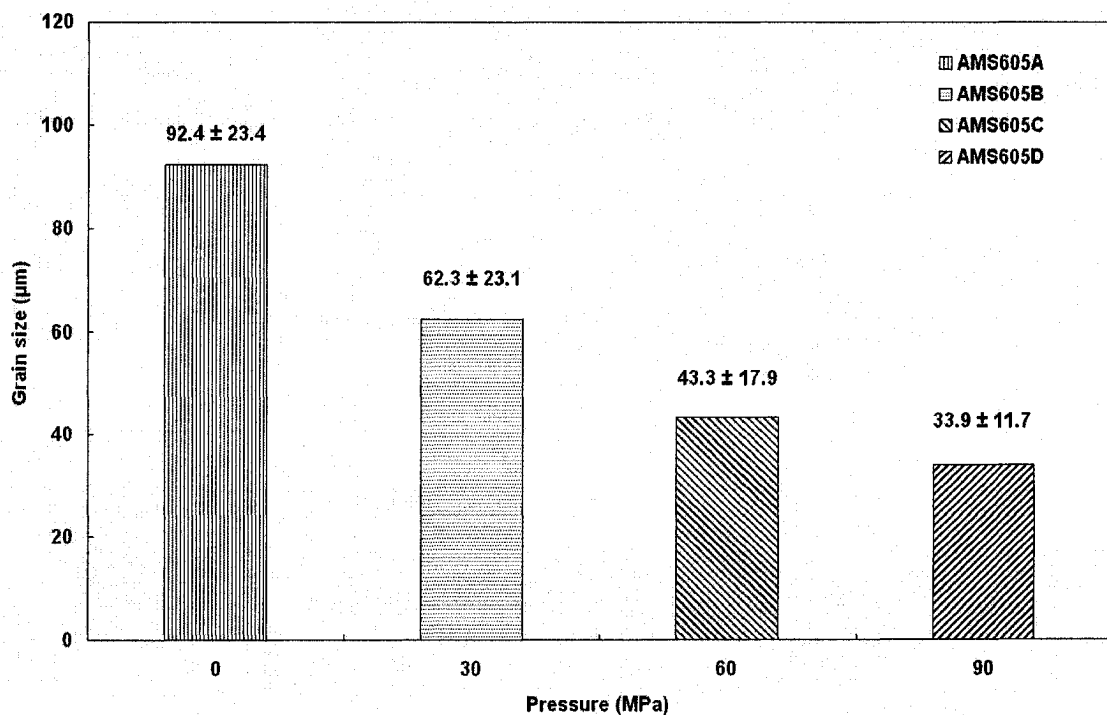
Figure 4.15 Effect of applied pressure levels on grain size of AMS605 alloy.

4.2.4.2 Phase morphology

Figures 4.16 to 4.19 show the optical microstructures of the AMS605 alloys squeeze cast under pressures of 0, 30, 60, and 90 MPa in the as-cast condition, respectively. It can be seen that the secondary phase (intermetallic Mg-Al-Sr phase) are precipitated around grain boundaries, There is also a third phase that is an intermetallic of Al-Mn phase which has a round or triangle shape.

By comparing the optical microstructural characteristics, it is obvious that there were loose, discontinuous secondary phases at grain boundaries surrounding relatively large grains in AMS605A. As the applied pressure increases from 30 to 90 MPa, the grain structure of the alloy tends to become a fine, continuous, closed network, which should be effective in inhibiting grain boundary migration and sliding during deformation.
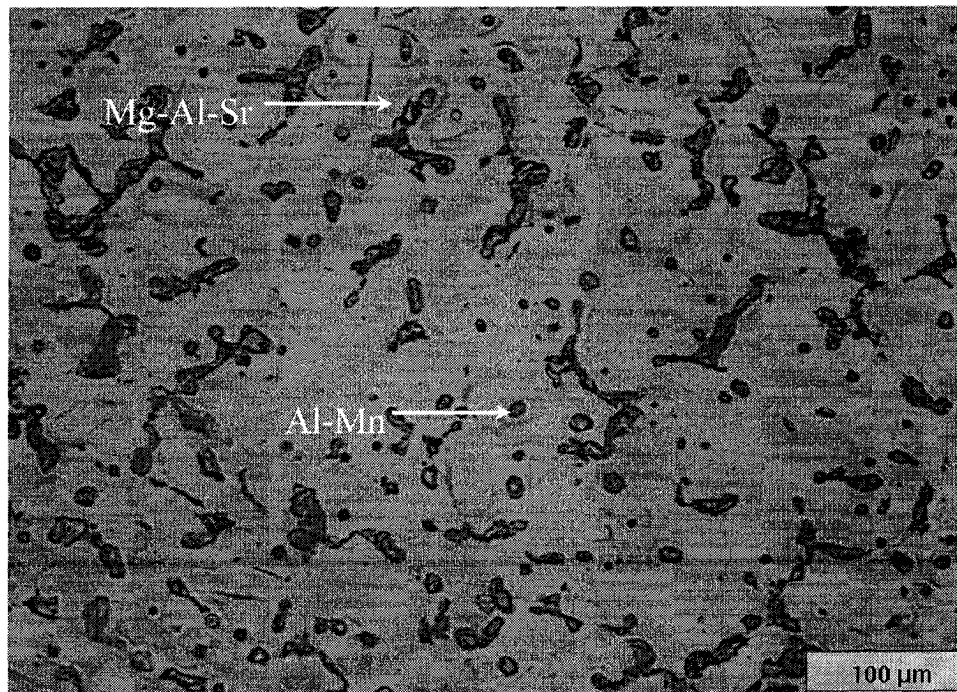
Figure 4.16 Optical micrograph showing microstructure of AMS605A alloy.

63
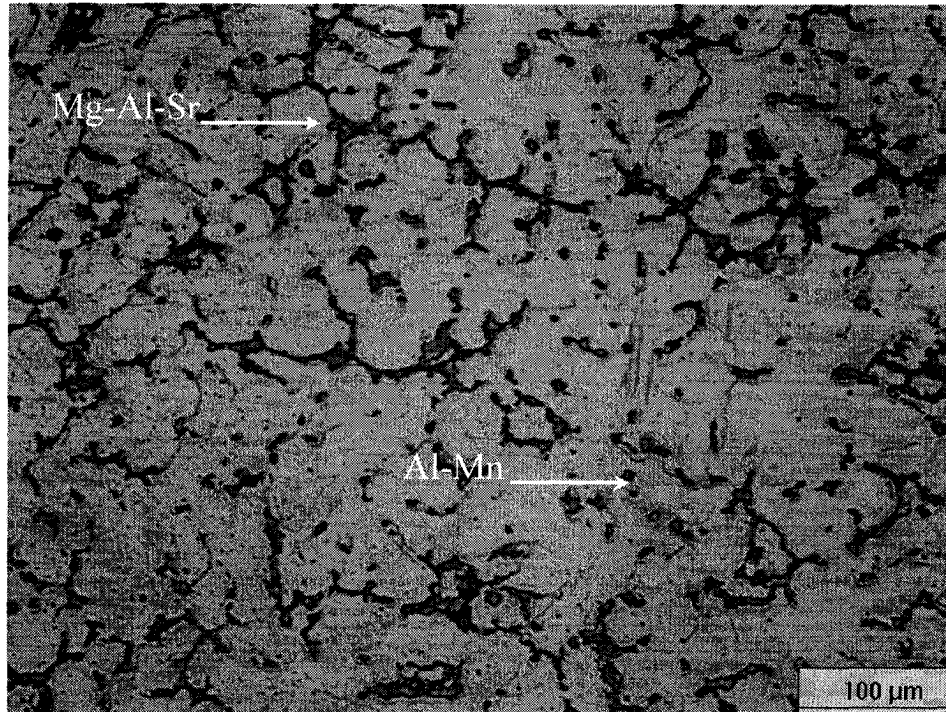
Figure 4.17 Optical micrograph showing microstructure of AMS605B alloy.
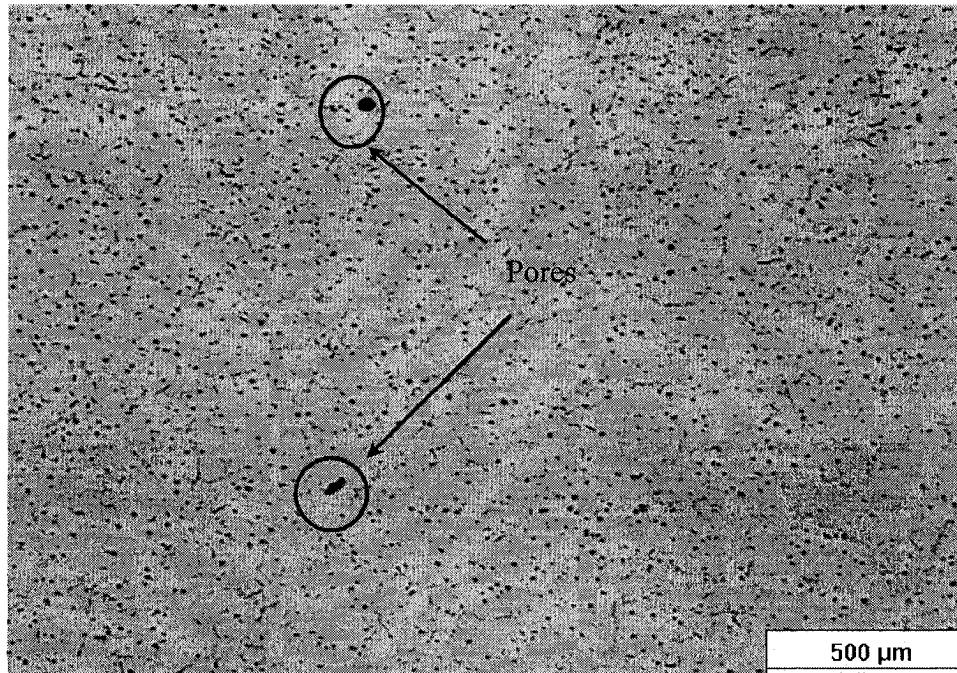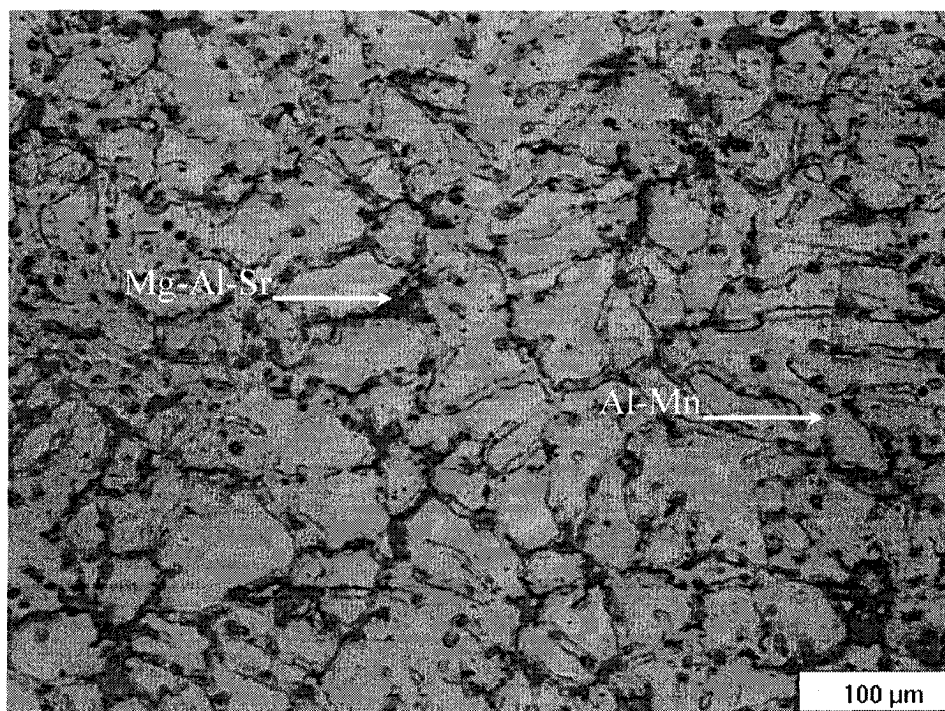

Figure 4.18 Optical micrograph showing microstructure of AMS605C alloy.

64
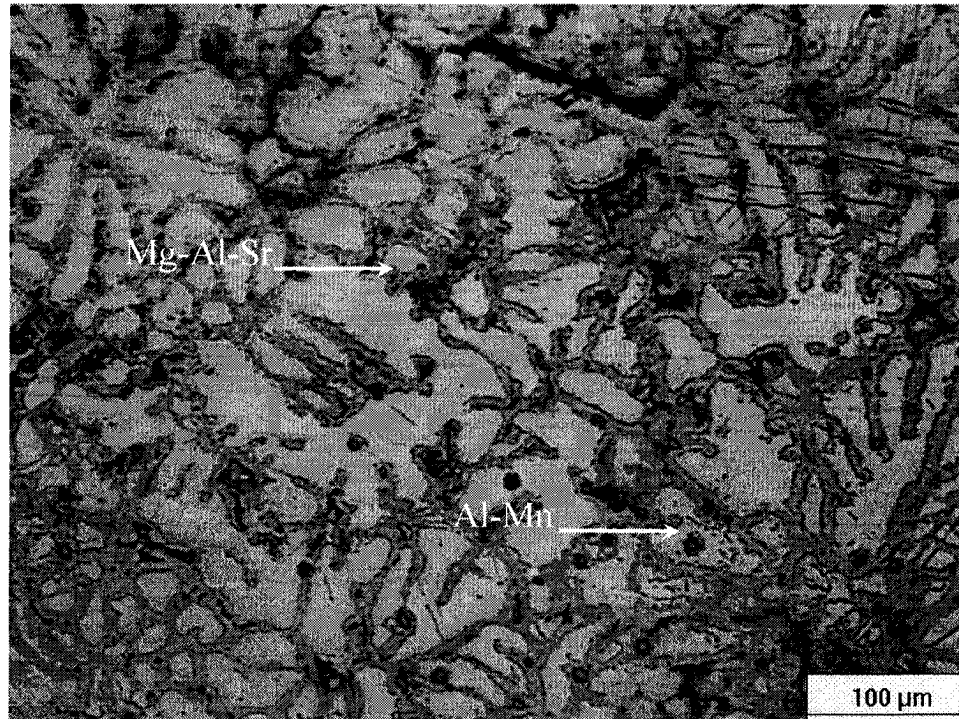
Figure 4.19 Optical micrograph showing microstructure of AMS605D alloy.

4.2.4.3 SEM/EDS analysis

SEM and EDS were utilized for the elemental analysis of microstructural features

observed in AMS605 alloy. Figures 4.20 – 4.24 present the results of SEM and EDS

analysis for AMS605B. Figure 4.20 shows the SEM microstructure of squeeze cast

AMS605B. It can be seen that the Mg-Al-Sr eutectic phase (bright contrast) precipitates

around grain boundaries. To facilitate the presentation of EDS spectra, the visible

primary and secondary phases in the microstructure of the alloy were identified with "A",

"B", "C" and "D". Figures 4.21 – 4.24 show the EDS spectra for point A (Figure 4.19),

which is the Mg-Al-Sr eutectic phase; point B (Figure 4.20), which is the primary α-Mg

matrix; point C (Figure 4.21), which is the secondary $Mg_{17}Al_{12}$ eutectic phase, and point

65

D (Figure 4.22), which is the Al-Mn intermetallic phase. Oxygen peak which appeared on many spectra resulted from surface oxidation during and after sample preparation and had removed the element symbol. The detailed elemental data in both the atomic and weight percentages are listed in Tables 4.3-4.6. Examination of the spectra data reveals that, besides the presence of three common phases, (Primary α-Mg, $Mg_{17}Al_{12}$ eutectic, and Al-Mn intermetallic), the same as the ones in Mg-Al alloys [18], the relatively low amount (0.5 wt%) of Sr addition results in the formation of the new Mg-Al-Sr eutectic in the alloy. It appears that the secondary Mg-Al-Sr phase should be $(Mg_{10})Al4Sr$ based on the atomic percentage of each element involved in the phase in which Mg may be picked from the matrix.
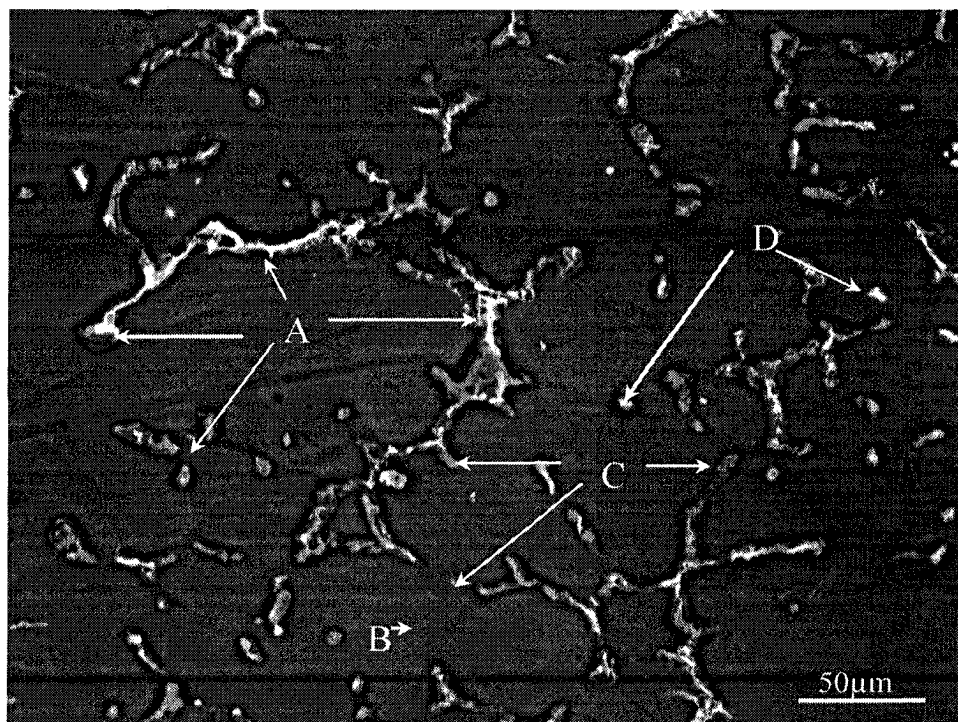
Figure 4.20 SEM micrographs showing microstructure of squeeze cast AMS605B.

66
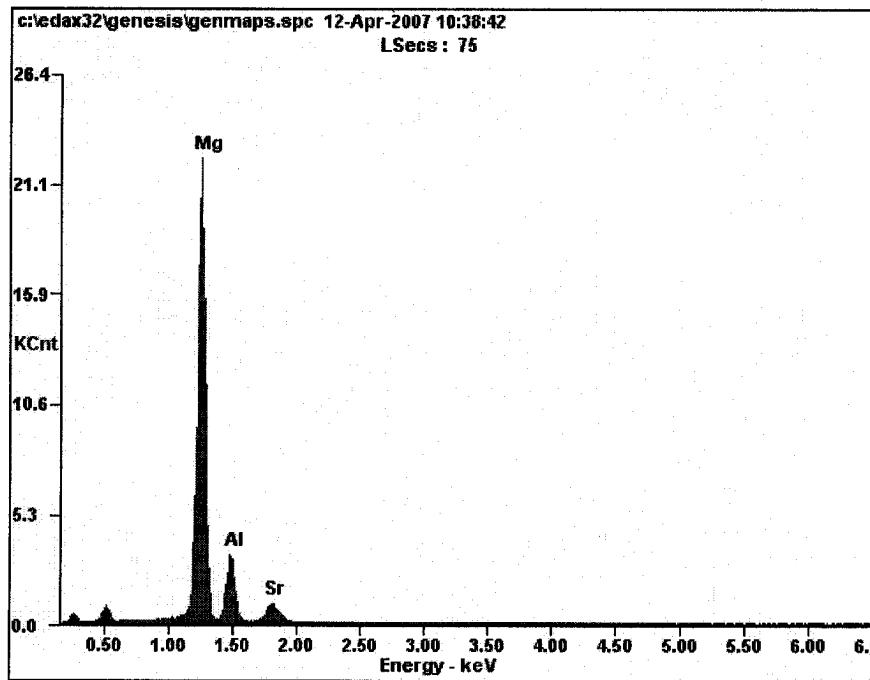
Figure 4.21 EDS spectrum from the region marked "A" in Figure 4.20, i.e., the eutectic

Mg-Al-Sr phase.

Table 4-3 Atomic and weight percent of element at point "A" (Mg-Al-Sr eutectic)

Element	Mg	Al	Sr
At%	71.73	23.27	5.000
	65.68	28.02	6.310
	71.39	24.27	4.340
Wt%	62.06	22.34	15.60
	54.96	26.02	19.02
	62.64	23.64	13.72

67

c:\edax32\genesis\genmaps.spc 12-Apr-2007 10:51:11
LSecs : 32
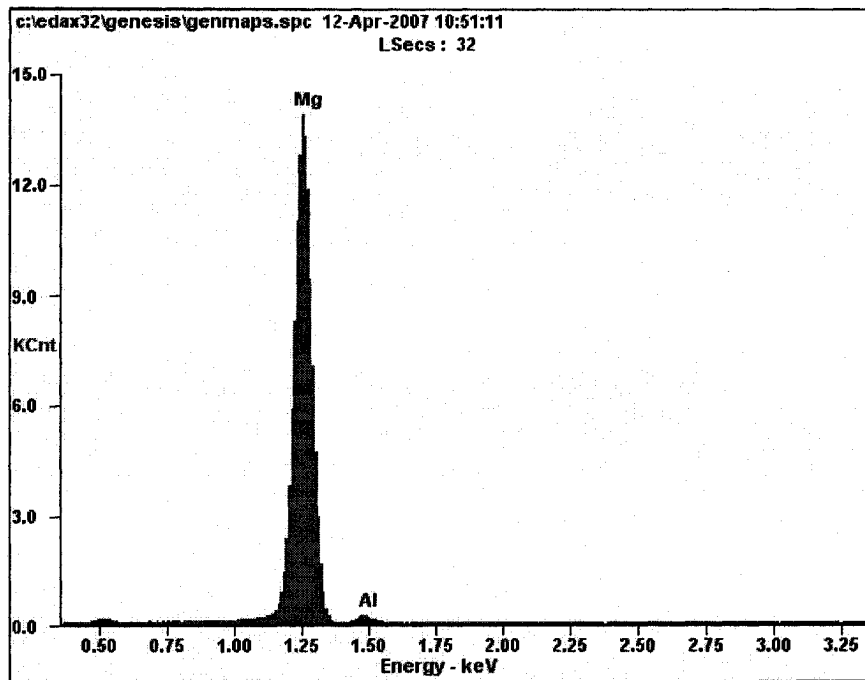
Figure 4.22 EDS spectrum from the region marked "B" in Figure 4.20, i.e. primary α-Mg.

Table 4-4 Atomic and weight percent of element at point "B" (α-Mg)

Element	Mg	Al
At%	96.53	3.47
	95.57	4.43
	97.53	2.47
Wt%	96.17	3.83
	95.10	4.90
	97.27	2.73

68

c:\edax32\genesis\genmaps.spc 12-Apr-2007 10:45:20
LSecs : 37
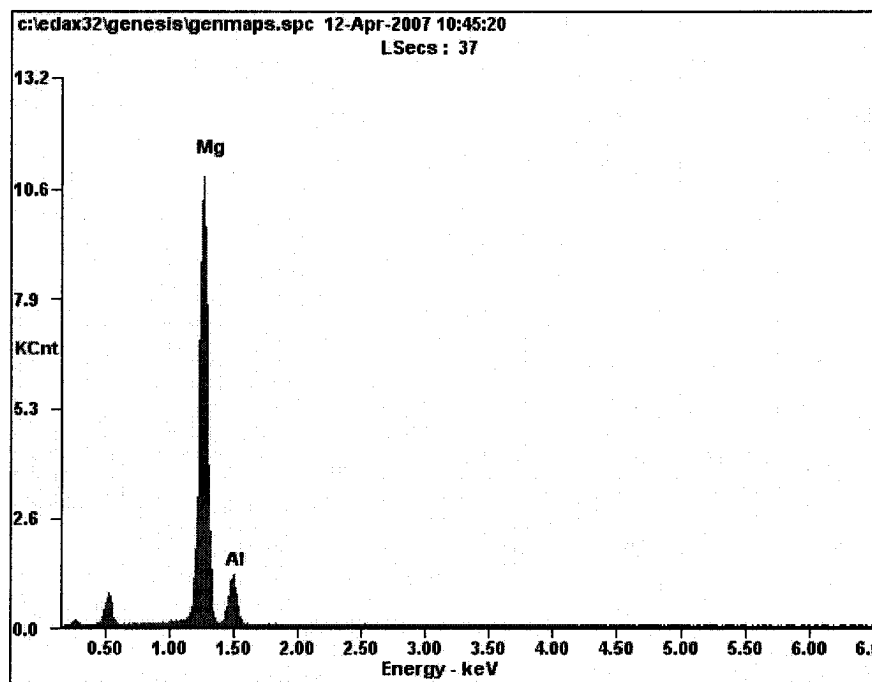
Figure 4.23 EDS spectrum from the region marked "C" in Figure 4.20, i.e., the eutectic

phase $Mg_{17}Al_{12}$.

Table 4-5 Atomic and weight percent of element at point "C" (eutectic phase $Mg_{17}Al_{12}$)

Element	Mg	Al
At%	79.21	20.97
	82.97	17.03
	77.09	22.91
Wt%	77.44	22.56
	81.45	18.55
	75.20	24.80

69
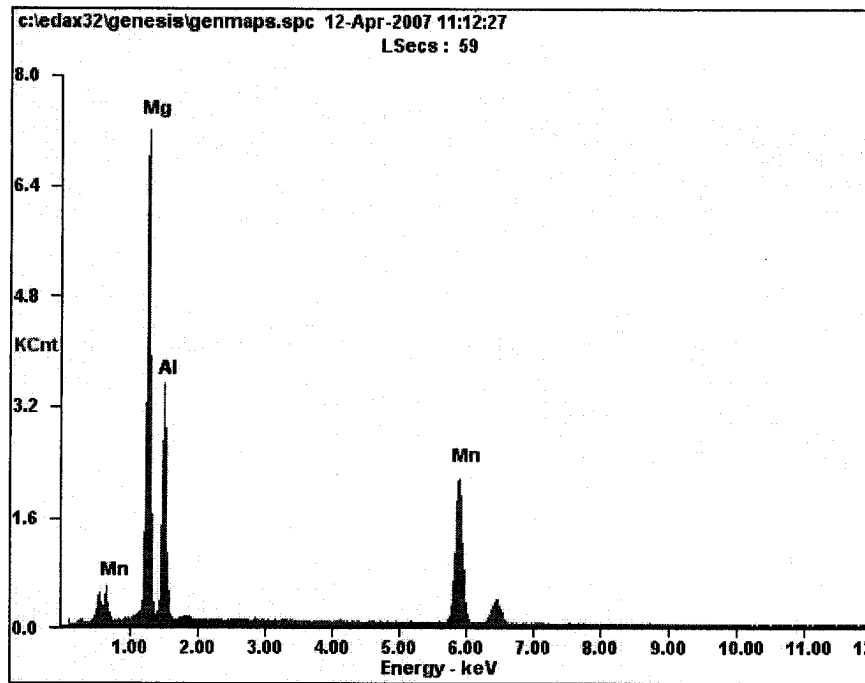
Figure 4.24 EDS spectrum from the region marked "D" in Figure 4.20, i.e., Al-Mn

intermetallics.

Table 4-6 Atomic and weight percent of element at point "D" (Al-Mn intermetallics)

Element	Al	Mn
At%	29.84	21.05
	24.99	14.46
Wt%	25.51	36.65
	27.56	32.49

70

4.2.5 Tensile Behaviour

4.2.5.1 Effect of applied pressure levels on tensile properties

Figure 4.25 shows representative engineering stress and strain curves for squeeze cast AMS605 alloys at room temperature. The curves show that under tensile loading, the alloy deformed elastically first. Then, once the yield point reached, plastic deformation of the alloy set in. It is obvious that the ultimate tensile strength (UTS), yield strength (YS) and elongation of the sample cast under 0 MPa are much lower than those cast under applied pressure. The effect of applied pressure on tensile properties of squeeze cast AMS605 alloy is shown in Table 4.7 and Figure 4.26. It can be seen from the results that an increase in pressure levels brings a significant improvement in UTS and E_f, and some improvement in yield strength (YS). The E_f, UTS and YS of the AMS605D squeeze cast under an applied pressure of 90MPa are 6.07%, 181.83MPa and 87.55 MPa respectively, which results in increases of 270% in enlongation, 153% in UTS and 82% in YS over AMS605A cast under 0 MPa.

The aforementioned tensile behaviour of the alloys might be interpreted as follows. It is evident that an applied pressure leads to a significant change in the microstructure of the squeeze cast Mg-Al-Sr alloys. When the pressure increased from 0 MPa to 90 MPa, the grain size decreased from 92.4 μm to 33.9 μm. The finer microstructure provides a greater total grain boundary area to impede slip and dislocation motion, which improves the yield strength of the squeeze cast Mg-Al-Sr alloys. Meanwhile, the applied pressure reduces the porosity content and densifies the alloys. Porosity is deleterious to the UTS and elongation for two reasons: (1) Pores reduce the cross-sectional area across which a tensile load is applied, and (2) They act as stress

71

concentrators for crack initiation. As a result, the reduction in porosity enhances considerably both the UTS and elongation. Furthermore, the fine, continuous network of the eutectics, $Mg_{17}Al_{12}$ and Mg-Al-Sr phases, resulting from the applied pressure, also restricts dislocation motion in which the same way as grain boundaries, which accounts for high UTS and YS of the alloys [18].
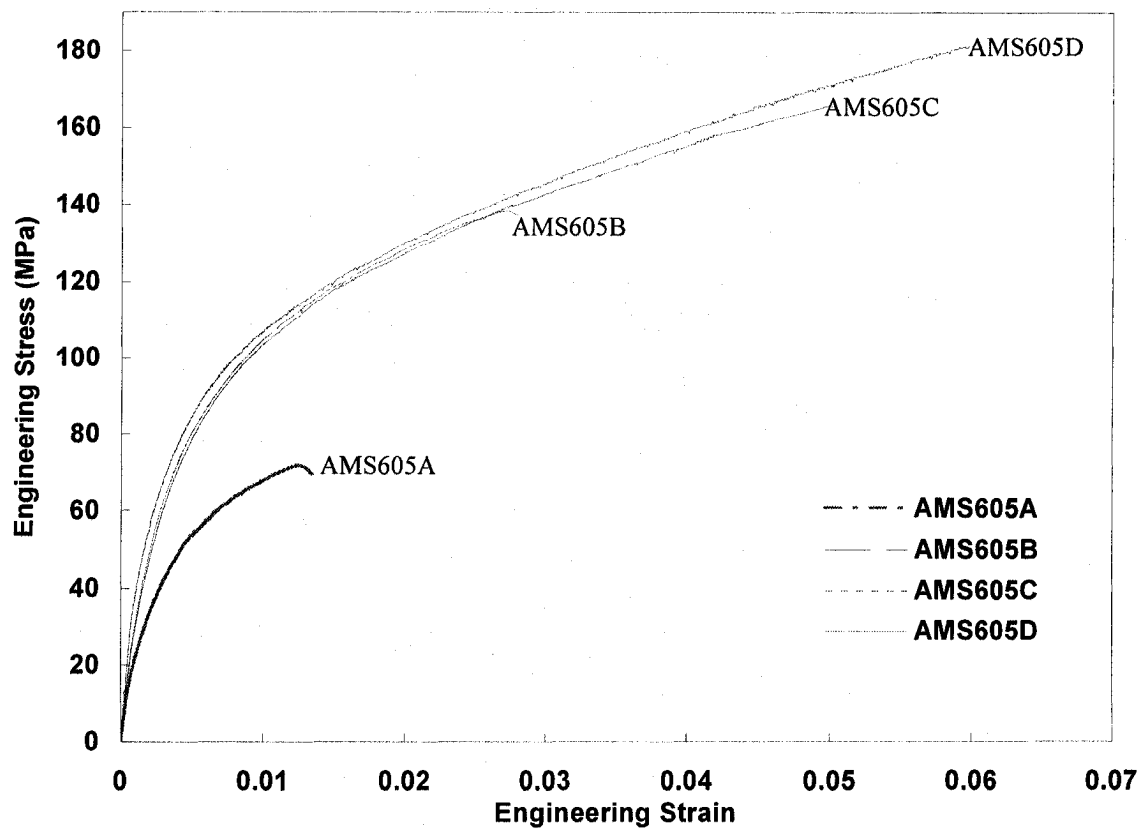
Figure 4.25 Engineering stress-strain curves of AMS605 alloy.

72

Table 4-7 Effect of pressure levels on UTS, YS and Elongation of AMS605

Pressure (MPa)	Alloy Symbol	UTS (MPa)	YS (MPa)	Elongation (%)
0	AMS605A	71.74 ± 3.80	48.03 ± 2.97	1.64 ± 0.29
30	AMS605B	138.22 ± 7.35	80.36 ± 3.78	2.85 ± 0.16
60	AMS605C	165.68 ± 8.31	82.33 ± 4.09	5.02 ± 0.09
90	AMS605D	181.83 ± 9.28	87.55 ± 2.78	6.07 ± 0.018
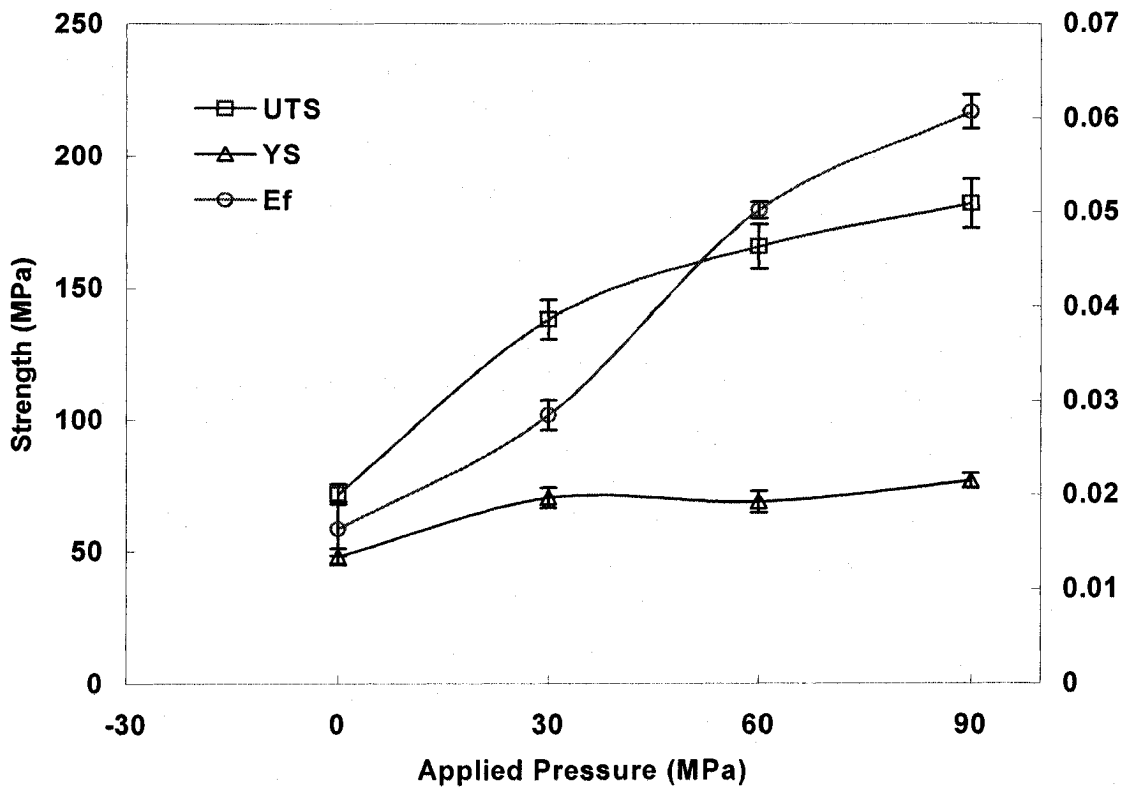
Figure 4.26 Effect of pressure levels on UTS, YS and Elongation of AMS605 Alloy.

73

4.2.5.2 Strain-hardening

Figure 4.27 gives true stress vs strain curves for AMS605 alloys. To elucidate the strain-hardening behavior of the AMS 605 alloy, a plot of strain-hardening rate ($d\delta/d\varepsilon$) versus true plastic strain (ε), is illustrated in Figure 4.28, which is derived from true stress-strain curves. It can be seen from Figure 4.26 that as the applied pressure rises, the strain-hardening rate of AMS605 alloy increases. It suggests that AMS605 alloys cast under high pressure levels are able spontaneously to strengthen themselves increasingly to certain extent, in response to large plastic deformation prior to fracture. The high strain hardening rates of the alloy cast under higher applied pressure may be attributed to the high dislocation densities exist in samples that squeeze cast under high-applied pressure [17].
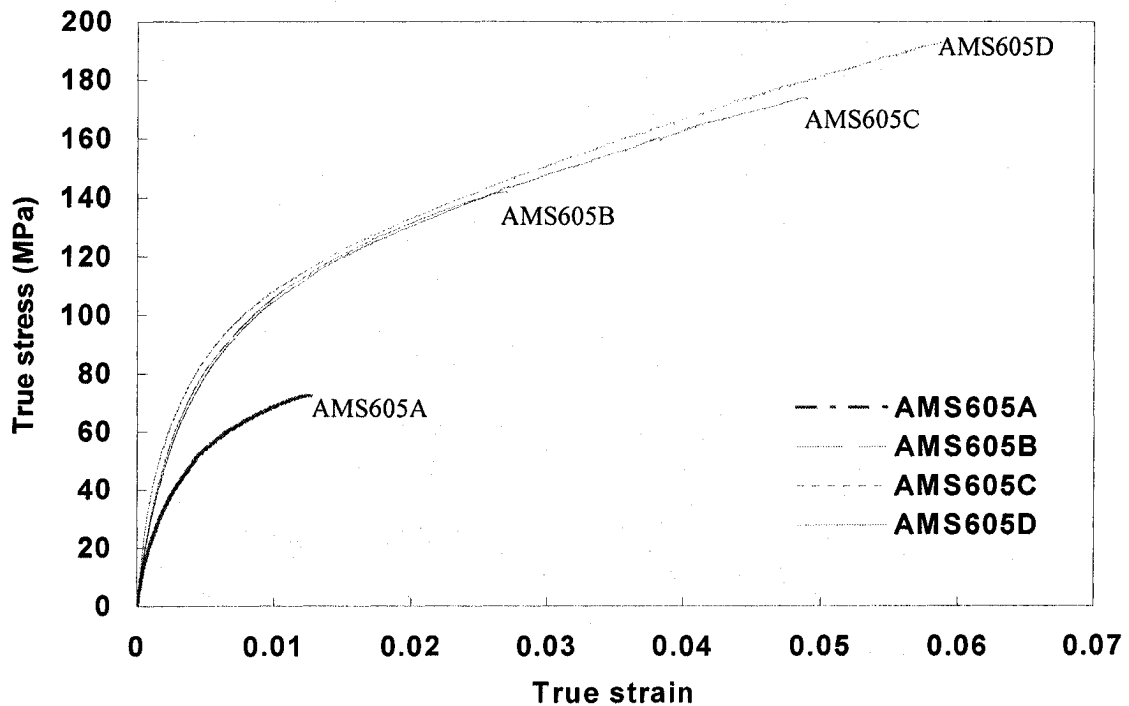
Figure 4.27 True stress-strain curves of AMS605 alloy.

74
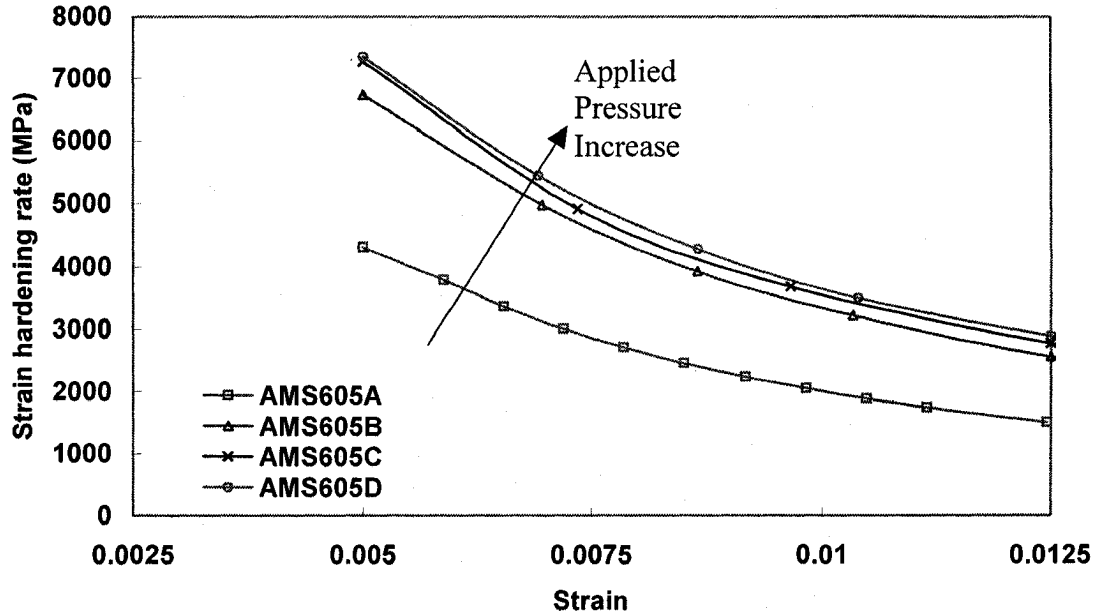
Figure 4.28 Strain hardening rate versus strain of AMS605 alloy.

4.2.6 Fracture behaviour

The tensile fractured surfaces of the squeeze cast AMS605A and AMS605C are shown in Figures 4.29 ~ 4.32 respectively. The observed fracture mode of the samples under 0 and 60 MPa is dimple rupture. In this mechanism the alloy fail by microvoid coalescence when fractured under a continual rising load. The microviods nucleate in the material at areas of localized high plastic deformation such as that associated with second phase particles, inclusions and grain boundaries. As the load on the material increases, microviods grow, coalesce, and eventually form a continuous fracture surface. A considerable amount of energy is consumed in the process of the formation of microvoids and finally leading to creation of cracks.

The analysis of SEM fractography shows the applied pressure levels influence the fracture behavior of the squeeze cast AMS605 alloys. As the pressure level increases, the

75

fracture of alloy tends to transit from brittle to ductile. The fracture surface of AMS605A (under 0 MPa pressure) shows the space (voids and microvoids) and brittle behavior (Figures 4.29 and 4.30). The fracture surface of AMS605C (under 60 MPa pressure) shows primarily ductile in nature, which is characterized by the presence of deep dimples with extensive deformation marks along the walls of individual craters (Figure 4.31, 4.32). The brittle behavior of AMS605A alloy can be attributed to high porosity (high amount of voids and microvoids) percentage. It seems that the failure of AMS605A alloy is caused by a combined brittle fracture mechanism coalescence and intergranular fracture.

4.2.6.1 SEM fractography
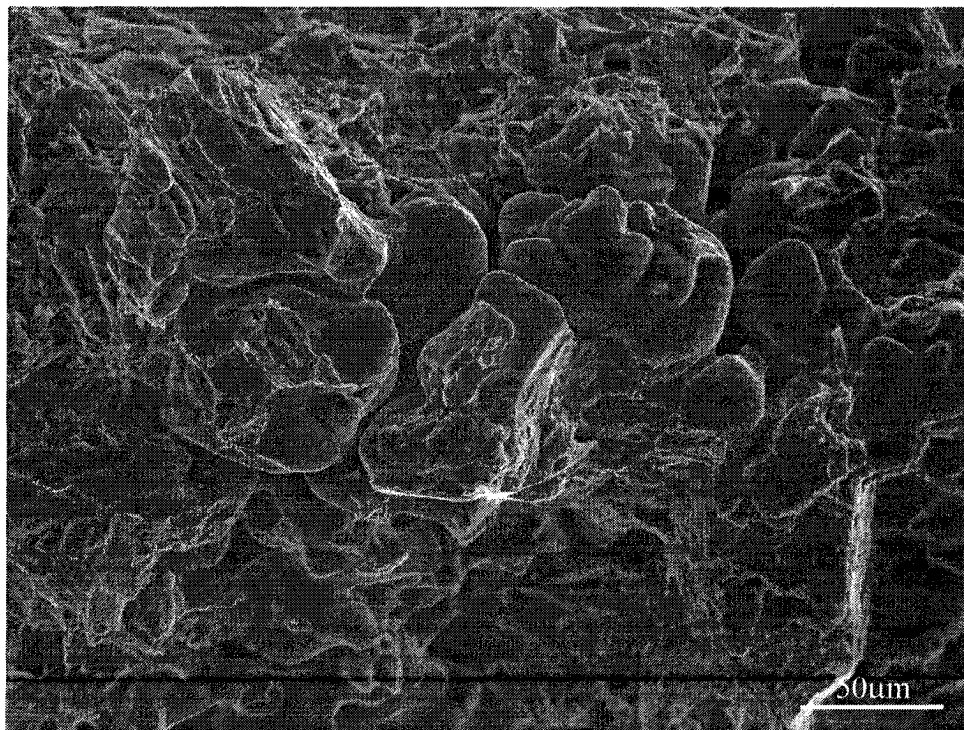
Figure 4.29 SEM fractographs of AMS605A (X500).

76
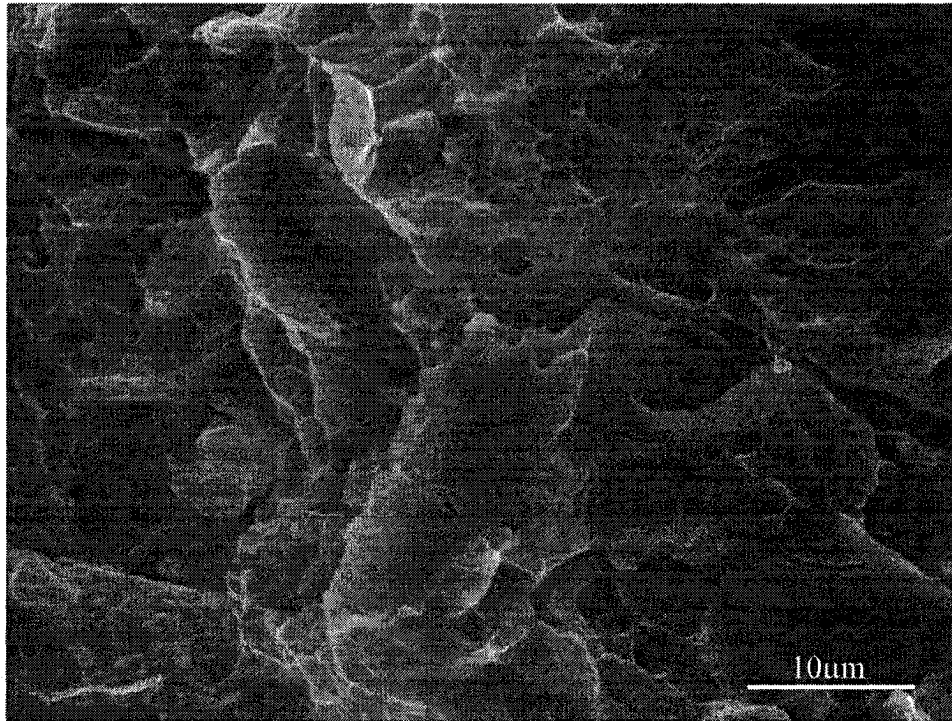
Figure 4.30 SEM fractographs of AMS605A (X3000).
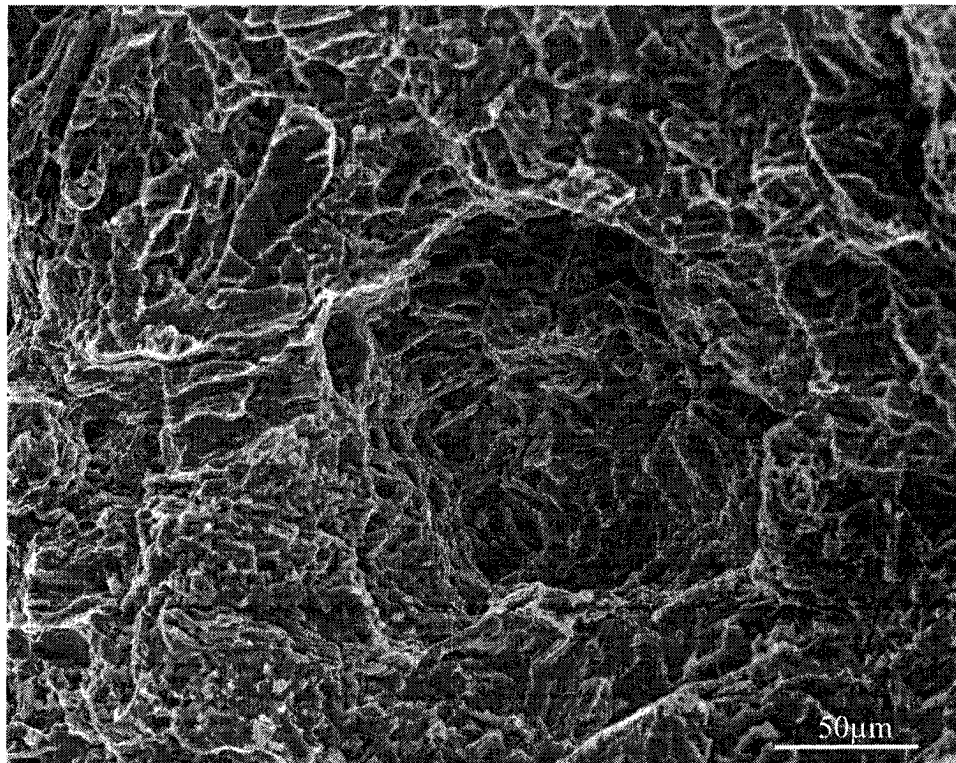
Figure 4.31 SEM fractographs of AMS605C (X500).
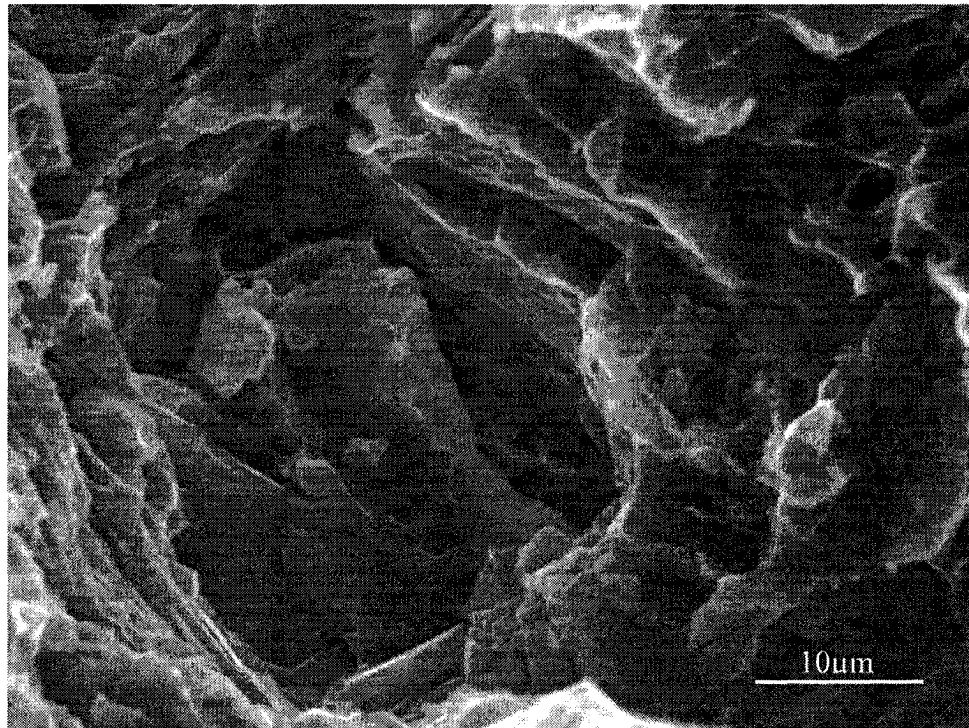
Figure 4.32 SEM fractographs of AMS605C (X3000).

78

4.2.6.2 Optical analysis of crack origins

The initiation point of cracks possibly began with the internal discontinuity due to the presence of porosity. The porosity presence cause stress concentration and cracks can form at points of stress concentration, and spread rapidly over the section. The final fracture results from the growth and coalescence of the cracks. For alloy AMS605C, the segreation brittle eutectics β-$Mg_{17}Al_{12}$ and Mg-Al-Sr along the grain boundaries is the likely main cause of the intergranular fracture. The damaged microstructure underneath the fractured surfaces presented in Figure 4.33 and 34, at least in part, supports this interpretation [17, 18].
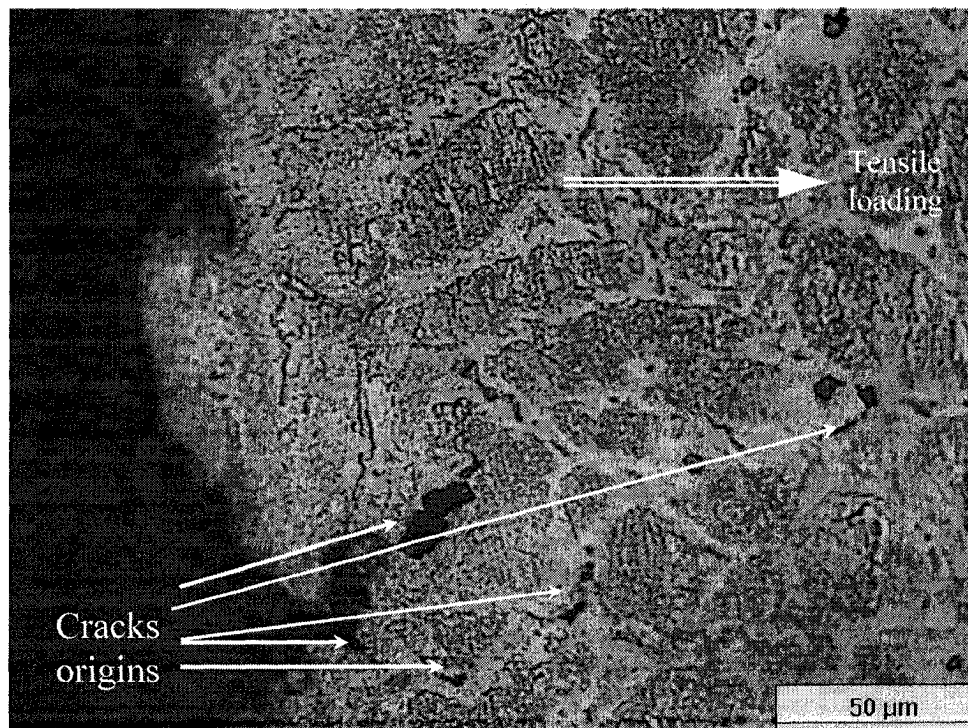
Figure 4.33 Optical micrograph showing crack origin in AMS605A.
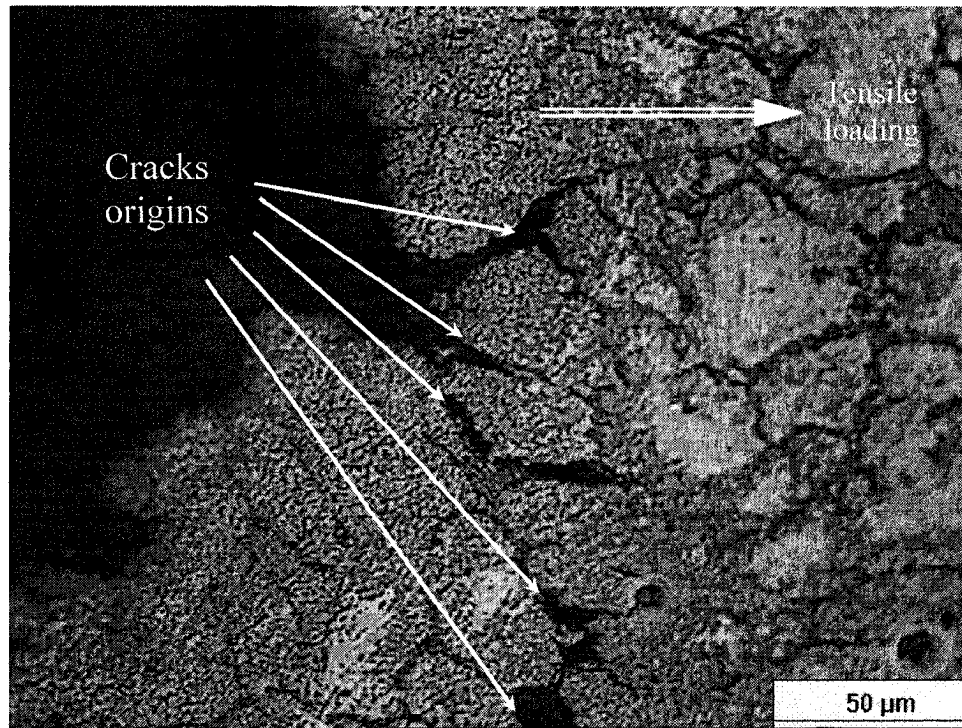
Figure 4.34 Optical micrograph showing crack origin in AMS605C.

4.3 Effect of Strontium Contents on Tensile Properties and

Microstructure of Squeeze Cast Mg-Al-Sr Alloys

To investigate the effect of strontium content on microstructure and mechanical properties of the squeeze cast Mg-Al-Sr alloys, the AM60B alloy with different percentages of strontium addition, 0, 0.5, 1.5, 2.0, 3.0 wt.% were squeeze cast under two applied pressure levels of 30 and 90 MPa. The AMS-B series alloys (AMS600B, AMS605B, AMS615B, AMS620B and AMS630B) for a low pressure level of 30 MPa were tested and analyzed. Also under a high pressure of 90 MPa, the AMS-D series alloys (AMS600D, AMS605D, AMS615D, AMS620D and AMS630D) were considered with a brief discussion of the experimental results.

80

4.3.1 Effect of Strontium on Surface cracking of Mg-Al-Sr alloys

As discussed in the previous section (4.2.2), surface crecking as shown in Figure 4.1 took place in the surface of AMS630A when no applied pressure was exerted. However, no cracks appeared on the surfaces of AMS600A (Figure 4.35), AMS605A (Figure 4.36), AMS615A (Figure 4.37), and AMS620A (Figure 4.38). The observation indicates that, with the low content (< 3 wt.%) of Sr addition, no surface cracks were present in the Mg-Al-Sr alloys even in case that no external pressure was applied. However, once strontium increased to 3 wt.%, surface cracking occurred in the alloys solidified just under atmospheric pressure.
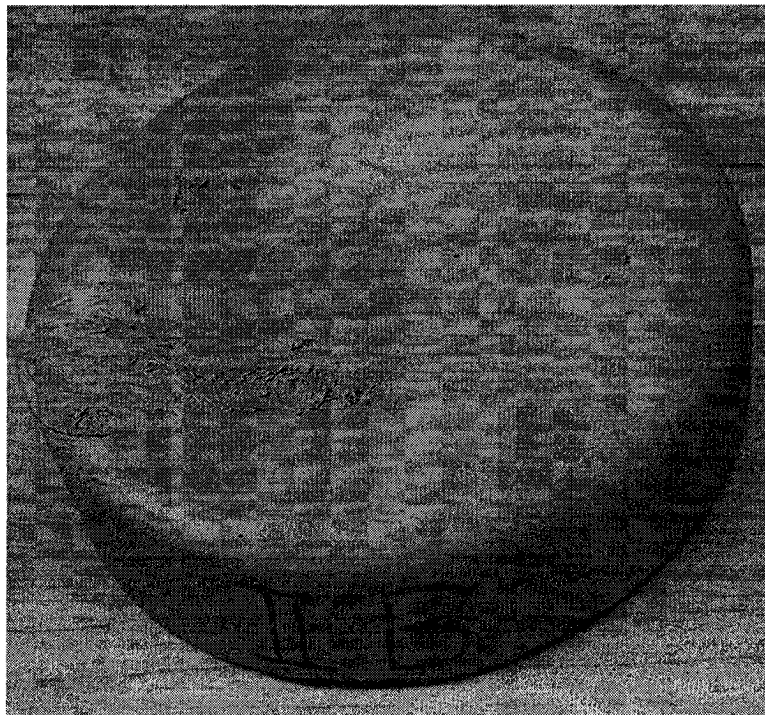
Figure 4.35 Alloy AMS600A, no crack formation in the sample solidified under zero
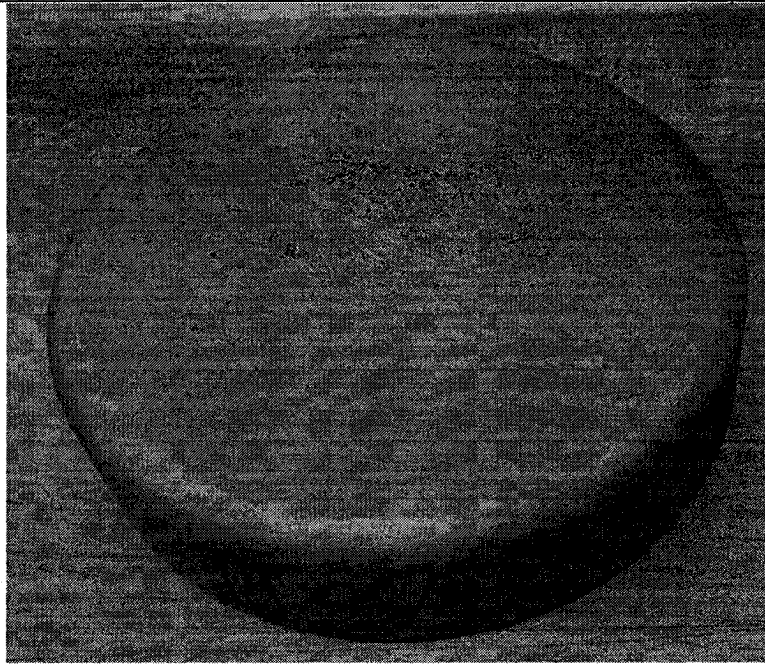
applied pressure.

Figure 4.36 Alloy AMS605A, no crack formation in the sample solidified under zero
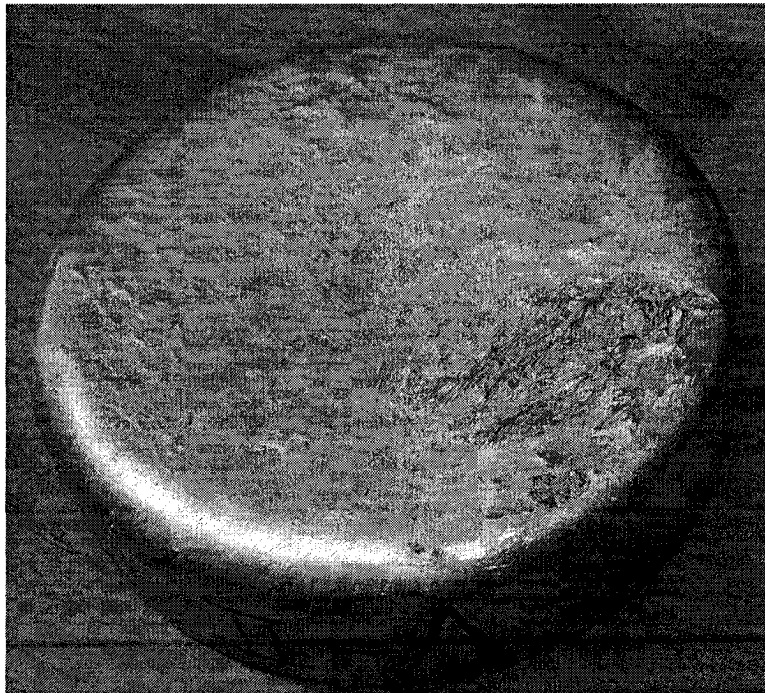
applied pressure.

Figure 4.37 Alloy AMS615A, no crack formation in the sample solidified under zero
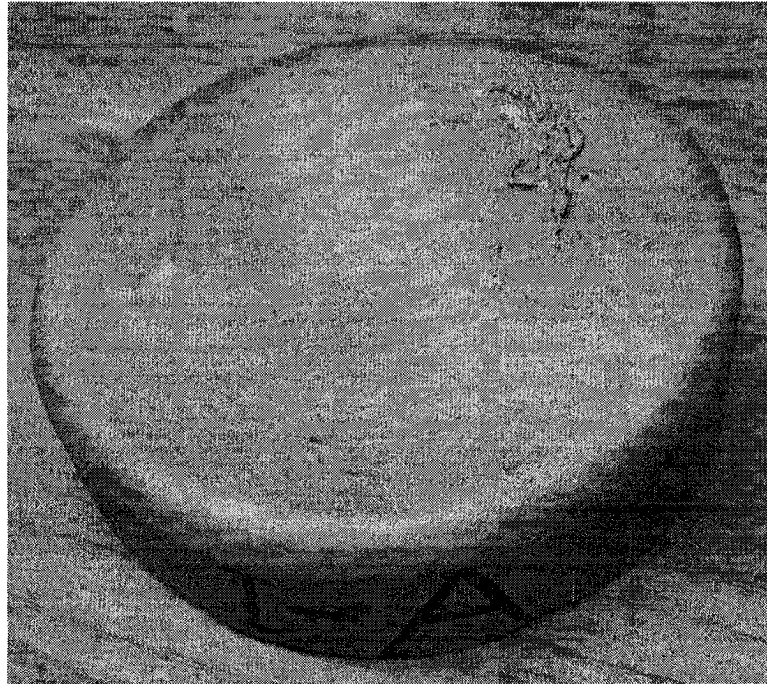
applied pressure.

Figure 4.38 Alloy AMS620A, no crack formation in the sample solidified under zero

applied pressure.

4.3.2 Strontium effect at low pressure level (30 MPa)

4.3.2.1 Density and porosity variation

Figures 4.39 and 4.40 present the density and porosity measurements of the series

of AMS-B alloys squeeze cast with different strontium contents of 0 wt% (AMS600B),

0.5 wt% (AMS605B), 1.5 wt% (AMS615B), 2.0 wt% (AMS620B), and 3.0 wt%

(AMS630B), under the applied pressure of 30 MPa. It is evident from Figures 4.39 and

4.40 that the densities of the squeeze cast AMS-B series alloys increases considerably

once the Sr content increases to and above 1.5 wt.%. But its porosity also increases with

an increase in the content of strontium addition.

83

Optical and SEM micrographs given in Figures 4.41 and 4.42 show almost no porosity present in alloy AMS600B. However, as the strontium content increases to 3 wt.%, the existence of tiny pores in alloy AMS630B solidified even under 30 MPa is revealed by SEM and optical microscopy as illustrated in Figures 4.43 and 4.44. The SEM observation on AMS-B alloys supports porosity measurements.

The increase in the densities of the squeeze cast AMS-B series alloys should be attributed to the fact that the strontium density (2630 kg/m^3) is higher than that of the based alloy AM60B (1800 kg/m^3). This indicates that the introduction of Sr addition offsets the light-weight advantage of magnesium alloys slightly. Meanwhile, it has been observed that, their porosities become high when Sr was added to aluminum-silicon alloys [8]. The previous study [7] on Sr-treated magnesium alloy shows that low amount of Sr addition reduces shrinkage porosity of AZ91D. These observations suggest that relatively high amount ($\geq$ 0.5 wt.%) of Sr addition may introduce extra porosity, which has an adverse effect on casting quality.
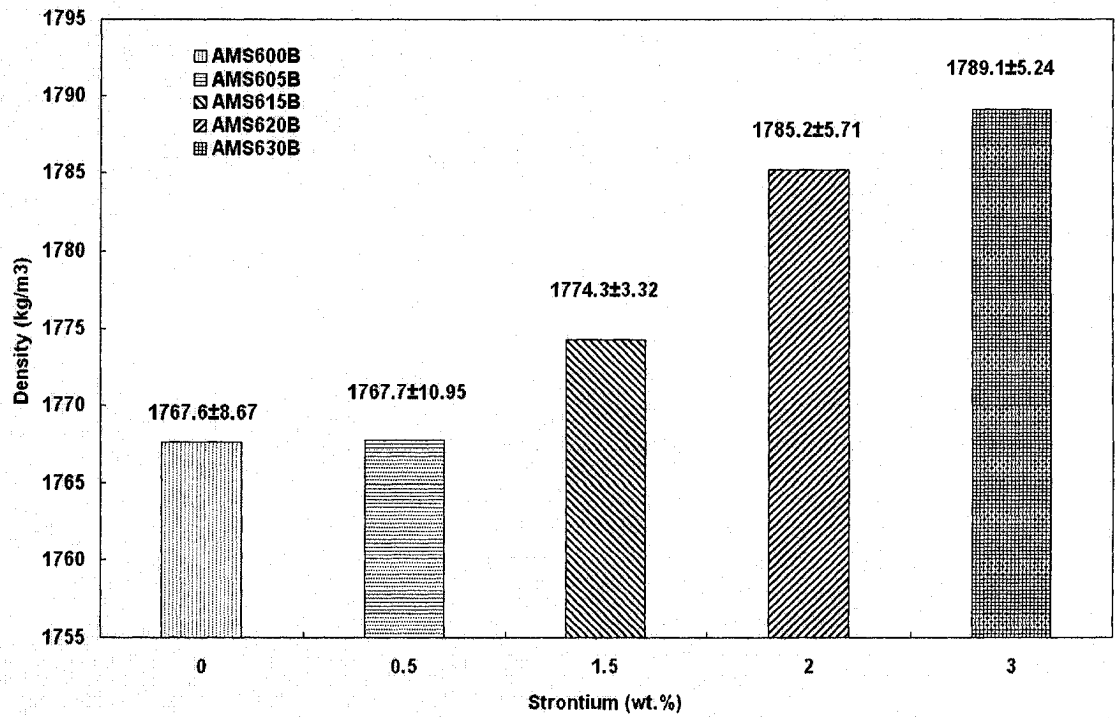
Figure 4.39 Effect of strontium content on density of AMS-B series alloys.
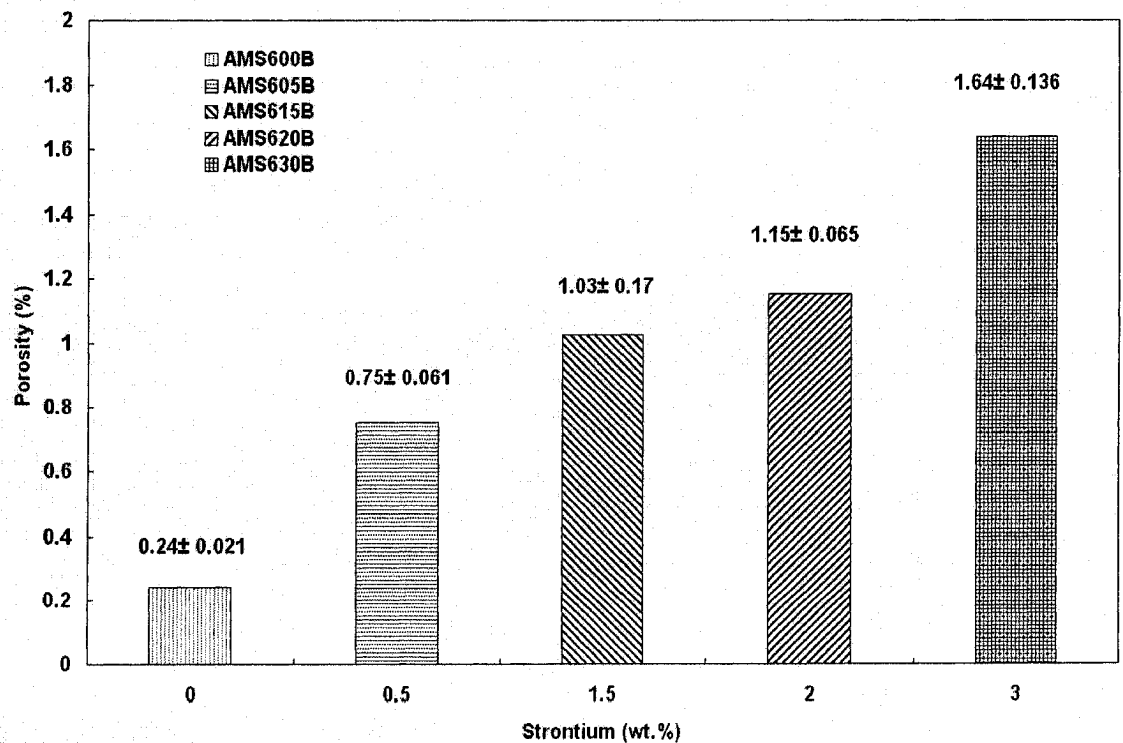
Figure 4.40 Effect of strontium content on porosity of AMS-B series alloys.
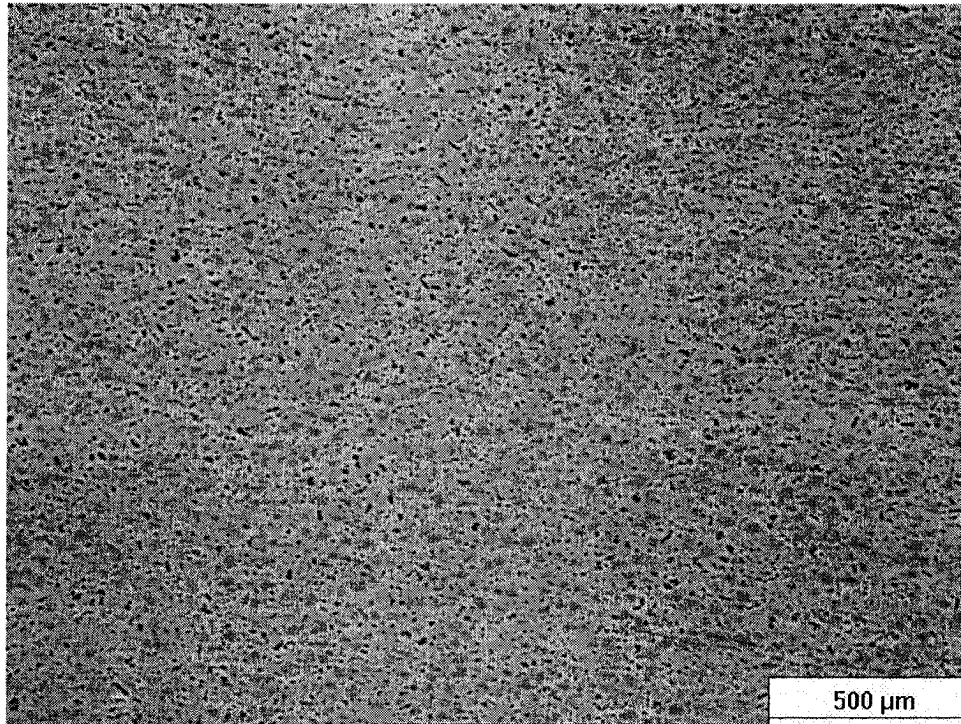
Figure 4.41 Optical micrograph showing no-porosity in AMS600B alloy.
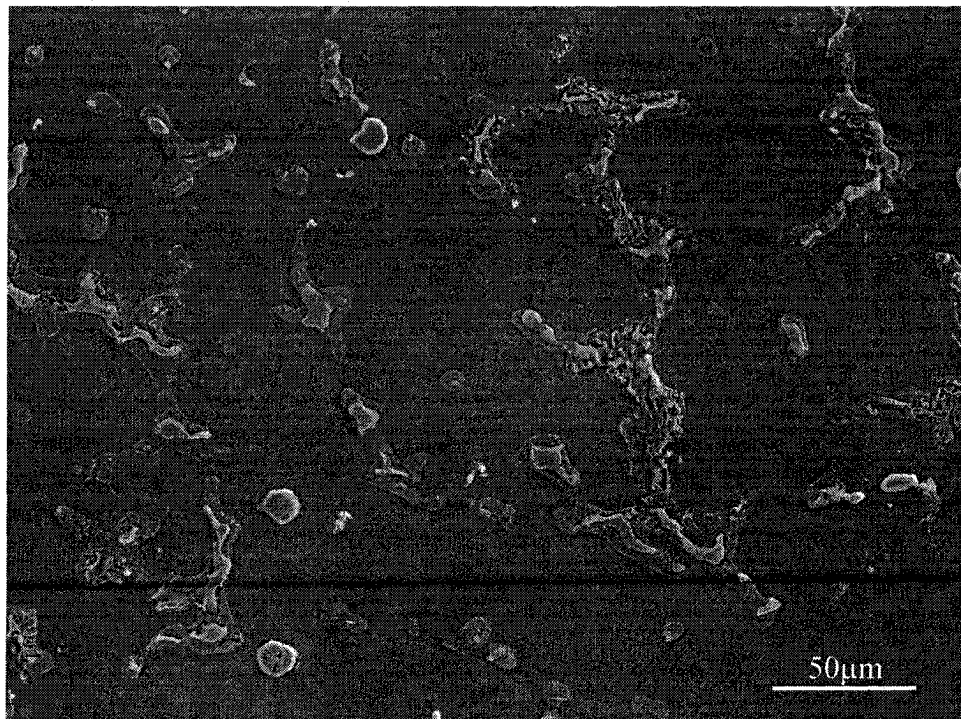
Figure 4.42 SEM micrograph showing no porosity in AMS600B alloy.

86
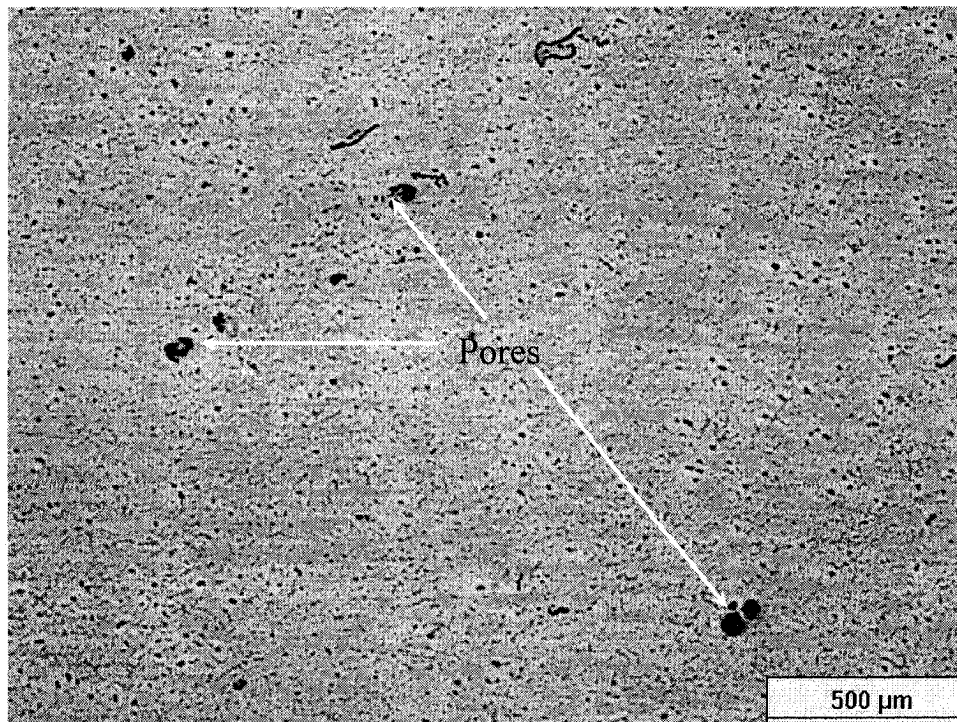
Figure 4.43 Optical micrograph showing porosity in AMS630B alloy.
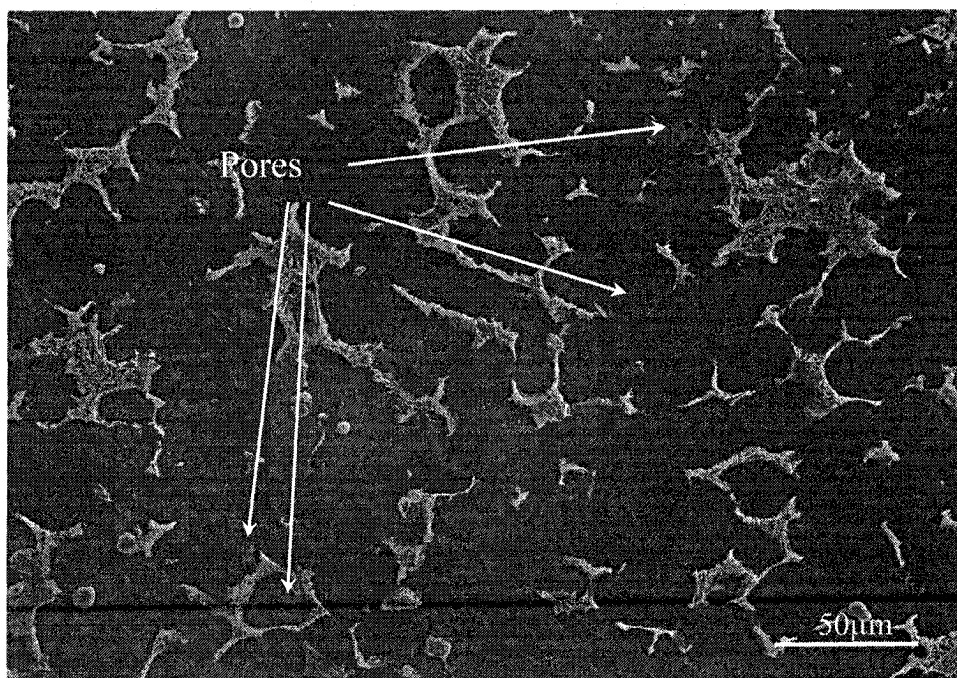
Figure 4.44 SEM micrograph showing porosity in AMS630B alloy.

87

4.3.2.2 Microstructure Analysis

4.3.2.2.1 Variation of grain size with strontium levels

The grain sizes of AMS-B series alloys were measured by using an Optical Image Analyzer. Figure 4.45 shows the grain size variation among AMS-B series alloys. It is interesting to note that 0.5 wt.% Sr addition reduces the grain size of the alloy slightly from 62.7 μm to 62.3 μm. However, further increases in Sr addition level up to 3 wt.% from 0.5 wt.% result in a significant reduction in grain size to 38.5 μm from 62.3 μm. This experimental observation indicates that in general, an increase Sr content levels leads to a decrease in grain size for the squeeze cast Mg-Al-Sr alloy, which results from the grain refinement effect of Sr on Mg-Al alloys.
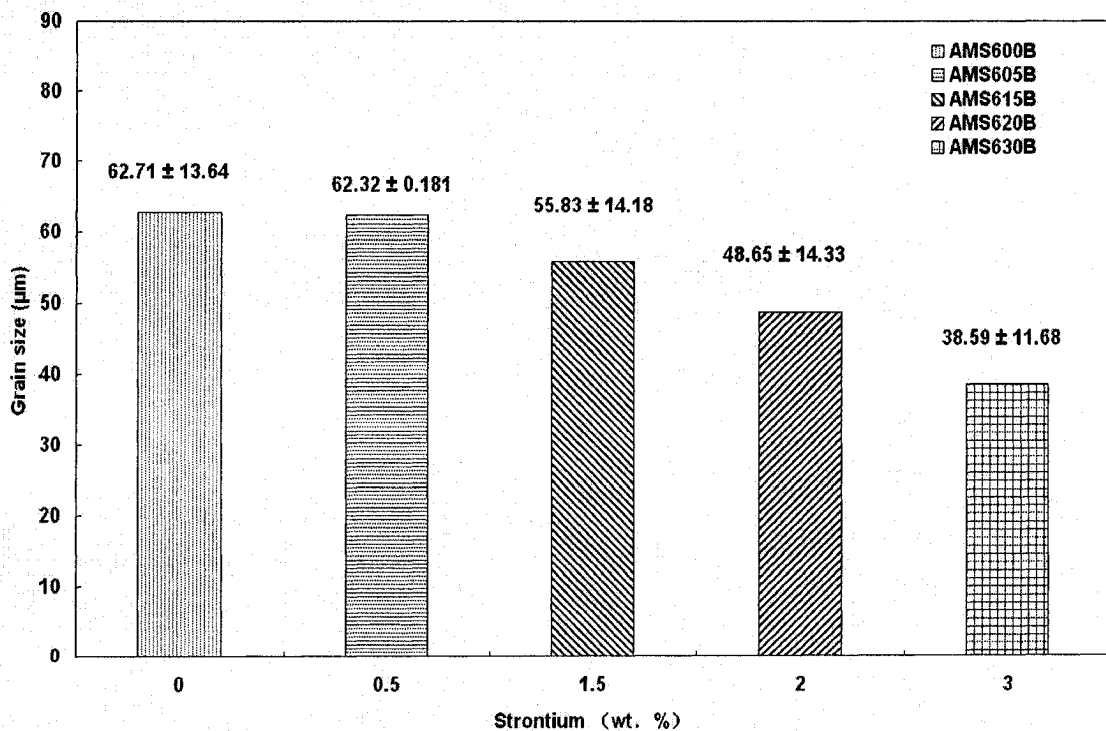
Figure 4.45 Effect of Strontium content on grain size of AMS-B series alloys.

4.3.2.2.2 Phase morphology

Figures 4.46 to 4.49 show the optical microstructure of AMS-B series alloy squeeze cast under the Sr content of 0, 1.5, 2.0, 3.0 wt% in the as-cast condition, respectively. It can be seen that the secondary phases $Mg_{17}Al_{12}$ and Mg-Al-Sr, are precipitated around grain boundaries, There is also a third phase that is intermetallic Al-Mn phase which has a round or triangle shape.

Comparison of the optical microstructural features in the squeeze cast Mg-Al-Sr alloys with different contents of Sr addition manifests that loose and divorced secondary phases containing both $Mg_{17}Al_{12}$ and Mg-Al-Sr phases are present at grain boundaries. As Sr content increases, Mg-Al-Sr secondary phase grows into relatively large sizes, tends to form a continuous network around grain boundaries, and becomes predominant compared to $Mg_{17}Al_{12}$ phase.
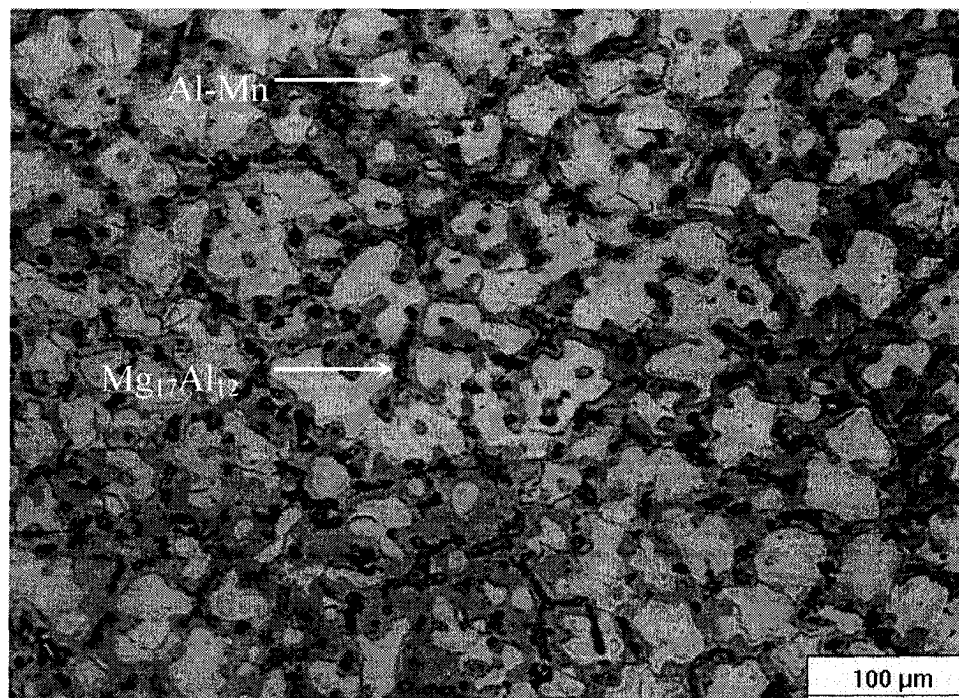
Figure 4.46 Optical micrograph showing microstructure of AMS600B alloy.
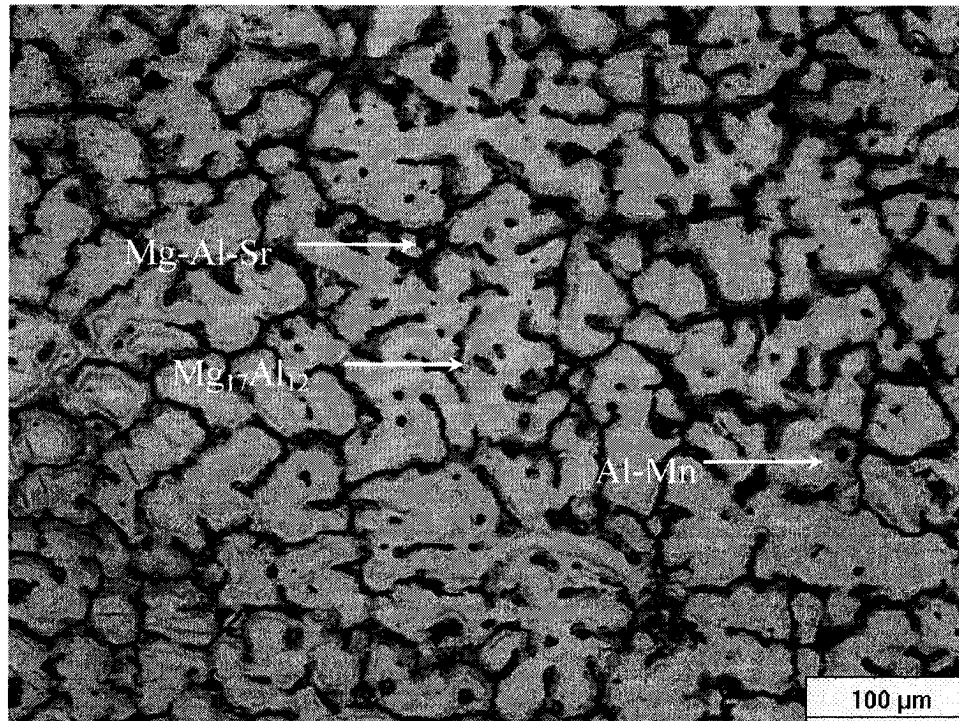
Figure 4.47 Optical micrograph showing microstructure of AMS615B alloy.
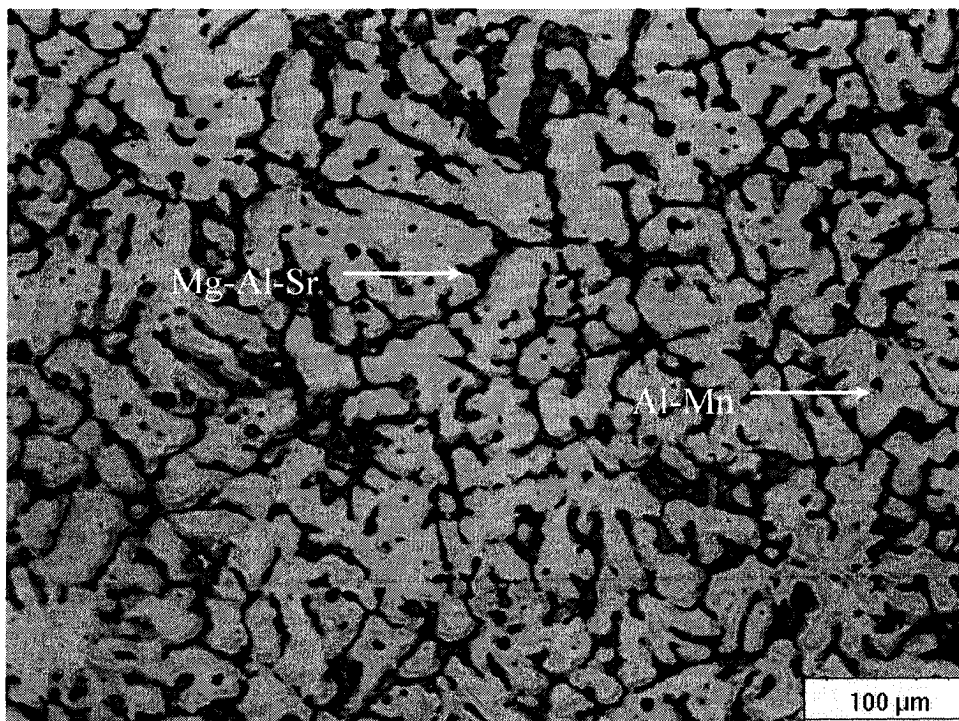
Figure 4.48 Optical micrograph showing microstructure of AMS620B alloy.

90
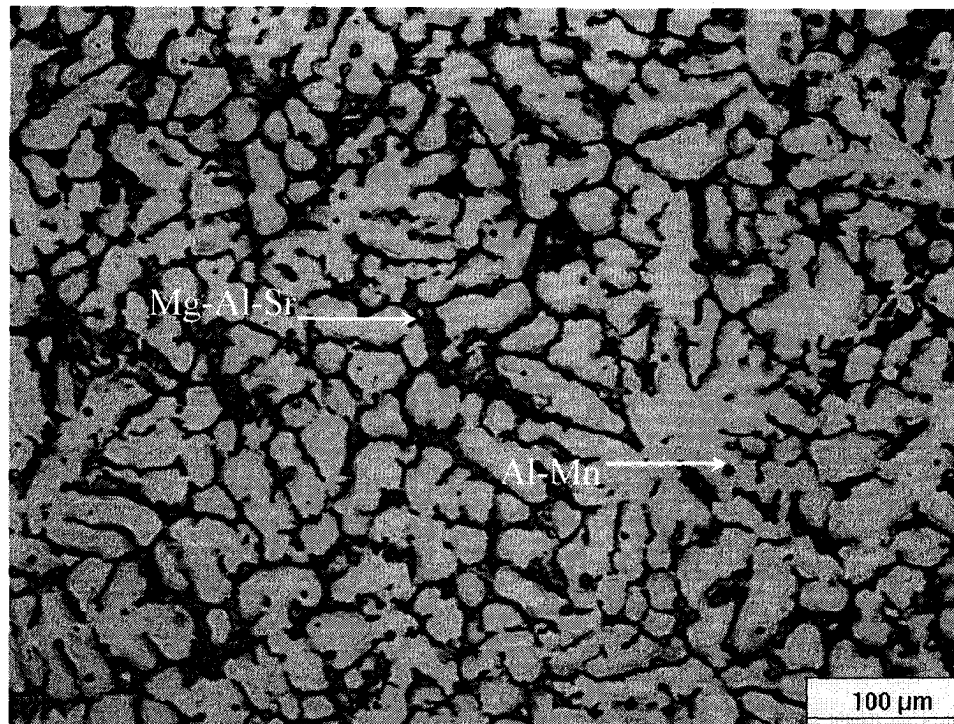
Figure 4.49 Optical micrograph showing microstructure of AMS630B alloy.

4.3.2.2.3 SEM/EDS analysis

SEM and EDS were also utilized for the elemental analysis of microstructural

features observed in AMS-B series alloys. Figures 4.50 – 4.53 present the results of SEM

and EDS analysis for the representative alloy AMS630B. Figure 4.50 presents SEM

micrograph showing the microstructure of the squeeze cast AMS630B. It can be seen

from Figure 4.50 that the Mg-Al-Sr eutectic phase precipitates around grain boundaries.

Also, to simplify the discussion about EDS spectra, the identified primary and secondary

phases in the microstructure of the alloy were labled as "A", "B" and "C". Figures 4.51 –

4.53 show the EDS spectra for point A (Figure 4.51), which is the Mg-Al-Sr eutectic

phase; point B (Figure 4.52), which is Al-Mn intermetallic phase; point C (Figure 4.53),

which is the primary α-Mg matrix. Oxygen peak which appeared on many spectra esulted from surface oxidation during and after sample preparation, and had been removed the element symbol.

The detailed data of elemental analysis in both the atomic and weight percentages are summarized in Tables 4-8 ~ 4-10. It should be pointed out that in the alloy with 3 wt.% Sr addition, only three phases were found. They are the Al-Mn intermetallic, primary α-Mg, and secondary Mg-Al-Sr. Apparently, $Mg_{17}Al_{12}$ was completely depleted by the emerging Mg-Al-Sr phase.
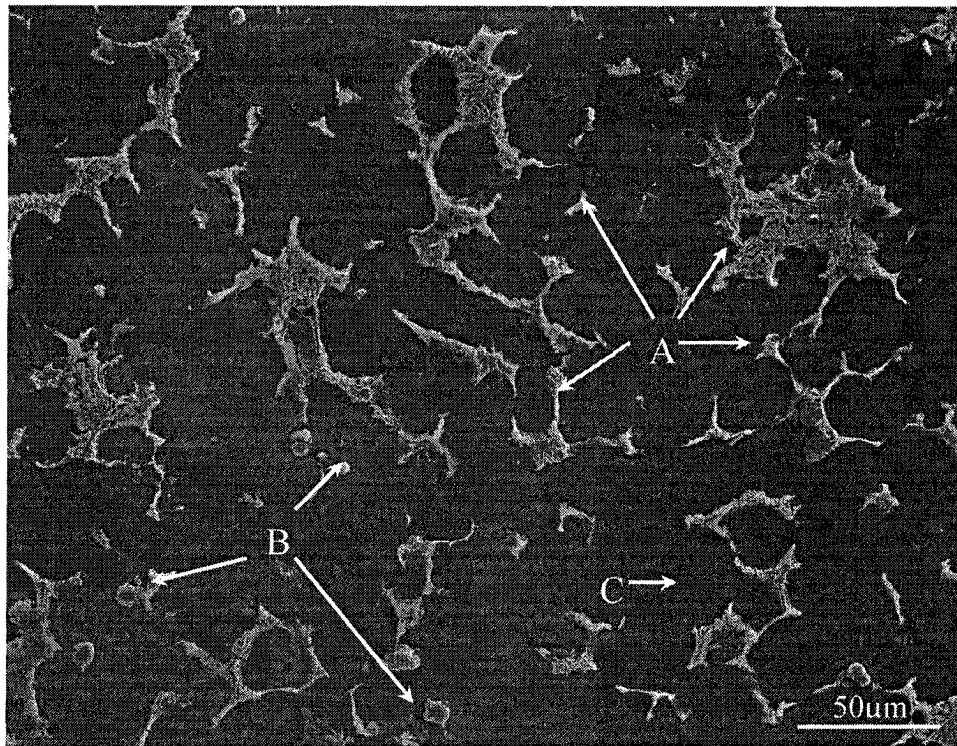
Figure 4.50 SEM micrographs showing microstructure of squeeze cast AMS630B.

92
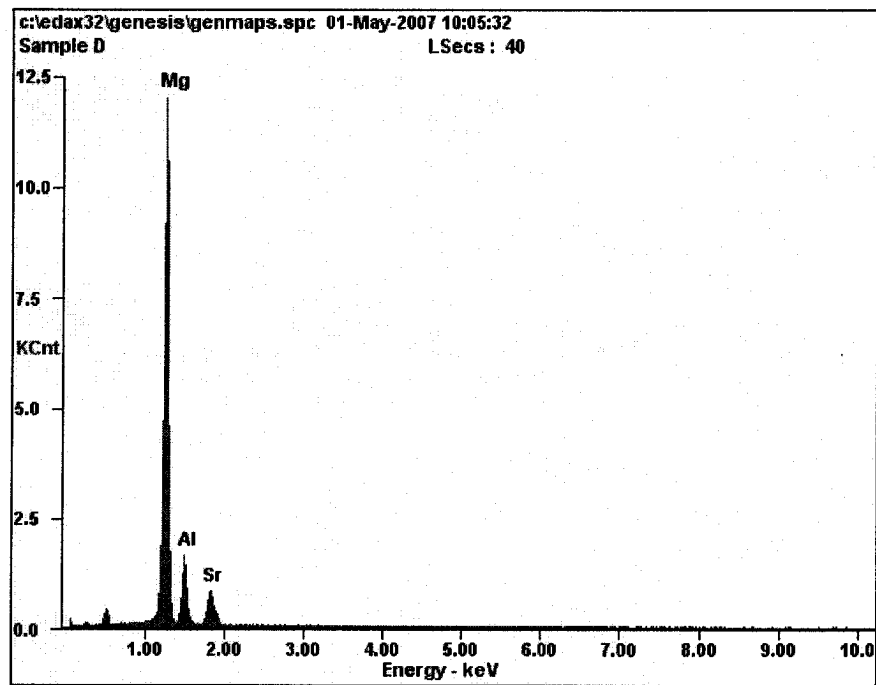
Figure 4.51 EDS spectrum from the region marked "A" in Figure 4.50, i.e. Mg-Al-Sr

Phase.

Table 4-8 Atomic and weight percent of element at point "A" ($Mg_{10} Al_4Sr$ eutectic)

Element	Mg	Al	Sr
At%	72.45	20.55	6.99
	65.98	26.82	7.19
	69.72	23.29	6.99
Wt%	60.14	18.94	20.92
	54.23	24.46	21.31
	57.74	21.40	20.86

93
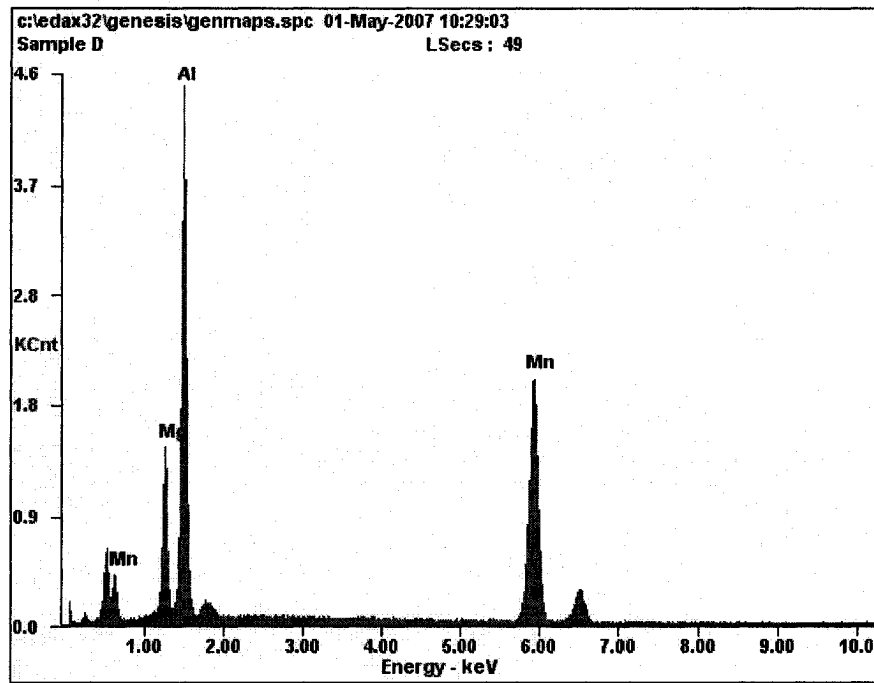
Figure 4.52 EDS spectrum from the region marked "B" in Figure 4.50, i.e. Al-Mn phase.

Table 4-9 Atomic and weight percent of element at point "B" (Al-Mn phase)

Element	Al	Mn
At%	39.48	28.95
	43.87	34.61
	50.20	31.46
Wt%	31.12	46.46
	32.80	52.69
	38.38	48.98

94
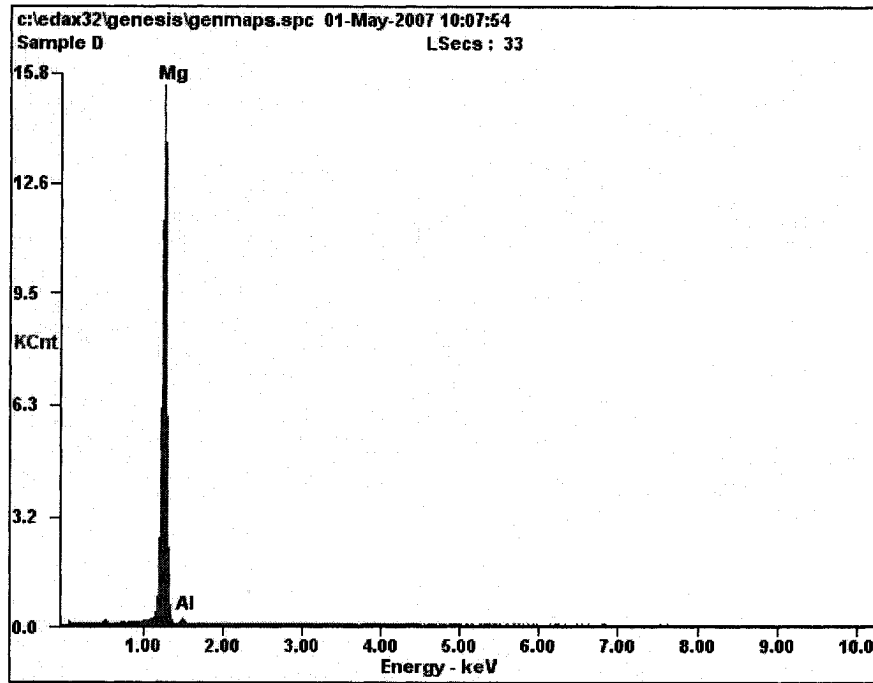
Figure 4.53 EDS spectrum from the region marked "C" in Figure 4.50, i.e. primary α-Mg

Table 4-10 Atomic and weight percent of element at point "C" (primary α-Mg)

Element	Mg	Al
At%	97.14	02.86
	96.37	03.63
Wt%	96.84	03.16
	95.99	04.01

95

4.3.2.2.4 TEM analysis

Baril et al. [5] have tentatively identified the $Mg_5Al_{17}Sr_3$, $Mg_{13}Al_{10}Sr$, and $Mg_{13}Al_3Sr$ phase in AJ52 and in AJ51 alloys. However, with the increased aluminum content, Al_4Sr phase emerged in AJ62 alloy. Using x-ray diffraction, Parvez et al. [24] found Al_4Sr to be dominating phase in the magnesium-aluminum alloys containing strontium varying from 3.32 wt.% to 32.0 wt.% .

Figure 4.54 shows TEM micrographs of (a) Al_4Sr phase in AMS630B alloys, (b) Al_4Sr phase at high magnification, (c) EDS spectrum from the Al_4Sr phase, (d) selected area diffraction pattern of Al_4Sr phase, and (e) Indexing of diffraction pattern in (d). The Al_4Sr phase has a typical lamellar structure with a regular shape. The lamellar eutectic has been indexed as arising from a binary Al-Mg compound Al_4Sr with a body centred tetragonal structure. The present TEM observation on squeeze cast Mg-6 wt.%Al-3 wt.%Sr alloy is consistent with the results given in reference [39].
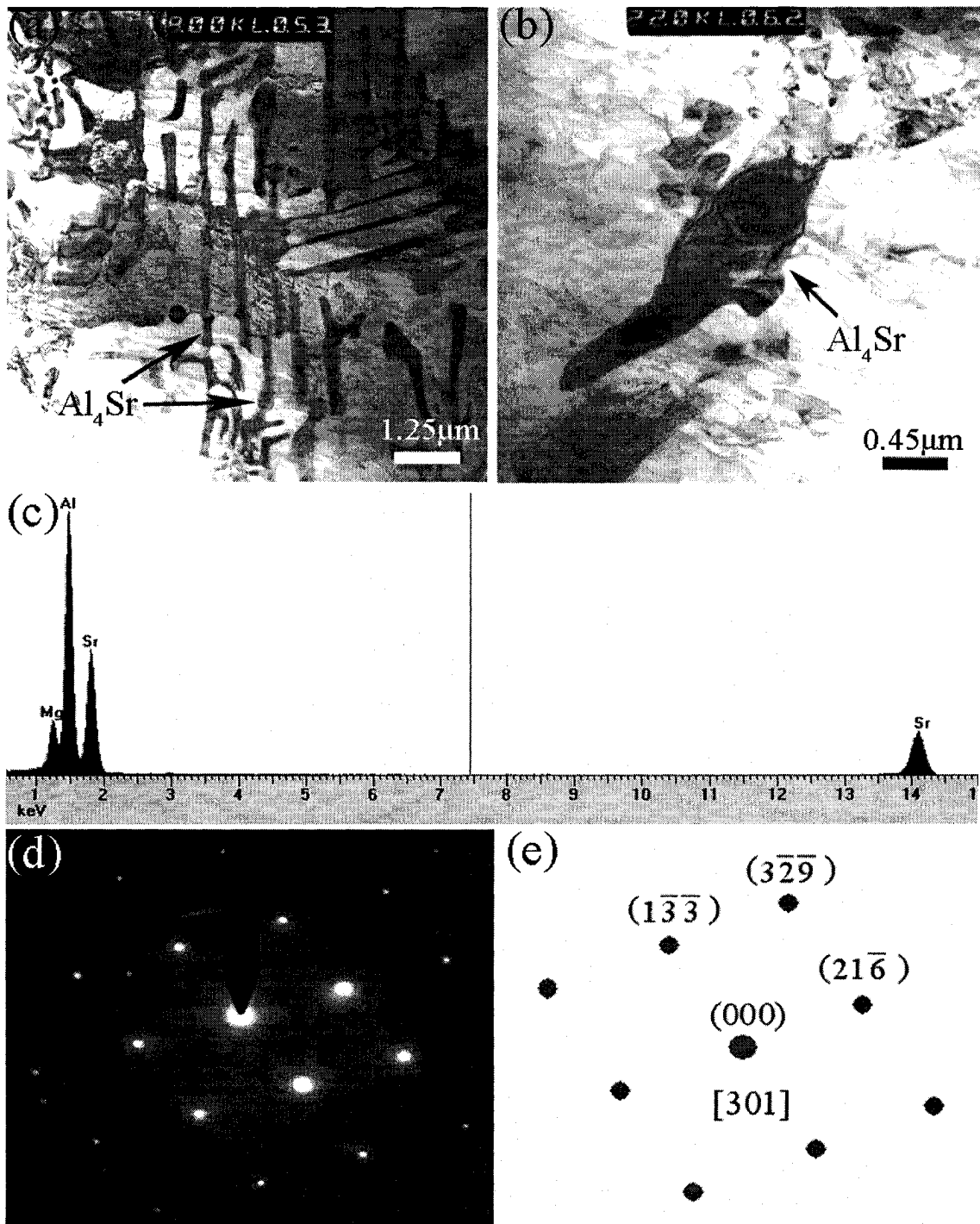
Figure 4.54 TEM micrographs of AMS630B. (a) Al₄Sr phase in AMS630B alloys, (b) Al₄Sr phase at high magnification, (c) EDS spectrum from the Al₄Sr phase, (d) selected area diffraction pattern of Al₄Sr phase, and (e) Indexing of diffraction pattern in (d).

97

4.3.2.3 Tensile behaviour of AMS-B series alloys

4.3.2.3.1 Effect of Sr content on tensile properties

Figure 4.55 shows representative engineering stress and strain curves for squeeze cast AMS-B series alloys at room temperature. The curve shows that under tensile loading, the alloy deformed elastically at first. Then, once the yield point reached, plastic deformation of the alloy set in. It is obvious that the ultimate tensile strength (UTS), yield strength (YS) and elongation of AM60 alloy cast (0 wt% strontium) are much higher than those with strontium addition under the same pressure of 30 MPa.

The effect of strontium content on tensile properties of the squeeze cast AMS-B series alloys is presented in Table 4.11, and in Figure 4.56. It is observed from the results that an increase in strontium content levels brings a significant decrease in UTS and E_f, and a somewhat decrease in yield strength (YS). The elongation, UTS and YS of the AMS630B is 0.64%, 58.93MPa and 45.61 MPa respectively. The Sr addition of 3 wt.% results in a decrease of 493% in enlongation, 154% in UTS and 69% in YS under those of AMS600B.

The grain size measurements indicate that the grain structure of the squeeze cast Mg-Al-Sr alloy was refined as Sr content increased from 0 to 3.0 wt.%. It implies that the tensile properties should increase accordingly. Unfortunately, the results of tensile testing show that the tensile properties of the alloy decrease considerably with increasing Sr addition. The decrease in tensile properties of the alloy should be attributed to an increase in porosity as Sr content increases. The porosity measurements reveal that the porosity level of the alloys increases 583 % over AM60 while Sr addition increases to 3.0 from

zero percent. It seems that the adverse effect of Sr addition on tensile properties due to porosity increase offsets its positive grain refinement on microstructure of the squeeze cast Mg-Al-Sr alloys.
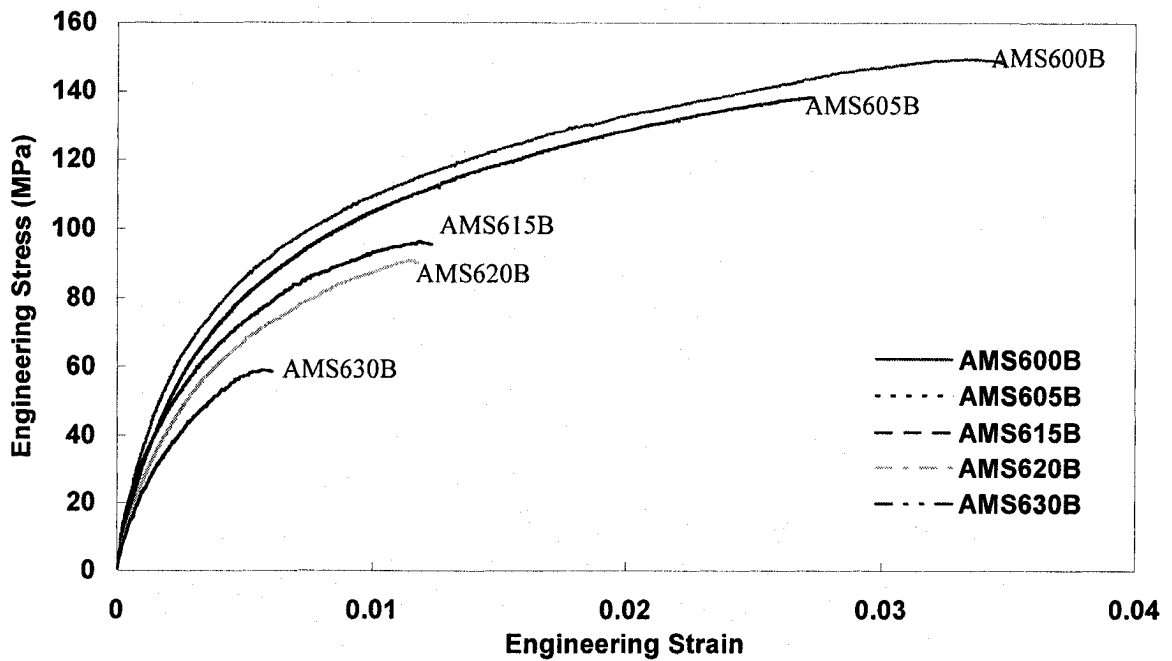
Figure 4.55 Engineering stress-strain curves of AMS-B alloys under 30 MPa pressure.

Table 4-11 Effect of strontium content on UTS, YS and Elongation of AMS-B alloys

Strontium(wt%)	Alloy Symbol	UTS (MPa)	YS (MPa)	Elongation (%)
0	AMS600B	149.65 ± 4.37	77.13 ± 1.85	3.8 ± 0.15
0.5	AMS605B	138.22 ± 3.69	70.36 ± 2.13	2.85 ± 0.13
1.5	AMS615B	96.24 ± 5.51	63.24 ± 4.77	1.19 ± 0.09
2.0	AMS620B	92.67 ± 5.86	56.07 ± 4.01	1.17 ± 0.11
3.0	AMS630B	58.93 ± 6.27	45.61 ± 3.65	0.64 ± 0.14

99
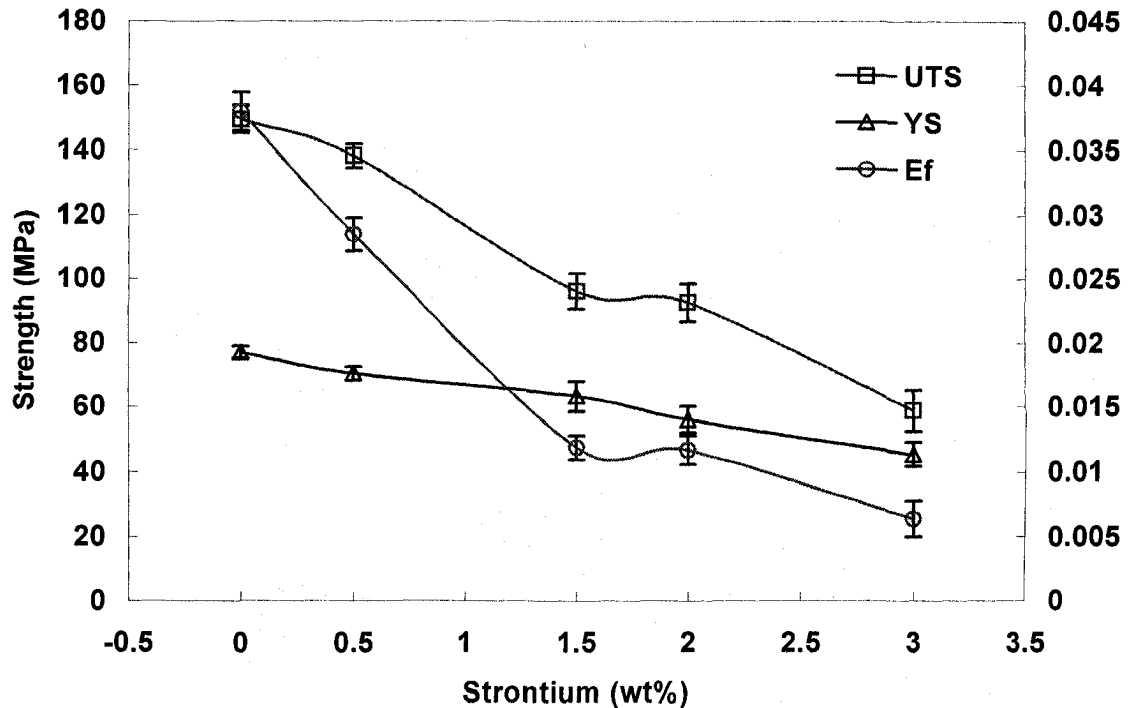
Figure 4.56 Effect of Sr contents on UTS, YS and Elongation of AMS-B Alloys under 30

MPa pressure.

4.3.2.3.2 Effect of Sr content on strain-hardening

Figure 4.57 gives true stress-strain curves for AMS-B series alloys. To elucidate

the strain-hardening behaviors of the AMS-B alloys, a plot of strain-hardening rate (dδ/dε)

versus true plastic strain (ε), is illustrated in Figure 4.58, which is derived from true

stress-strain curves. It can be seen from Figure 4.58 that, as the strontium content rises,

the strain-hardening rates of AMS-B alloys decrease. It suggests that AMS-B alloys cast

under low strontium content are able spontaneously to strengthen themselves increasingly

to certain extent, in response to large plastic deformation prior to fracture. The high strain

hardening rates of the alloys cast under low strontium content may be attributed to the

relatively low porosity level in the alloys.

100
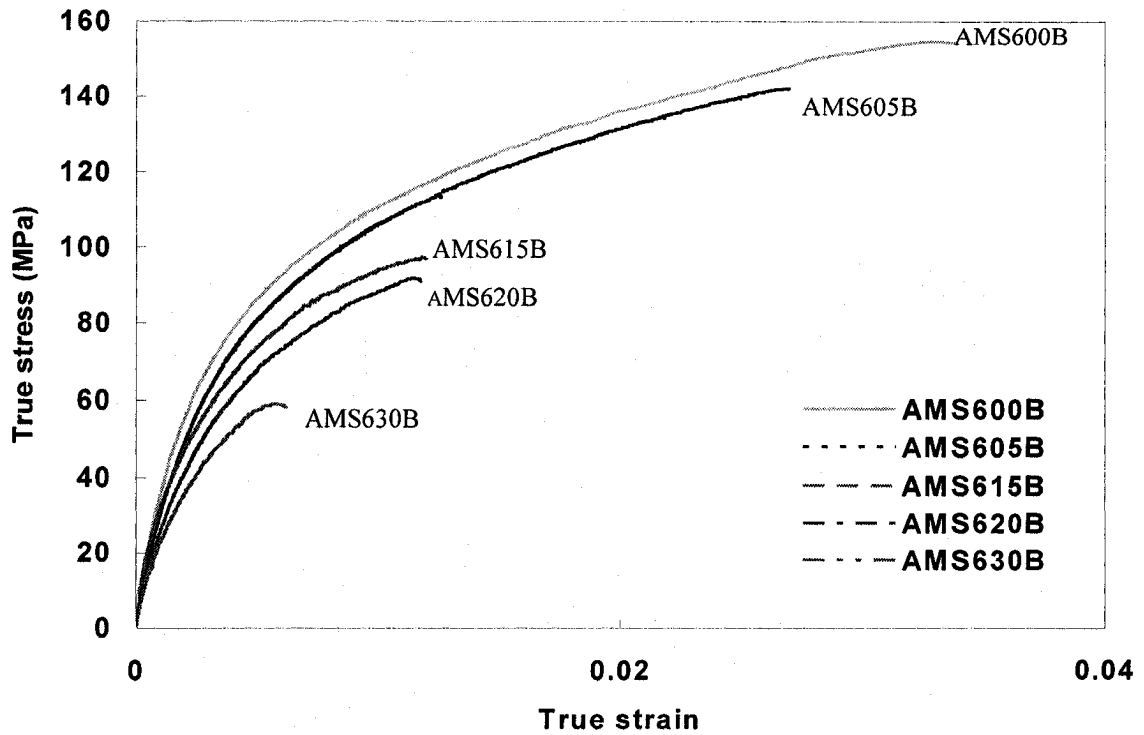
Figure 4.57 True stress-strain curves of AMS-B series alloys.
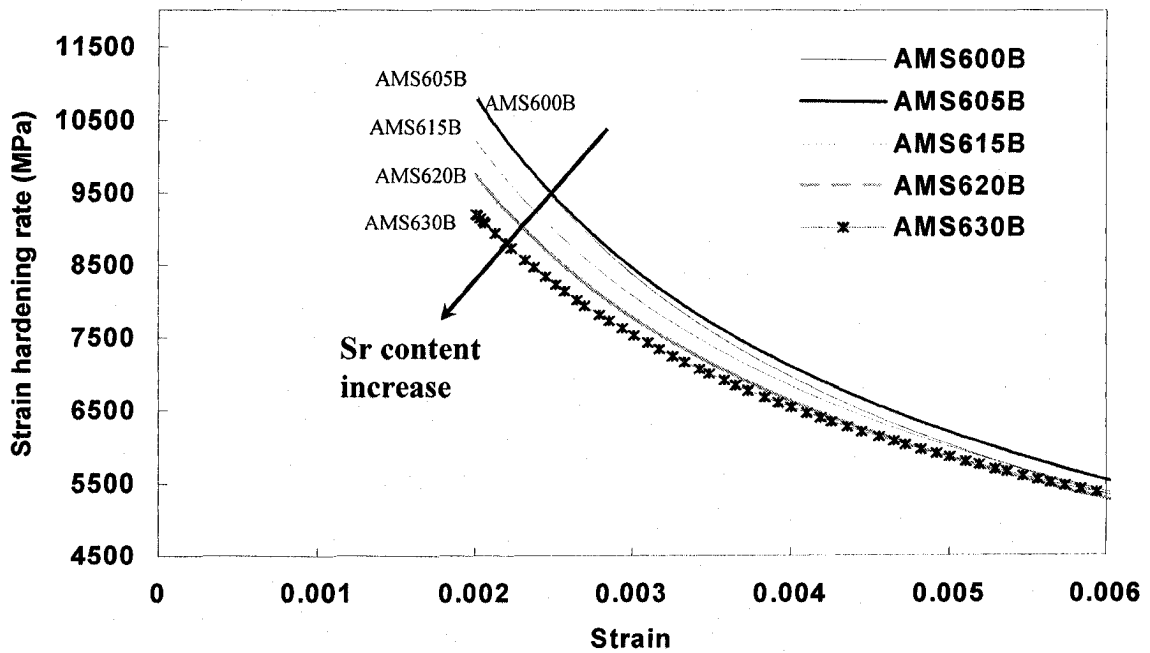
Figure 4.58 Strain hardening rate versus strain of AMS-B series alloys.

101

4.3.2.4 Fracture behavior

The tensile fractured surfaces of squeeze cast AMS600B and AMS630B are shown in Figures 4.59 ~ 4.62. The observed fracture in the alloys with 0 and 3wt.% strontium is brittle in nature. Brittle fracture is characterized by rapid crack propagates with less expenditure of energy than with ductile fractures, and without appreciable gross plastic deformation. The fractured surface has a bright appearance, is generally of the flat type that is perpendicular to the direction of tensile loading.

Quasi-cleavage and cleavage should be considered as the fracture modes on a microscopic level for the alloys with 0 and 3 wt.% Sr, respectively. The characteristic feature of cleavage, i.e., flat facets, is observed on both the fractured surfaces of the alloys as shown in Figures 4.60 and 4.62. The flat facets in alloy AMS600B are partially covered by river markings and tiny dimples. The river markings are the results of cracks moving through grains along a number of parallel planes that forms a series of plateaus and connecting ledges. The tiny dimples are caused by the localized microvoid coalescence. Those features are indications of the absorption of energy through certain local plastic deformation that occurred during tensile testing. However, almost no dimples are present in the fractured face of the AMS630B (3 wt.%). This indicated that very limited deformation took place during fracture of AMS630B alloy. In general, the SEM observations on the fractured surfaces of the squeeze cast Mg-Al-Sr alloy show a good agreement with the elongation data listed in Table 4-11.

Figures 4.63 and 4.64 show the damaged microstructure underneath the fractured surfaces for alloys AMS600B and AMS630B, respectively. It can be seen from Figure

102

4.63 that cracks in AMS600B originated in the secondary phase, $Mg_{17}Al_{12}$, due to its

brittleness in nature. However, the initiation point of cracks in AMS630B began with the

internal discontinuity due to the presence of pores and porosity. The porosity presence

cause stress concentration and cracks can form at points of stress concentration, and

spread rapidly over the section. The final fracture results from the growth and

coalescence of the cracks.
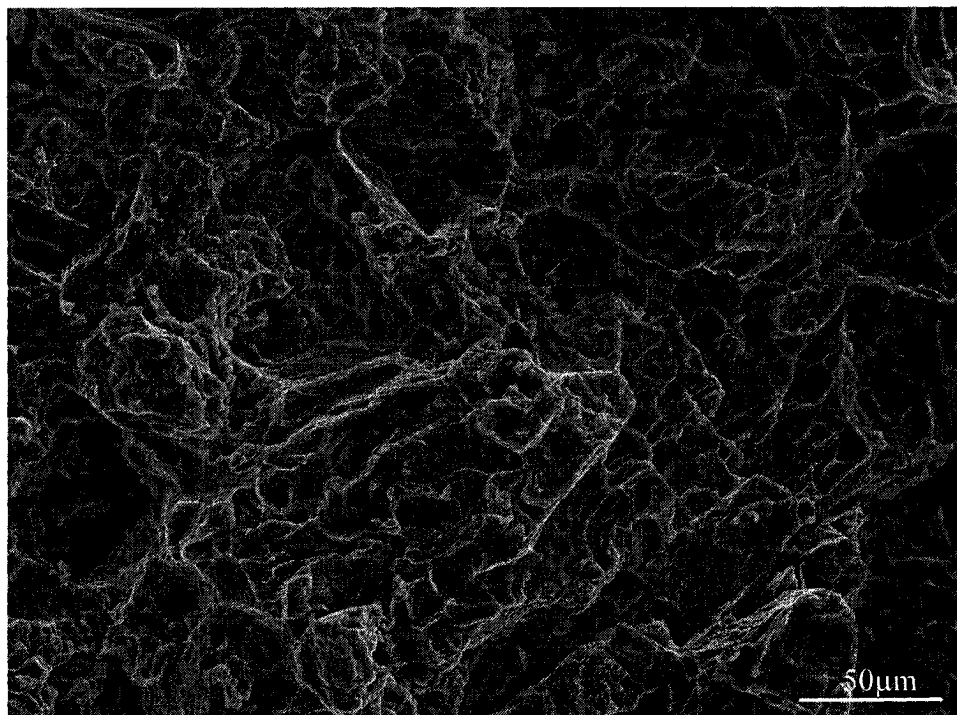
Figure 4.59 SEM fractographs of AMS600B (X500).

103
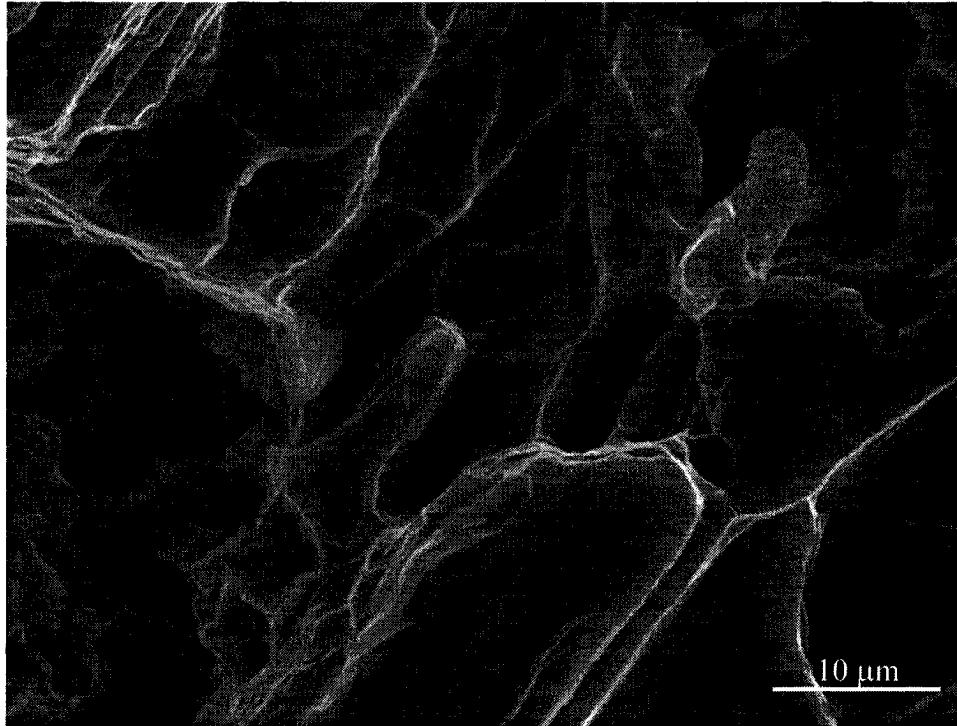
Figure 4.60 SEM fractographs of AMS600B (X3000).
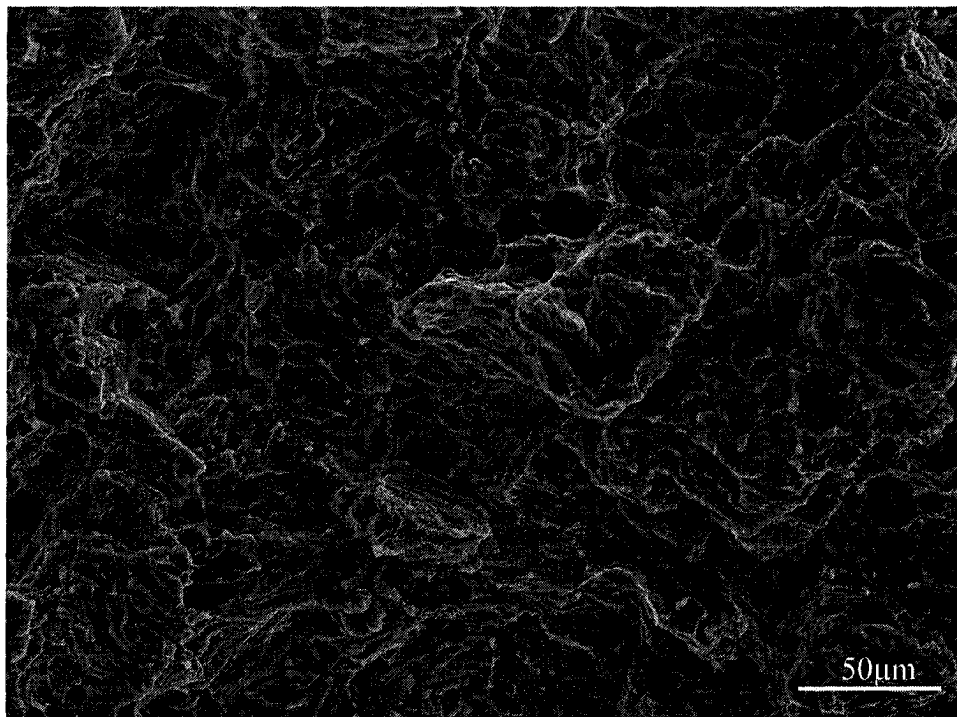
Figure 4.61 SEM fractographs of AMS630B (X500).
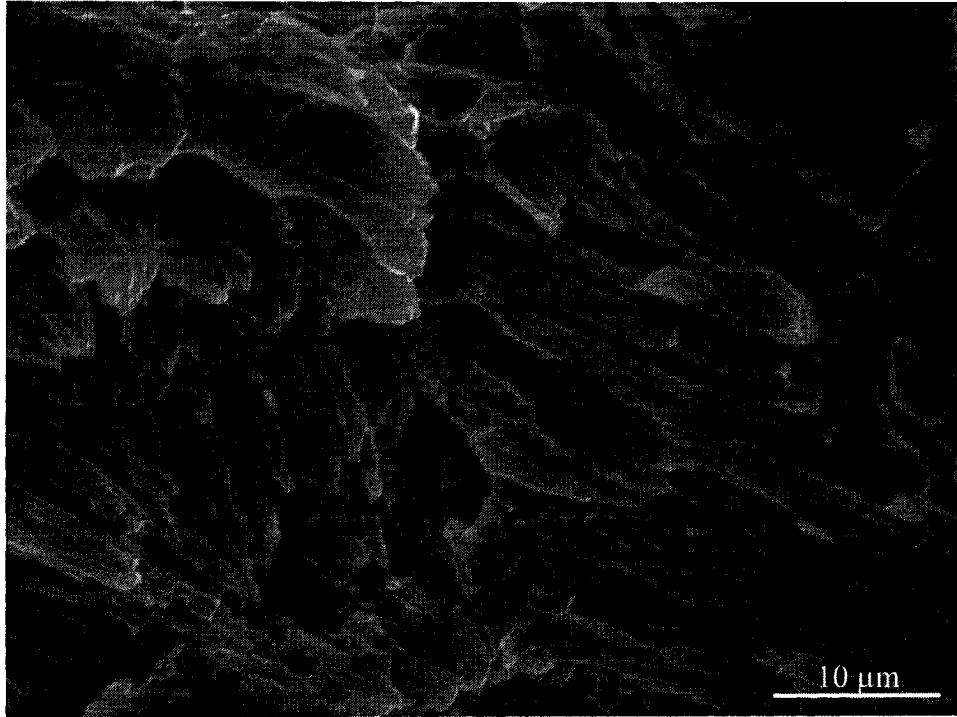
Figure 4.62 SEM fractographs of AMS630B (X3000).

105
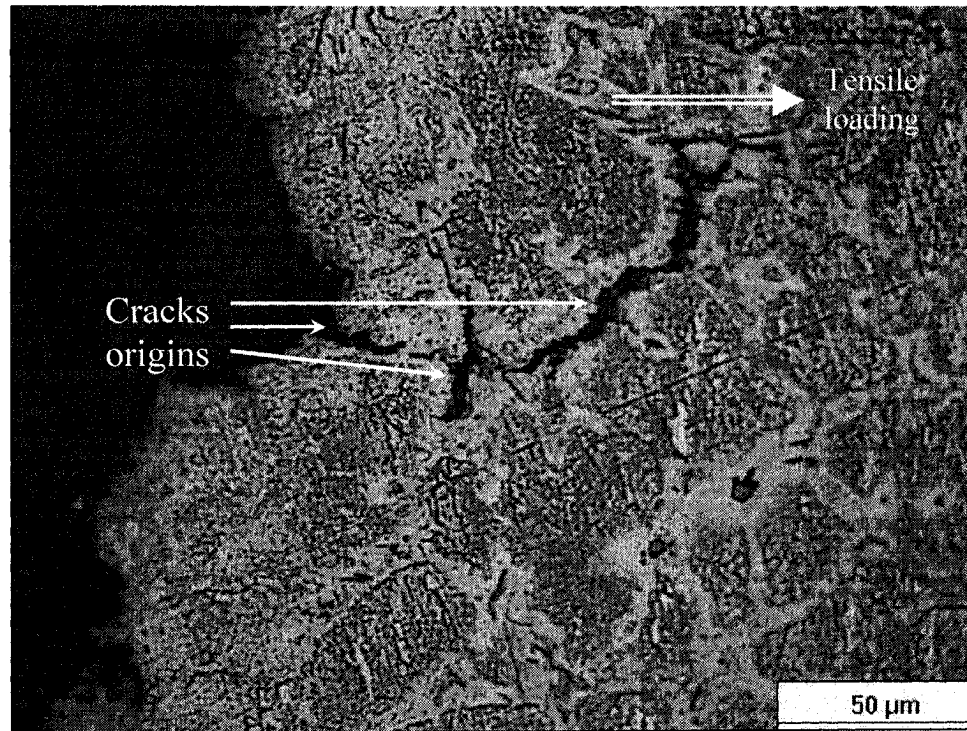
Figure 4.63 Optical micrograph showing crack origin in AMS600B alloy.
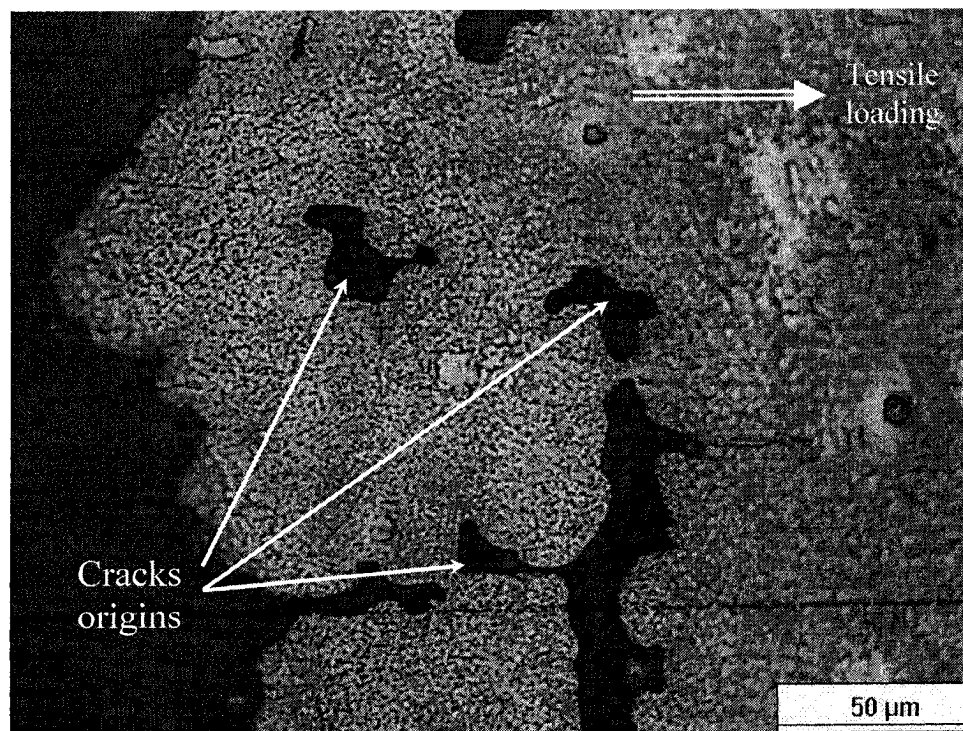
Figure 4.64 Optical micrograph showing crack origin in AMS630B alloy.

106

4.3.3 Strontium effect at high pressure (90 MPa)

4.3.3.1 Tensile behaviour of AMS-D series alloys

Figure 4.65 shows representative engineering stress and strain curves for squeeze cast AMS-D series alloys at room temperature. The curve shows that, under tensile loading, the alloy deformed elastically first. Once yield point reaches, plastic deformation of the alloy set in. It is evident that the elongation (6.41%) of the alloy with 0 wt% strontium content is much higher than that (1.79%) of the one with 3.0 wt% strontium content. The ultimate tensile strength (UTS) of the alloy without strontium is also higher than that of the alloys with strontium addition. However, as strontium content increases from 0 to 3.0 wt.%, the yield strengths (YS) of the alloys squeeze cast under 90 MPa increase from 74.65 to 86.35 MPa.

The effect of strontium content on tensile properties of squeeze cast AMS-D alloy in high pressure is given in Table 4.12 and Figure 4.66. It is observed from the results that an increase in strontium content levels brings a significant decrease in E_f and slightly decrease in UTS, but some increase in yield strength (YS). The elongation and UTS of the AMS630D are only 1.79% and 141.02 MPa which results in a significant decrease of 258% in and 34% compared to those of AMS600D, respectively. However, the YS of the AMS630D is 86.35 MPa, which increases slightly by 16% over that of AMS600D. The YS variation of the alloys cast under high pressure with Sr content is somewhat different from those of the alloys cast with a low applied pressure.

The difference in the YS variation with Sr content for the alloys between high (90 MPa) and low (30 MPa) applied pressure cases may give rise to the fact that the grain structure is primarily responsible for the YS. An increase in both the Sr content and

107

applied pressure level leads to a very fine microstructure due to grain refinement caused

by not only Sr addition but also fast cooling by eliminating air gap between the casting

and mould with the high applied pressure.
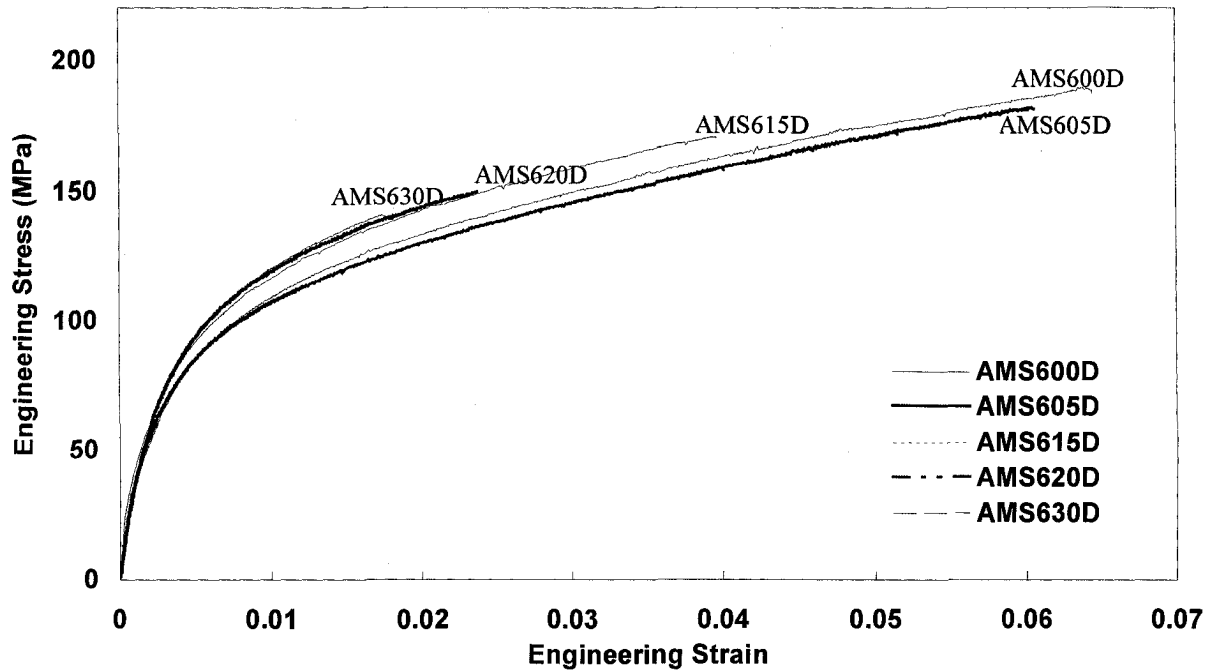
Figure 4.65 Engineering stress-strain curves of AMS-D series alloys.

Table 4-12 Effect of strontium content on UTS, YS and Elongation of AMS-D alloys

Strontium(wt%)	Alloy Symbol	UTS (MPa)	YS (MPa)	Elongation (%)
0	AMS600D	189.04 ± 6.35	74.65 ± 2.97	6.41 ± 0.26
0.5	AMS605D	181.83 ± 4.17	76.84 ± 2.18	6.07 ± 0.13
1.5	AMS615D	170.86 ± 2.18	84.93 ± 3.42	3.97 ± 0.27
2.0	AMS620D	149.95 ± 2.31	85.72 ± 4.05	2.37 ± 0.21
3.0	AMS630D	141.02 ± 4.69	86.35 ± 3.89	1.79 ± 0.14

108
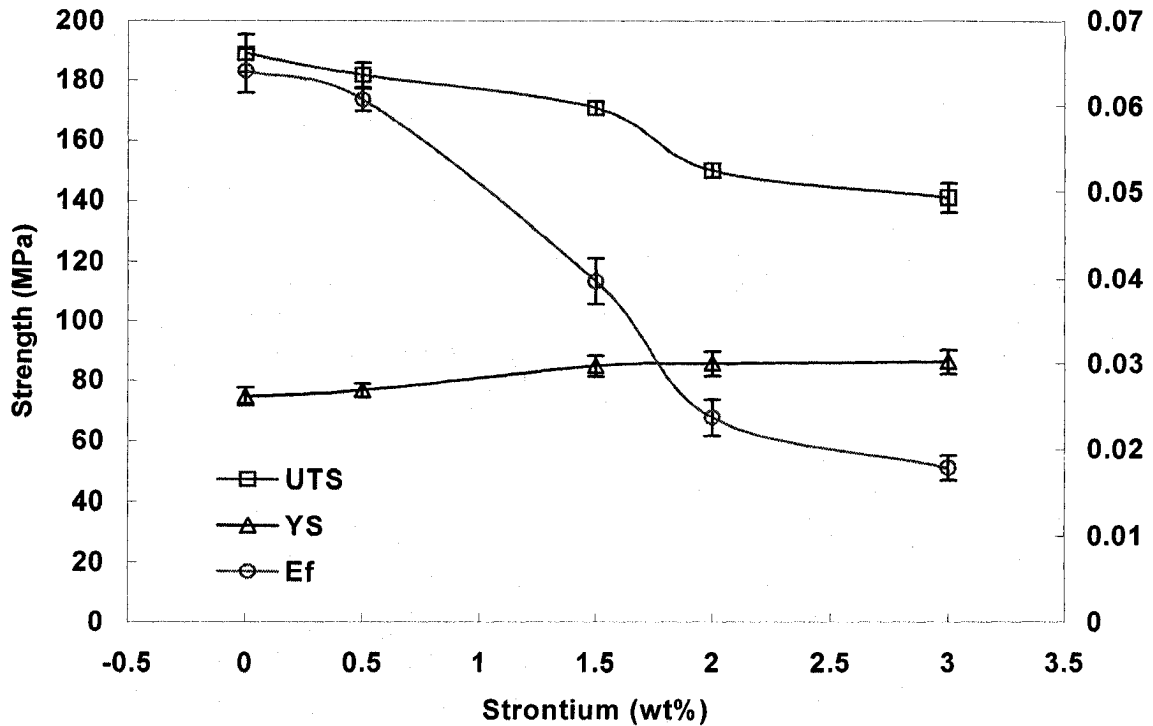
Figure 4.66 Effect of Sr contents on UTS, YS and Elongation of AMS-D series alloys.

4.3.3.2 Microstructure analysis

Optical and SEM micrographs given in Figures 4.67 and 4.68 show almost no porosity present in alloy AMS605D. However, as the strontium content increases to 3 wt.%, the existence of tiny pores in alloy AMS630D solidified even under 90 MPa is revealed by SEM and optical microscopy as illustrated in Figures 4.69 and 4.70.
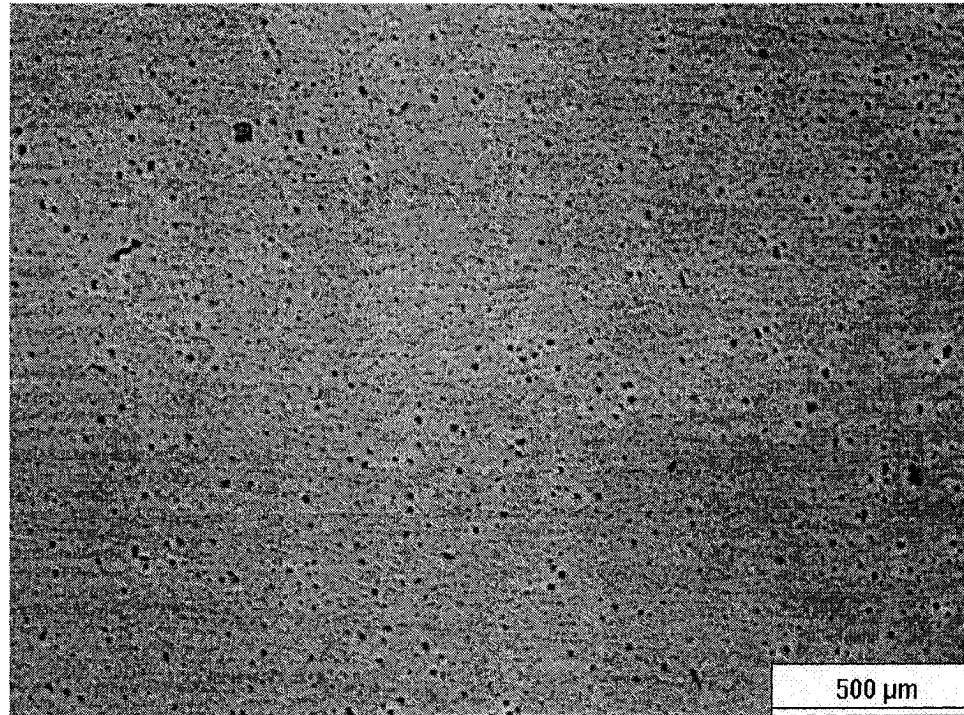
Figure 4.67 Optical micrograph showing almost no-porosity in AMS605D alloy.
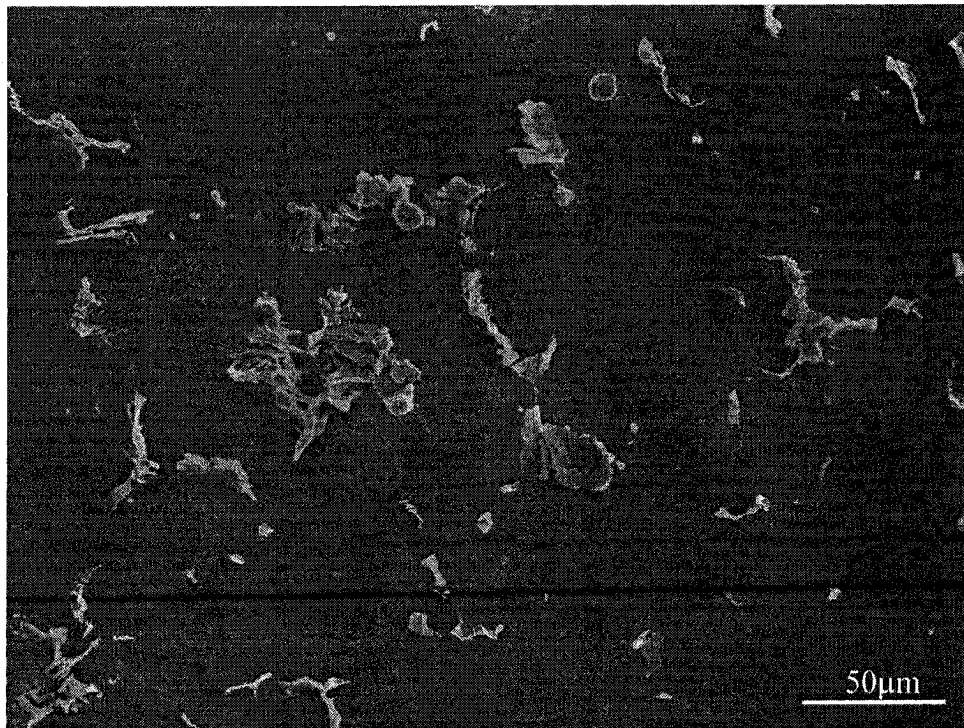
Figure 4.68 SEM micrograph showing no porosity in AMS605D.

110
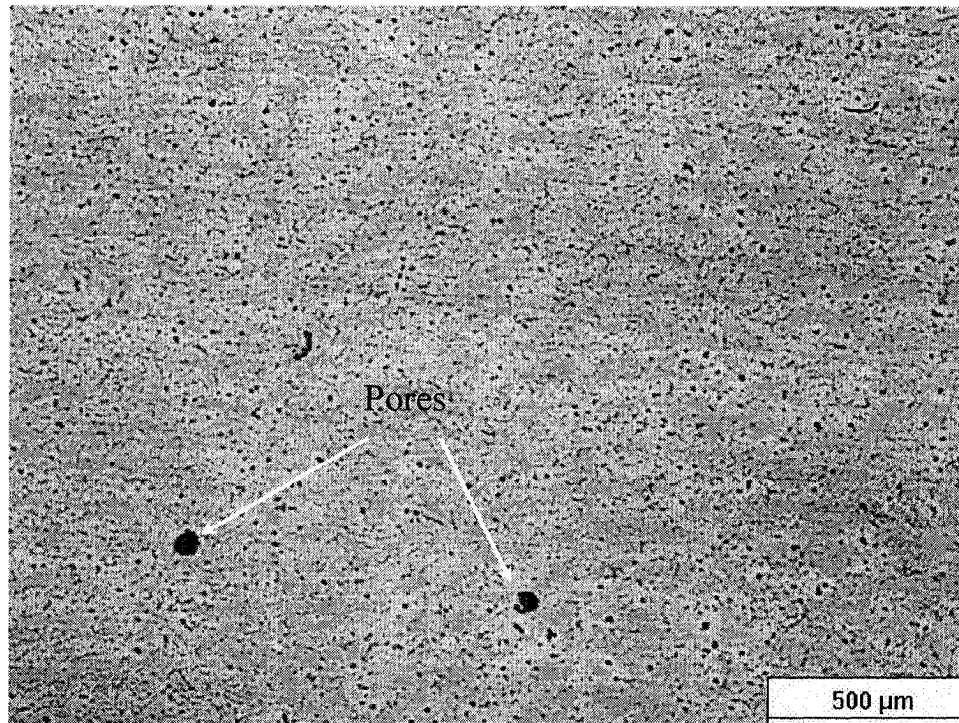
Figure 4.69 Optical micrograph showing porosity in AMS630D alloy.
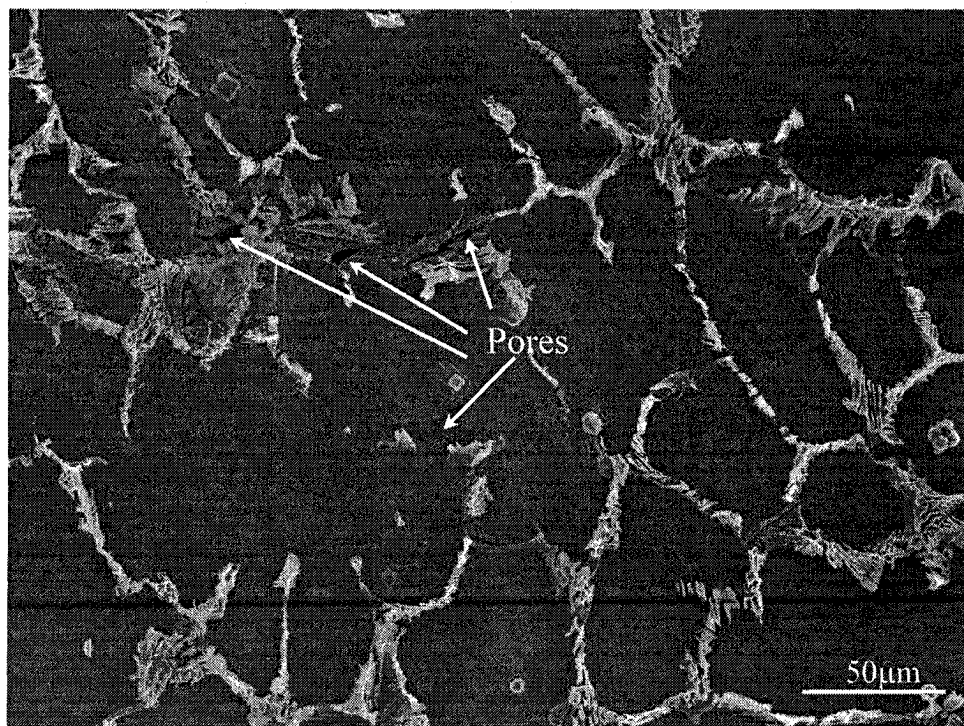
Figure 4.70 SEM micrograph showing porosity in AMS630D.

111

4.4 Summary

The effect of applied pressure levels on tensile properties and microstructure of squeeze cast Mg-Al-Sr alloys was investigated through experiments. The microstructural features of the AMS605 alloys were studied via metallography and SEM/EDS analysis. The microstructure for all samples of AMS605 alloy contains the same types of phases: the primary α-Mg, Mg-Al-Sr intermetallic phase, β-$Mg_{17}Al_{12}$ intermetallic phase, and Al-Mn phases. The applied pressure has a significant influence on microstructure of AMS605 alloy. Large primary α-Mg grains and pores tend to be present in AMS605 squeeze cast under the low applied pressure. In contrast, AMS605D cast under the high pressure present a fine grain and porosity-free microstructure. The observation via SEM fractography illustrates that the fracture behavior of the squeeze cast AMS605 alloys is influenced by applied pressure levels. As the pressure increases, the fracture of AMS605 alloy tends to transit from brittle (AMS605A) to ductile (AMS605C) mode.

The results of tensile testing indicate that the mechanical properties, UTS, YS, and E_f, increase significantly with an increase in applied pressure. The applied pressure also leads to an increase in the strain-hardening rates of the alloys, which benefits the alloys to sustain during plastic deformation. The materials densification, porosity reduction, and fine grain structure should be responsible for the increase in mechanical properties.

The effect of strontium levels on tensile properties and microstructure of squeeze cast Mg-Al-Sr alloys was also investigated through experiments. Under low pressure (30 MPa), the microstructural features of the AMS-B alloys were studied via

112

metallography and SEM/EDS analysis. The microstructure for all samples of AMS-B series alloys with 3.0 wt.% Sr consists of primary α-Mg, Mg-Al-Sr secondary phase, and Al-Mn intermetallics. The strontium content has a significant influence on microstructure of AMS-B alloys. High porosity levels were found in AMS630B. In contrast, AMS600B presents a fine grain and almost porosity-free microstructure. The observed fracture of the AMS-B series alloys is brittle in nature. As strontium contents increase, the brittleness of the alloys arises.

The results of tensile testing indicate that the an increase in strontium content brings a significant decrease in UTS and E_f, and a somewhat decrease in yield strength (YS). The increase in porosity level should be responsible for the decrease in mechanical properties.

Under high pressure (90MPa), the results of tensile testing indicate that an increase in strontium content levels brings a significant decrease in E_f and slight decrease in UTS, but an increase in yield strength (YS).

CHAPTER V

CONCLUSIONS

The conclusions drawn from this study can be classified into three categories based on two research objectives:

I: Effect of pressure levels on tensile properties and microstructure of squeeze cast AMS605 alloys

1. The microstructure of the squeeze cast Mg-Al-Sr alloy with 0.5 wt.% Sr contains the primary α-Mg, the secondary β-$Mg_{17}Al_{12}$, Mg-Al-Sr and Al-Mn intermetallic phases;

2. The grain size of the alloy decreases significantly from 92.4 to 33.9 μm when applied pressure increases from 0 to 90 MPa;

3. With an increase in the applied pressure to 90 MPa, the enlongation, UTS and YS of the alloy with 0.5 wt.% Sr rise to 6.07 %, 182 MPa and 88 MPa, respectively, which results in an increase of 270 % in elongation, 153 % in UTS and 82 % in YS over the same alloy cast under 0 MPa; and

4. The material densification and porosity reduction, as well as the grain refinement should be responsible for the increase in tensile properties of the squeeze cast Mg-Al-Sr alloy.

114

II: Effect of strontium contents on tensile properties and microstructure of squeeze cast AMS-B series alloys cast under low pressure (30 MPa)

1. The Sr content influences a number of phases present in the squeeze cast Mg-Al-Sr alloys. The alloy with low amount of Sr addition (0.5 wt.%) contains the primary α-Mg, the secondary phases Mg-Al-Sr and $Mg_{17}Al_{12}$, and Al-Mn intermetallic phase. However, once Sr content increases to 3.0 wt.%, only three phases, the primary α-Mg, the secondary phases Mg-Al-Sr and Al-Mn intermetallics are present in the alloy;

2. There is a decrease in grain size with increasing the strontium content. This indicate that strontium refines the grain structure of AMS-B series alloy;

3. The results of tensile testing indicate that there are decreases of 490% in enlongation, 154% in UTS and 69% in YS when the strontium content is increased from 0 to 3.0 wt%; and

4. The increase in porosity level by Sr addition, which seems to offset its grain refinement effect, should be responsible for the decrease in tensile properties.

III: Effect of strontium contents on tensile properties and microstructure of squeeze cast AMS-B series alloys cast under high pressure (90 MPa)

1. The results of tensile testing indicate that the tensile properties of the alloys decrease by 258% in enlongation, and 34% in UTS, but, an increase of 16% in YS with the strontium content increase from 0 to 3.0 wt%; and

115

2. The variation in tensile properties of the alloys with Sr contents under high pressure should be attributed to the combining effects of the fine microstructure resulting from Sr refinement and fast cooling due to air gap elimination, and also high porosity level caused by increasing Sr addition.

CHAPTER VI
FUTURE WORK

The future work for this study will be continued in follow two research objectives:

I: Effect of pressure levels on tensile properties and microstructure of squeeze cast AMS605 alloys

1. The tensile behaviour of AMS605 alloys should be investigated at high temperature over 150 ^{0}C; and

2. The effect of casting geometry such as aspect ratio and section thicknesses on tensile behaviour and microstructure of squeeze cast Mg-Al-Sr alloys should be studied.

II: Effect of strontium content on tensile properties and microstructure of squeeze cast AMS-B and AMS-D series alloys

1. The tensile behaviour of AMS-B and AMS-D alloys should be investigate at high temperature over 150^{0}C;

2. Under high pressure condition, the tensile properties and microstructure of squeeze cast AMS-D series alloys should be studied in detail; and

3. Detailed studies on phase identification for the squeeze cast Mg-Al-Sr need to be carried out.

117

REFERENCES

[1] H. Hu, A. Yu, N. Li and J. E. Allison, " Potential Magnesium Alloys for High Temperature Die Cast Automotive Applications: A Review", Materials and Manufacturing Processes, Vol. 18, No. 5, pp. 687-717, 2003.

[2] M. M. Avedesian and H. Baker, "Magnesium and Magnesium Alloys", AMS Specialty Handbook, Publisher Materials Park, OH, ASM International, 1999, pp. 177-193

[3] William D. Callister, Jr "Materials Science and Engineering", Text book, JOHN WILEY & SONS, INC. January 1991, pp. 383-384.

[4] William F. Smith "Foundations of Materials Science and Engineering", Text book, 2004, pp. 506-508.

[5] E. Baril, P. Labelle, and M. O. Pekguleryuz, "Elevated Temperature Mg-Al-Sr: Creep Resistance, Mechanical Properties, and Microstructure", Journal of Metals, November 2003, pp. 34-39.

[6] D. Argo, M. Pekguleryue, P. Labelle, M. Dierks, T. Sparks, and T. Waltemate, "Diecastability and Properties of Mg-Al-Sr Based alloys", Magnesium Technology 2001, TMS 2001, pp. 131-136.

[7] C.A. Aliravci, J.E. Gruzleski, and F.C. Dimayuga, "Effect of Strontium on the Shrinkage Microporosity in Magnesium Sand Castings" AFS Transactions, 1993, 92-115, pp. 353~362.

[8] D. Emadi and J. E. Gruzleski, "Combating Al-Si Porosity: The Strontium/Hydrogen Myth", Modern Casting, March 1995, pp. 46-47.

[9] H. Hu, "Squeeze Casting of Magnesium Alloys and Their Composites", Journal of Materials Science, Vol. 33, 1998, pp. 1579-1589.

[10] M. Zhou, H. Hu, N. Li and J. Lo, "Microstructure and Tensile Properties of Squeeze Cast Magnesium Alloy AM50", Journal of Materials Engineering and Performance, Vol. 14, No. 4, Aug. 2005, pp. 539-545.

[11] E-book: http://www.knovel.com/knovel2/Toc.jsp?BookID=1284 (May 15, 2007) "Magnesium Technology – Metallurgy, Design Data, Application" by: Friedrich, Horst E; Mordike, Barry L.

[12] J. Polmear, "Overview: Magnesium alloys and applications", Materials Science and Technology, January 1994, Vol.10, pp. 1-15.

[13] J. Bai, Y.S. Sun, F. Xue, J. Qing and T.B. Zhu, "Influence of annealing on microstructures, mechanical and creep properties of Mg-4Al-2Sr alloy", Materials Science and Technology, 2006, vol 22, No. 10, pp. 1208~1212.

[14] A. Luo, M. O. Pekguleryuz, "Review: Cast Magnesium Alloys for Elevated Temperature Applications", Journal of Materials Science, 29 (1994), pp. 5259~5271.

[15] M. O. Pekguleryuz, M. M. Avedesian, "Magnesium Alloying, Some Potentials for Alloy Development", Institute of Magnesium Technology (ITM), Quebec, Canada (Paper), 1990.

[16] M. O. Pekguleryuz, "Development of Creep Resistant Magnesium Diecasting Alloys—an Overview", Paper presented at the Magnesium Automotive Seminar, Aalen, Germany, September 29-30, 1999.

[17] Y. J. Chung and K. S. Shin, "Effect of Precipitates and Alloying Element on Microstructure and High Temperature Properties of Mg-Al", Materials Science Forum, Vols. 475-479, 2005, pp. 537-540.

[18] J. Kim, B. Park, J. Jun, K. Kim and W. Jung, "Microstructure and Properties of Mg-Al Based Casting Alloys Modified with Minor Alloying Elements", Materials Science Forum, Vols. 488-489, 2005, pp. 147-150.

[19] R. K. Singh, "Ductility troughs in Mg-Li alloys", Journal of Materials Science Letters, Vols. 13, January, 1994, pp. 744-745.

[20] H. Hu, M. Masoumi and N. Li, "Effect of Pressures Levels on Tensile Properties of Squeeze Cast Mg-Al-Ca Alloys", Magnesium Technology, 2007, Orlando, FL, TMS2007, pp. 109-114.

[21] A book edited by H. G. Paris, W.H. Hunt, "Advances in Magnesium alloys and Composites", The Minerals, Metals, & Materials Society, 1988, pp. 25-40.

[22] P. Zhao, Q. Wang, C. Zhai, and Y. Zhu, "Effects of Strontium and Titanium on the Microstructure, Tensile Properties and Creep Behavior of AM50 Alloys" Materials Science and Engineering :A Vol. 444, Issues 1-2, 25 January 2007, pp. 318-326.

[23] N.D. Saddock, A. Suzuki, K. Wu, S.C. Wildy, Y.A. Chang, T.M. Pollock and J. W. Jones, "Solidification and Microstructure of Mg-Al- (Ca, Sr, Ce, La) Ternary Alloys", Magnesium Technology 2005, TMS 2005, pp. 121-126.

[24] M.A. Parvez, M. Medraj, E. Essadiqi, A. Muntasar, and G. Denes, "Experimental study of the ternary Magnesium-aluminum-strontium system", Journal of Alloys and Compounds, 402, 2005, pp.170-185.

[25] Internet information: Strontium (May 2007)

http://en.wikipedia.org/wiki/Strontium.

[26] E-book: http://www.knovel.com/knovel2/Toc.jsp?BookID=688 (May 2007)
"Handbook of Inorganic Chemicals" by: Patnaik, Pradvot.

[27] Internet information: Strontium (May 2007)

http://periodic.lanl.gov/elements/38.html.

[28] Internet information: Strontium Products, Http://www.timminco.com, (March 2006).

[29] Internet information: Strontium

http://www.webelements.com/webelements/elements/text/Sr/, (April 2006).

[30] X. Zeng, Y. Wang, W. Ding, A. A. Luo and A. K. Sachdev, "Effect of Strontium on the Microstructure, Mechanical Properties, and Fracture Behavior of AZ31 Magnesium Alloy" Metallurgical and Materials Transactions A, Vol. 37A, April 2006, pp. 1333~1341.

[31] Kinji Hirai, Hidetoshi Somekawa, Yorinobu Takigawa, and Kenji Higashi, "Effects of Ca and Sr addition on mechanical properties of a cast AZ91 magnesium alloy at room and elevated temperature", Materials Science and Engineering A, Vol. 403, Issues 1-2, 25 August 2005, pp. 276-280.

[32] C.M. Dinnis, M.O. Otte, A.K. Dahle and J.A. Taylor, "The Influence of Strontium on Porosity Formation in Al-Si Alloys", Metallurgical and Materials Transactions A, Vol. 35A, November 2004, pp. 3531-3541.

121

[33] J.E. Gruzleski and C. A. Aliravci: U.S. Patent No. 5, 143, 564, 1992.

[34] Y. Wang, X. Zeng, W. Ding, A.A. Luo and A.K. Sachdev, "Effect of Strontium on the Microstructure and Mechanical Properties of AZ31Magnesium Alloy", Magnesium Technology 2005, TMS 2005, pp. 85-89.

[35] S. Li, W. Zheng, B. Tang and D. Zeng, "Effects of Rare Earths and Strontium Composite Additions on Microstructure and Properties of AM60 Magnesium Alloy", Foundry, January 2007, Vol.56, No.1, pp.18-22.

[36] D. Argo, M. Pekguleryue, P. Labelle, P. Vermette, R. Bouchard and M. Lefebvre, "Process Parameters and Diecasting of Noranda's AJ52 High Temperature Mg-Al-Sr alloy", Magnesium Technology 2002, TMS 2002, pp. 87-92.

[37] J. R. Franklin and A. A. Das, "Squeeze Casting- A Review of the Status", Br. Foundryman 77,1984, pp. 150-158.

[38] T. Ueno, M. Uichida, and M. Sose, "Squeeze Casting: Present and Future", proc.17th Int. Die Casting Congress and Exposition (Cleveland, OH, Oct. 1993), NADCA, 1993, pp. 413-418.

[39] J. Bai, Y. S. Sun, F. Xue, S. Xue, J. Qiang and T. B. Zhu, "Influence of annealing on microstructures, mechanical and creep properties of Mg-4Al-2Sr alloy", Materials Science and Technology, Vols. 22, 2006, pp. 1208-1212.

[40] Y. Fan, G. Wu and C. Zhai: "Effect of Strontium on Mechanical Properties and Corrosion Resistance of AZ91D", Materials Science Forum, Vols. 546-549, 2007, pp. 567-570.

[41] M. Zhou, "An Experimental Study of Die and Squeeze Cast Magnesium Alloy AM50", Master Thesis, University of Windsor, Windsor, Ontario, Canada, 2004

[42] A. Luo, H. Hu, and S. Lo, "Microstructure and Mechanical Properties of Squeeze Cast AZ91D Magnesium Alloy", Light Metals 1996, Montreal, Quebec, Canada, August, 1996, pp. 375~387.

[43] F. Yu, "Mathematical Modeling and Experimental Study of Squeeze Casting of Magnesium Alloy AM50A and Aluminum Alloy A356", PH.D. Thesis, University of Windsor, Windsor, Ontario, Canada, 2006.

[44] PROCEDURE FOR THE SAFE HANDLING OF THE PURE MAGNESIUM AND MAGNESIUM ALLOYS, Department of Mechanical, Automotive and Materials Engineering of University of Windsor, 2006

[45] "Standard Test Method for Density of High-Modulus Fibers", D3800-99, ASTM Standards, ASTM, Vol 15.03, 2002, pp. 186-187.

[46] "Standard Test Method for Dry and Wet Bulk Density, Water Absorption, and Apparent Porosity of Thin Sections of Glass-Fiber Reinforced Concrete," C948-81, ASTM Standards, ASTM, Vol 04.05, 2002, pp. 588-589.

[47] "Standard Test Methods of Tensile Testing Wrought and Cast Aluminum- and Magnesium-Alloy Products," B557M, ASTM Standards, ASTM, Vol 02.02, 2002, pp. 424.

APPENDIIX I: Mg-Al-Sr ALLOY PROPERTIES

		AMS600A	AMS600B	AMS600C	AMS600D
AMS600	Density (g/cm^3)	1.760138	1.767676	1.771696	1.772994
	UTS (MPa)	82.36	149.65	176.35	189.04
	YS (MPa)	46.62	77.13	76.14	74.65
	Ef	0.0179	0.0380	0.0569	0.0641
		AMS605A	AMS605B	AMS605C	AMS605D
AMS605	Density (g/cm^3)	1.760991	1.767709	1.774053	1.781138
	UTS (MPa)	71.74	138.22	165.68	181.83
	YS (MPa)	42.83	70.36	68.85	76.84
	Ef	0.016	0.0285	0.0502	0.0607
		AMS615A	AMS615B	AMS615C	AMS615D
AMS615	Density (g/cm^3)	1.768069	1.774304	1.778406	1.792715
	UTS (MPa)	70.69	96.24	156.09	170.86
	YS (MPa)	45.91	63.24	67.75	84.93
	Ef	0.0105	0.0119	0.0371	0.0397
		AMS620A	AMS620B	AMS620C	AMS620D
AMS620	Density (g/cm^3)	1.778101	1.785182	1.800502	1.806346
	UTS (MPa)	60.85	92.67	142.78	149.95
	YS (MPa)	39.21	56.07	86.86	85.72
	Ef	0.0098	0.0129	0.0236	0.0237
		AMS630A	AMS630B	AMS630C	AMS630D
AMS630	Density (g/cm^3)	1.784163	1.789121	1.810533	1.819216
	UTS (MPa)	41.89	58.93	130.34	141.02
	YS (MPa)	32.01	45.61	73.65	86.35
	Ef	0.0056	0.0064	0.0165	0.0179

124

APPENDIX II: DENSITY AND POROSITY DATA

AMS600A

	$A=W_a-0.006$	$B=W_w-0.006$	Density (g/cm^3) $C=A/(A-B)$	Porosity (%) $D=(1.772-C)/1.772$
1	1.7651	0.7681	1.770411	0.000897
2	1.7631	0.7660	1.768228	0.002129
3	1.7628	0.7573	1.753158	0.010633
4	1.7327	0.7429	1.750556	0.012102
5	1.7448	0.7525	1.758339	0.007709
Average			**1.760138**	**0.006694**

AMS600B

	$A=W_a-0.006$	$B=W_w-0.006$	Density (g/cm^3) $C=A/(A-B)$	Porosity (%) $D=(1.772-C)/1.772$
1	1.7726	0.7711	1.769950	0.001160
2	1.7816	0.7749	1.769743	0.001274
3	1.7721	0.7713	1.770683	0.000743
4	1.7759	0.7683	1.762505	0.005358
5	1.7738	0.7691	1.765502	0.003667
Average			**1.767676**	**0.002440**

AMS600C

	A=W_a -0.006	B=W_w -0.006	Density (g/cm^3) C=A/(A-B)	Porosity (%) D=(1.772-C)/1.772
1	1.7655	0.7703	1.774015	-0.001140
2	1.7615	0.7666	1.770530	0.000830
3	1.7691	0.7696	1.769985	0.001137
4	1.7738	0.7738	1.773800	-0.001.20
5	1.7636	0.7673	1.770150	0.001044
Average			**1.771696**	**0.000172**

AMS600D

	A=W_a -0.006	B=W_w -0.006	Density (g/cm^3) C=A/(A-B)	Porosity (%) D=(1.772-C)/1.772
1	1.7686	0.7702	1.771430	
2	1.7733	0.7709	1.769054	
3	1.7672	0.7726	1.776795	
4	1.7634	0.7689	1.773152	
5	1.7575	0.7671	1.774536	
Average			**1.772994**	**0**

126

AMS605A

	$A=W_a -0.009$	$B=W_w -0.009$	Density (g/cm^3) $C=A/(A-B)$	Porosity (%) $D=(1.781-C)/1.781$
1	1.7748	0.7572	1.774100	0.020717
2	1.7741	0.7748	1.775343	0.003176
3	1.7782	0.7644	1.753995	0.015163
4	1.7792	0.7724	1.767183	0.007758
5	1.7758	0.7693	1.764332	0.009359
Average			**1.760991**	**0.011255**

AMS605B

	$A=W_a -0.009$	$B=W_w -0.009$	Density (g/cm^3) $C=A/(A-B)$	Porosity (%) $D=(1.781-C)/1.781$
1	1.7638	0.7696	1.774090	0.003880
2	1.7712	0.7708	1.770492	0.005900
3	1.7830	0.7729	1.765172	0.008887
4	1.7898	0.7835	1.778595	0.001350
5	1.7782	0.7622	1.750197	0.017295
Average			**1.767709**	**0.007463**

AMS605C

	A=W_a -0.009	B=W_w -0.009	Density (g/cm^3) C=A/(A-B)	Porosity (%) D=(1.781-C)/1.781
1	1.7603	0.7661	1.770570	0.005857
2	1.7806	0.7768	1.773859	0.004009
3	1.7756	0.7731	1.771172	0.005518
4	1.7751	0.7757	1.776166	0.002714
5	1.7881	0.7827	1.778496	0.001406
Average			**1.774053**	**0.003901**

AMS605D

	A=W_a -0.006	B=W_w -0.006	Density (g/cm^3) C=A/(A-B)	Porosity (%) D=(1.781-C)/1.781
1	1.7511	0.7659	1.777410	
2	1.7471	0.7709	1.789695	
3	1.7440	0.7658	1.782866	
4	1.7406	0.7614	1.777574	
5	1.7433	0.7629	1.778152	
Average			**1.781138**	**0**

AMS615A

	A=W_a -0.009	B=W_w -0.009	Density (g/cm^3) C=A/(A-B)	Porosity (%) D=(1.793-C)/1.793
1	1.8056	0.7813	1.762765	0.016863
2	1.8075	0.7815	1.768437	0.013700
3	1.8123	0.7832	1.767768	0.014073
4	1.8091	0.7843	1.772101	0.011656
5	1.8103	0.7832	1.769276	0.013231
Average			**1.768069**	**0.013904**

AMS615B

	A=W_a -0.009	B=W_w -0.009	Density (g/cm^3) C=A/(A-B)	Porosity (%) D=(1.793-C)/1.793
1	1.7711	0.7653	1.760890	0.017911
2	1.7726	0.7714	1.770475	0.012562
3	1.7737	0.7745	1.775120	0.009972
4	1.7745	0.7723	1.770605	0.012490
5	1.7982	0.7961	1.794432	-0.000798
Average			**1.774304**	**0.010327**

AMS615C

	$A=W_a-0.009$	$B=W_w-0.009$	Density (g/cm^3) $C=A/(A-B)$	Porosity (%) $D=(1.793-C)/1.793$
1	1.7605	0.7715	1.780082	0.007211
2	1.7577	0.7688	1.777429	0.008684
3	1.7602	0.7713	1.779958	0.007274
4	1.7642	0.7710	1.776279	0.009326
5	1.7621	0.7772	1.778282	0.008208
Average			**1.778406**	**0.008140**

AMS615D

	$A=W_a-0.009$	$B=W_w-0.009$	Density (g/cm^3) $C=A/(A-B)$	Porosity (%) $D=(1.793-C)/1.793$
1	1.7388	0.7738	1.801871	
2	1.7358	0.7698	1.796894	
3	1.7351	0.7705	1.798777	
4	1.7331	0.7627	1.785965	
5	1.7329	0.7594	1.780072	
Average			**1.792715**	**0**

130

AMS620A

	$A=W_a -0.009$	$B=W_w -0.009$	Density (g/cm^3) $C=A/(A-B)$	Porosity (%) $D=(1.806-C)/1.806$
1	1.8305	0.8060	1.791362	0.008106
2	1.8235	0.7799	1.751638	0.030101
3	1.8248	0.7958	1.777908	0.015555
4	1.8296	0.8033	1.787317	0.010345
5	1.8266	0.7991	1.782281	0.013133
Average			**1.778101**	**0.015448**

AMS620B

	$A=W_a -0.009$	$B=W_w -0.009$	Density (g/cm^3) $C=A/(A-B)$	Porosity (%) $D=(1.806-C)/1.806$
1	1.8245	0.8031	1.786270	0.010923
2	1.8278	0.8010	1.780093	0.014345
3	1.8296	0.8064	1.788116	0.009903
4	1.8293	0.8067	1.788872	0.009484
5	1.8207	0.7993	1.782553	0.012983
Average			**1.785182**	**0.011527**

131

AMS620C

	A=W_a -0.009	B=W_w -0.009	Density (g/cm^3) C=A/(A-B)	Porosity (%) D=(1.806-C)/1.806
1	1.8111	0.8076	1.804783	0.000674
2	1.8223	0.8097	1.799625	0.003530
3	1.8194	0.8083	1.799426	0.003640
4	1.8178	0.8074	1.799089	0.003826
5	1.8228	0.8099	1.799585	0.003552
Average			**1.800502**	**0.003044**

AMS620D

	A=W_a -0.009	B=W_w -0.009	Density (g/cm^3) C=A/(A-B)	Porosity (%) D=(1.806-C)/1.806
1	1.7869	0.7976	1.806231	
2	1.7781	0.7938	1.806461	
3	1.7779	0.7925	1.804242	
4	1.7768	0.7933	1.806609	
5	1.7789	0.7951	1.808193	
Average			**1.806346**	**0**

AMS630A

	$A=W_a-0.009$	$B=W_w-0.009$	**Density (g/cm^3)** $C=A/(A-B)$	**Porosity (%)** $D=(1.819-C)/1.819$
1	1.8317	0.8038	1.781983	0.020350
2	1.8277	0.8042	1.785735	0.018287
3	1.8452	0.8115	1.785044	0.018667
4	1.8311	0.8033	1.781572	0.020576
5	1.8290	0.8052	1.786482	0.017877
Average			**1.784163**	**0.019152**

AMS630B

	$A=W_a-0.009$	$B=W_w-0.009$	**Density (g/cm^3)** $C=A/(A-B)$	**Porosity (%)** $D=(1.819-C)/1.819$
1	1.8234	0.8071	1.794155	0.013658
2	1.8223	0.8003	1.783072	0.019751
3	1.8291	0.8074	1.790252	0.015805
4	1.8238	0.8069	1.793490	0.014024
5	1.8239	0.8019	1.784638	0.018891
Average			**1.789121**	**0.016426**

133

AMS630C

	$A=W_a -0.009$	$B=W_w -0.009$	Density (g/cm³) $C=A/(A-B)$	Porosity (%) $D=(1.819-C)/1.819$
1	1.8423	0.8229	1.807240	0.006465
2	1.8251	0.8167	1.809897	0.005004
3	1.8173	0.8139	1.811142	0.004320
4	1.8052	0.8095	1.812996	0.003301
5	1.8161	0.8135	1.811390	0.004183
Average			**1.810533**	**0.004655**

AMS630D

	$A=W_a -0.009$	$B=W_w -0.009$	Density (g/cm³) $C=A/(A-B)$	Porosity (%) $D=(1.819-C)/1.819$
1	1.8368	0.8195	1.805564	
2	1.8337	0.8286	1.824396	
3	1.8359	0.8318	1.828404	
4	1.8329	0.8312	1.829789	
5	1.8195	0.8131	1.807929	
Average			**1.819216**	**0**

APPENDIX III. PHOTOGRAPHS OF GRAIN SIZE

MEASUREMENT

AMS605A

AMS605B

136

AMS605C

AMS605D

137
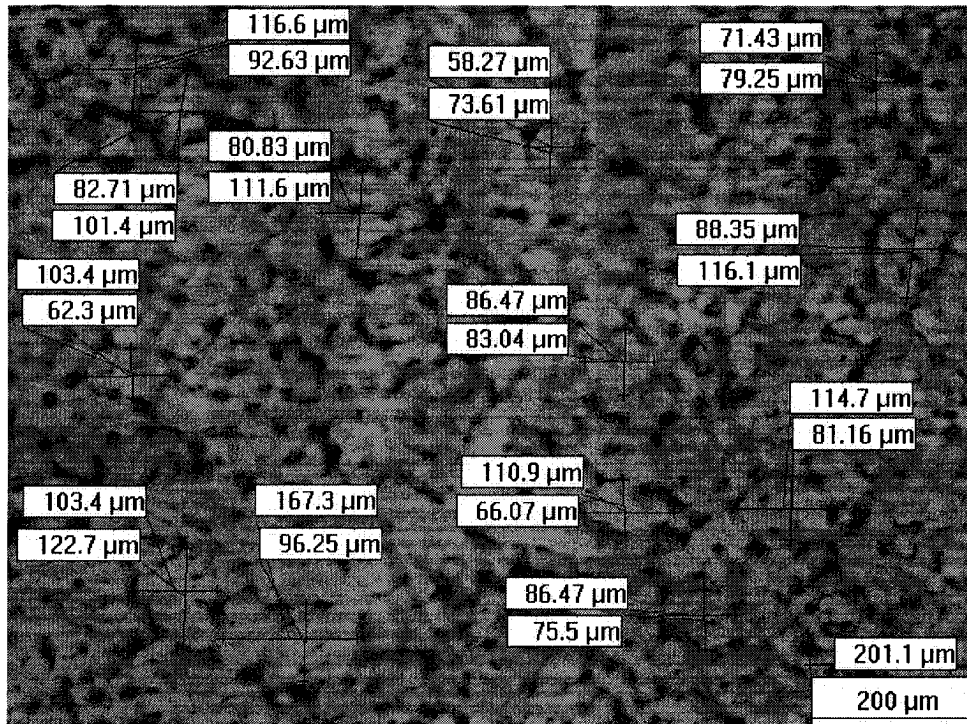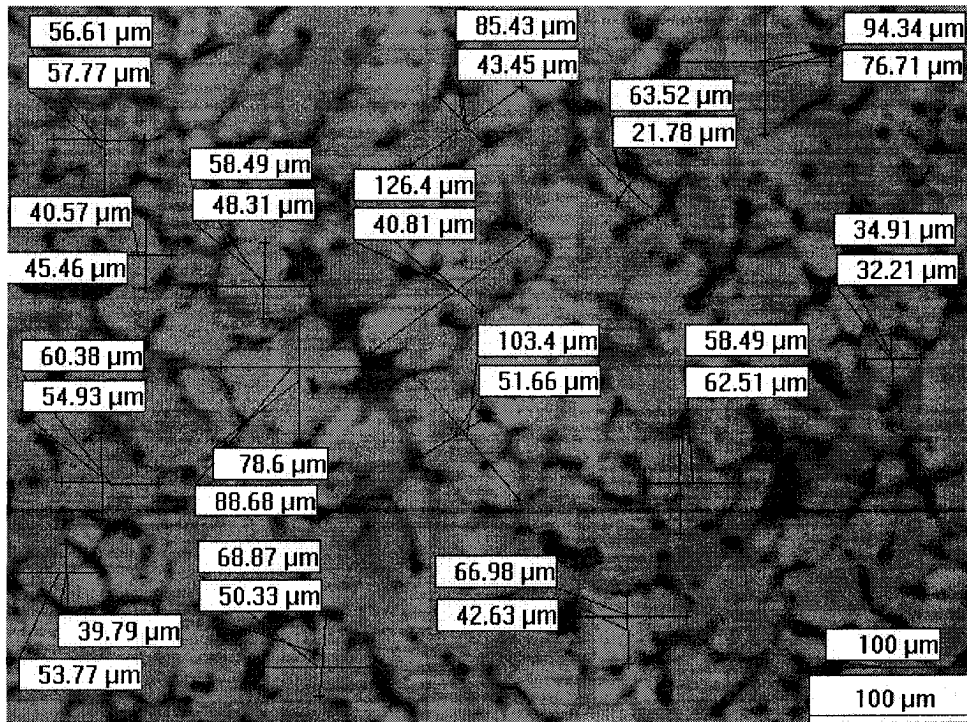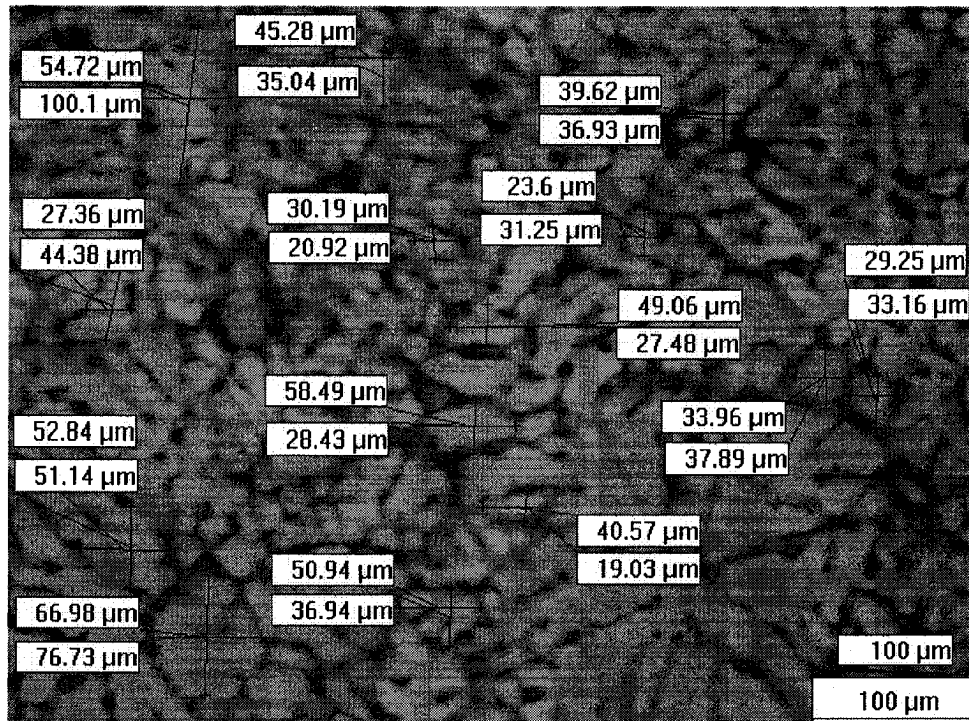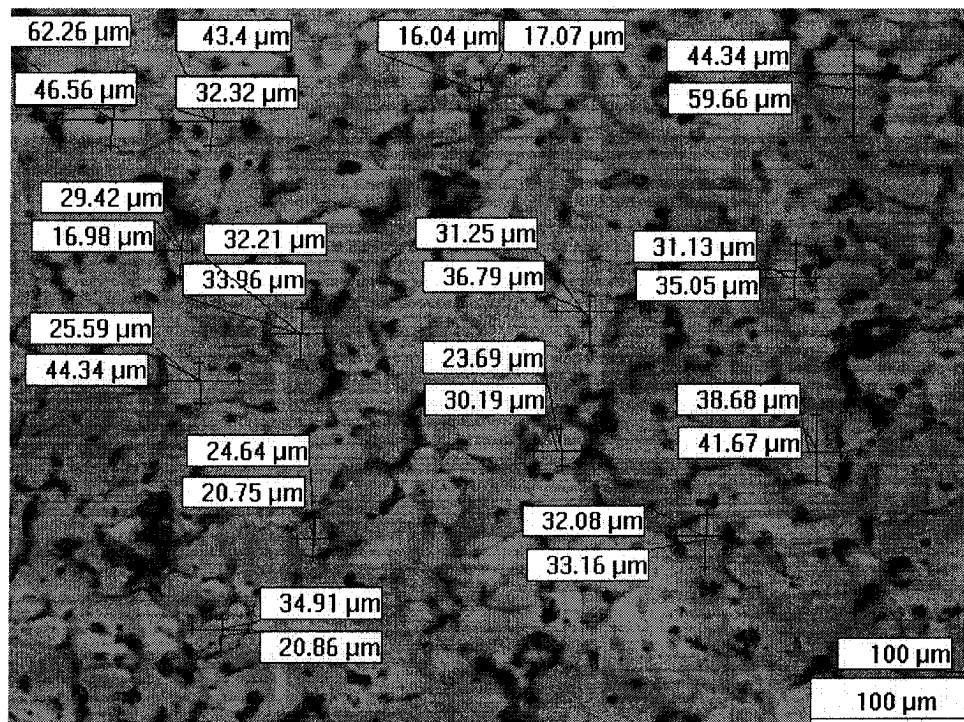
APPENDIX IV. GRAIN SIZE DATA

No.	Grain size (µm)			
	AMS605A	AMS605B	AMS605C	AMS605D
1	116.6	56.61	54.7	62.26
	92.63	57.77	100.1	46.56
2	82.71	40.57	27.36	43.4
	101.4	45.46	44.38	32.32
3	103.4	60.38	52.84	16.98
	62.3	54.93	54.14	29.42
4	103.4	53.77	66.98	33.96
	122.7	39.79	76.73	32.21
5	80.83	58.49	45.28	44.34
	111.6	48.31	35.04	25.59
6	167.3	88.68	30.19	20.75
	96.25	78.6	20.92	24.64
7	86.47	68.87	58.49	36.79
	83.04	50.33	28.43	31.25
8	110.9	85.43	50.94	30.19
	66.07	43.45	36.94	23.69
9	88.35	126.4	39.62	32.08
	116.1	40.81	36.93	33.16
10	71.43	103.4	23.6	44.34
	79.25	51.66	31.25	59.66
11	58.27	66.98	49.06	31.13
	73.61	42.63	27.48	35.05
12	114.7	94.34	33.96	38.68
	81.16	76.71	37.89	41.67
13	86.47	63.52	29.25	16.04
	75.5	21.78	33.16	17.07
Average	**92.4015**	**62.2758**	**43.2946**	**33.9842**

138

No.	Grain size (μm)			
	AMS600B	**AMS615B**	**AMS620B**	**AMS630B**
1	70.75	58.52	33.02	45.37
	61.56	62.51	34.09	52.09
2	52.08	59.46	37.74	42.45
	52.09	65.35	37.88	45.46
3	35.85	69.81	46.23	33.98
	55.88	59.66	37.13	35.15
4	62.26	44.34	43.41	22.73
	82.41	55.94	58.72	45.28
5	71.80	60.38	71.7	34.91
	65.34	25.59	55.9	30.36
6	54.73	52.83	32.08	52.83
	54.14	89.96	41.71	54.93
7	49.06	59.43	83.98	33.96
	69.82	38.84	66.32	31.48
8	60.38	42.45	43.4	37.74
	63.51	53.98	41.71	35.99
9	72.83	38.68	46.24	59.44
	65.54	45.49	42.66	42.66
10	53.77	73.58	51.89	17.92
	100.5	59.73	67.24	17.05
Average	**62.71**	**55.83**	**48.65**	**38.59**

APPENDIX V: TENSILE PROPERTIES CURVES

AMS600 alloy (AM60B ALLOY)
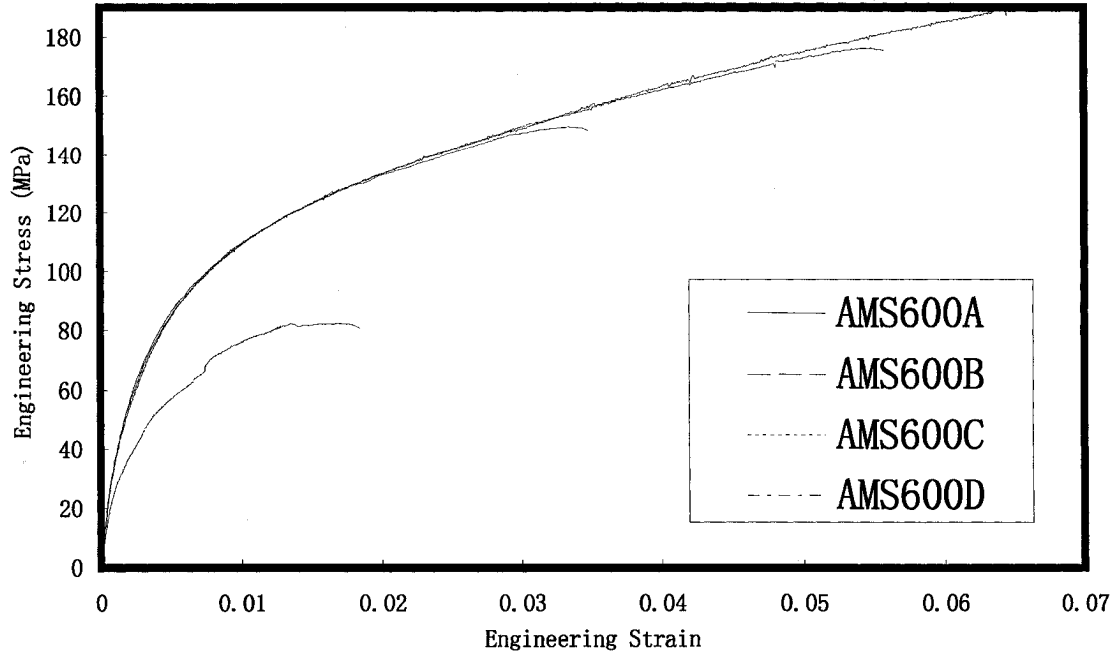
AMS605 alloy (0.5 wt% Sr)
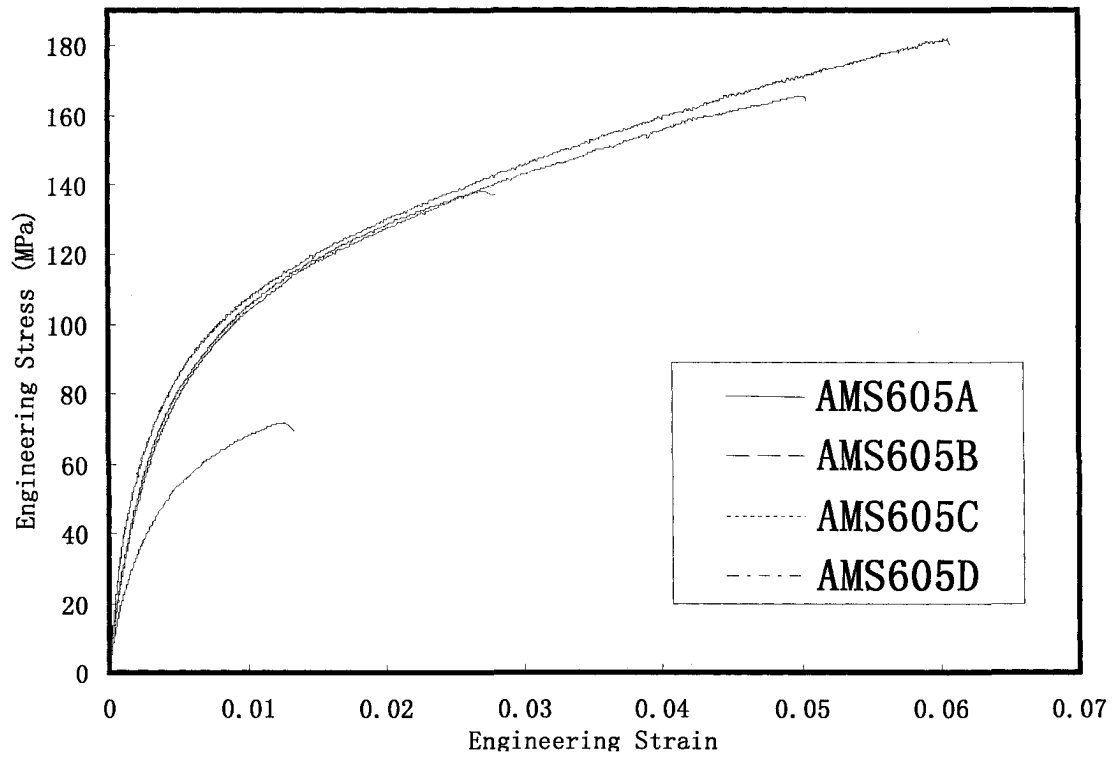
AMS615 alloy (1.5 wt% Sr)

141
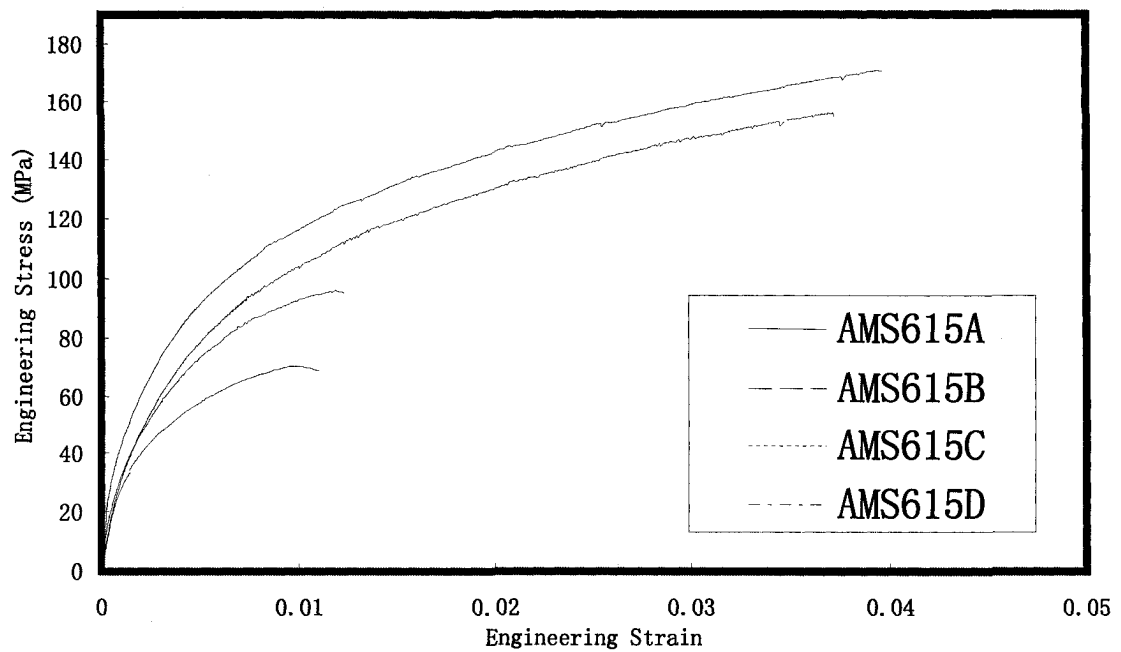
AMS620 alloy (2.0 wt% Sr)
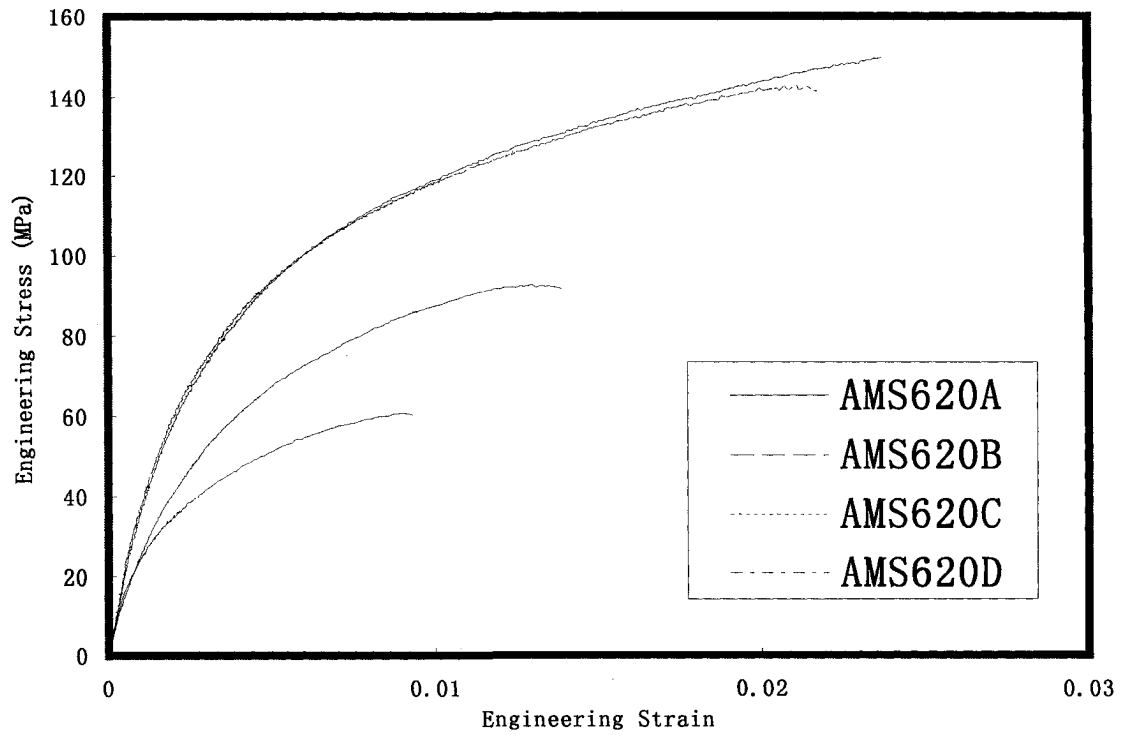
AMS630 alloy (3.0 wt% Sr)
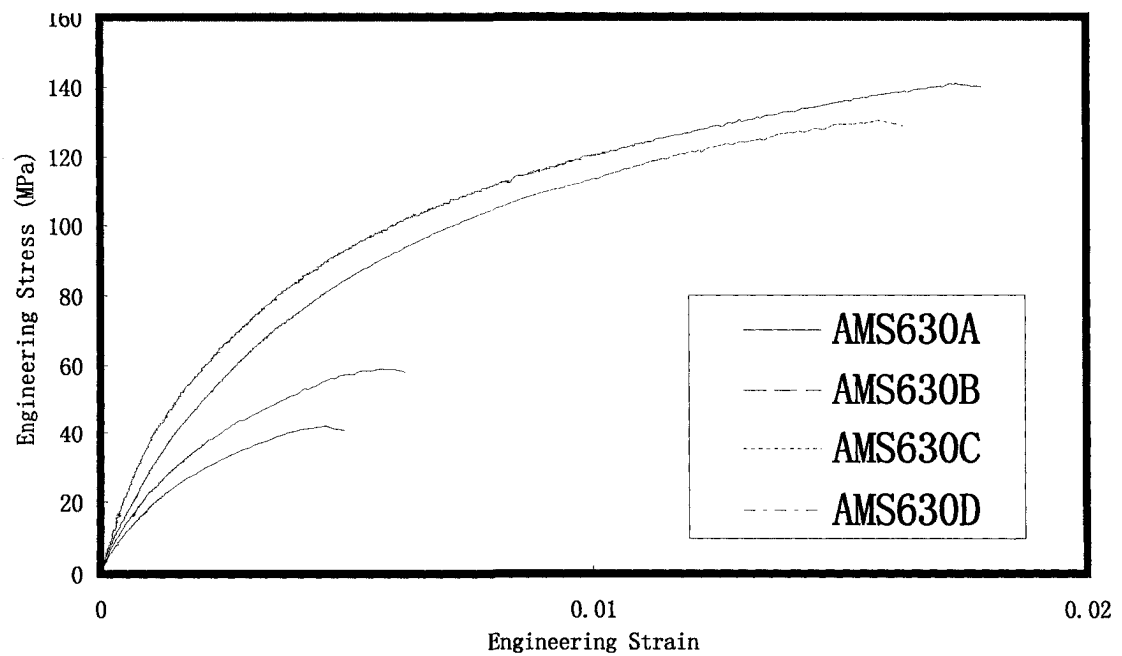
AMS-A SERIES ALLOY (0 MPa)
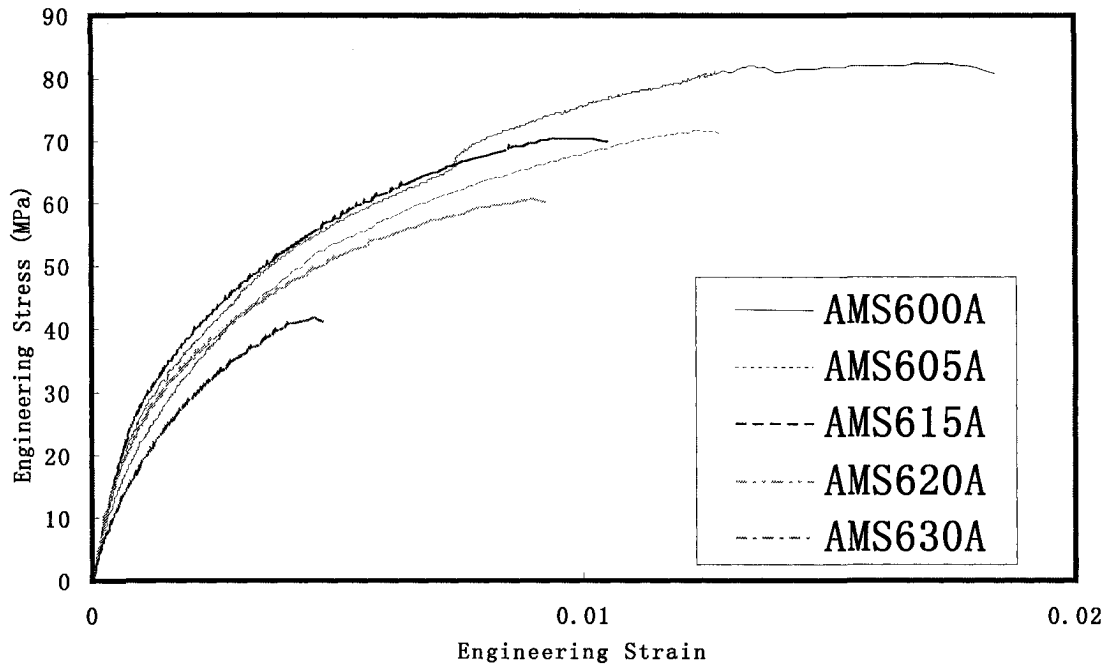
AMS-B SERIES ALLOY (30 MPa)

143
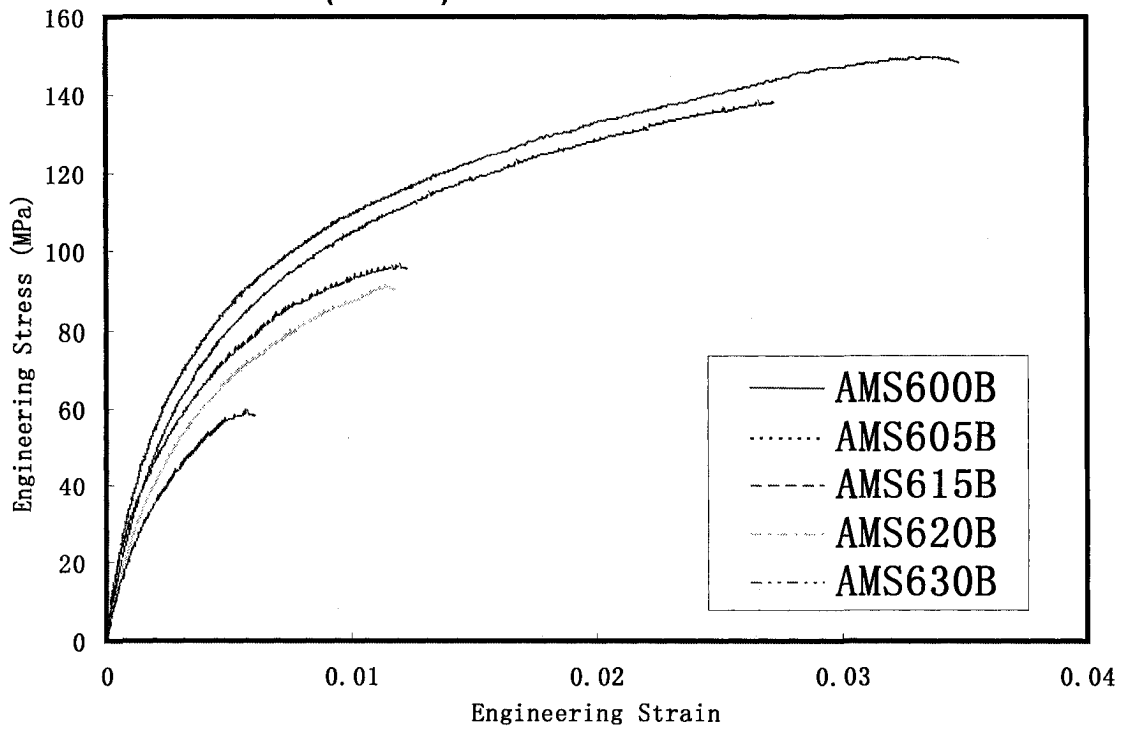
AMS-C SERIES ALLOY (60 MPa)
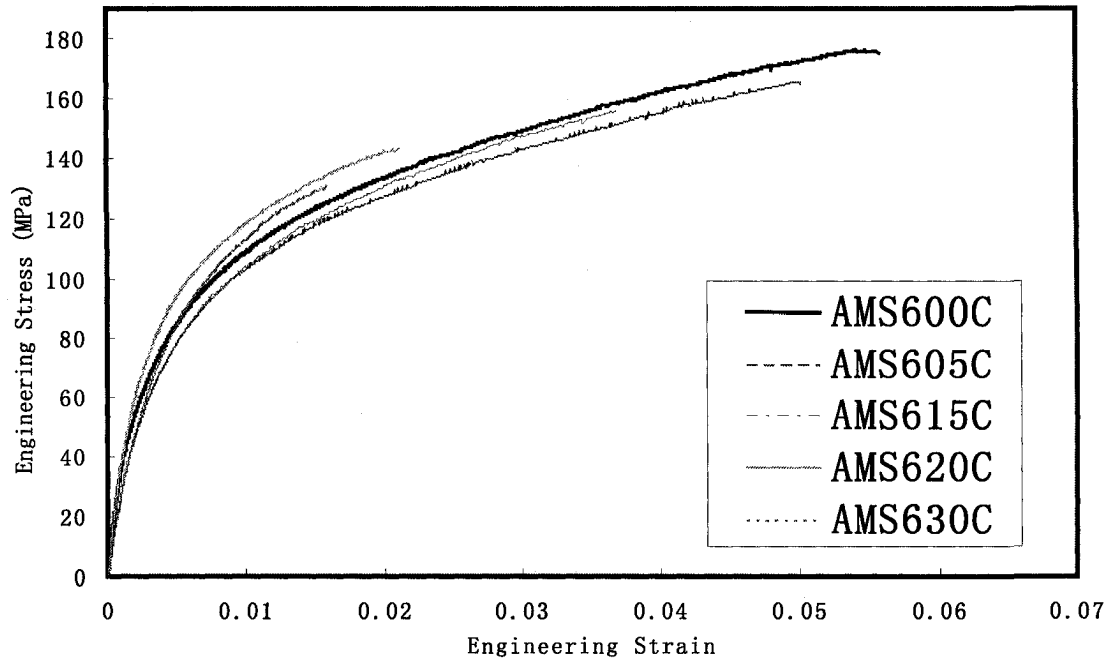
AMS-D SERIES ALLOY (90 MPa)
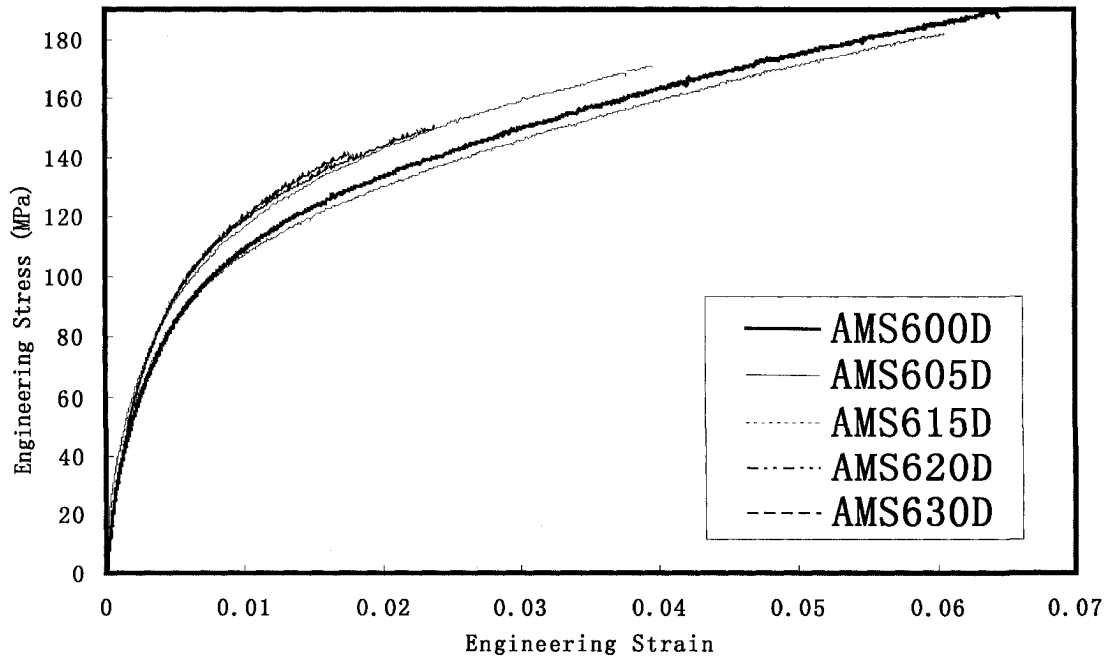
APPENDIX VI: FRACTURE SURFACE

145

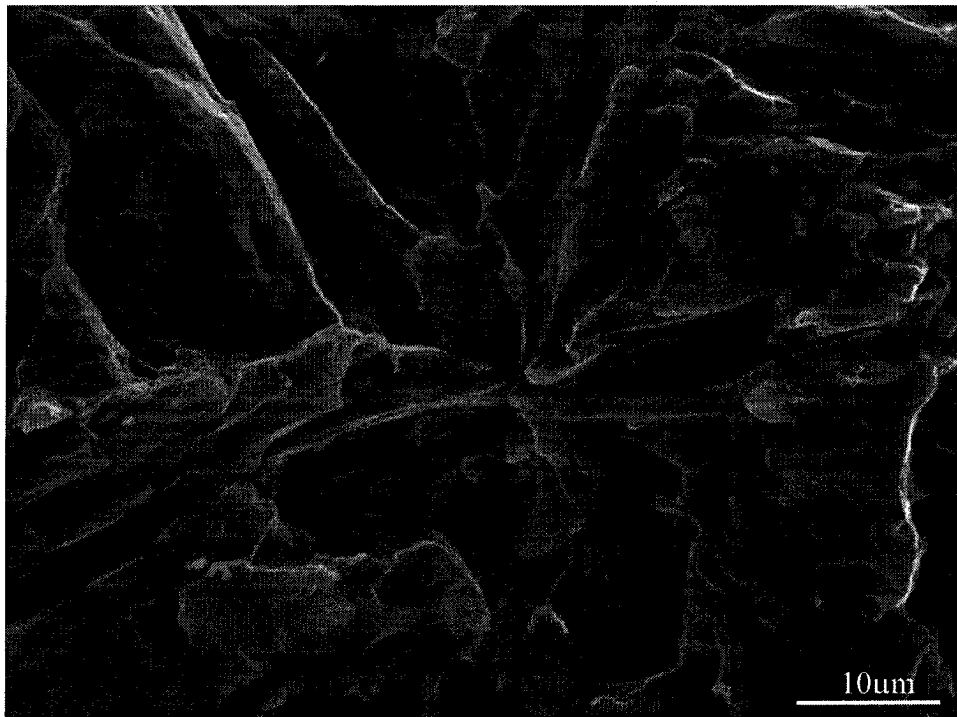AMS605A (X500)

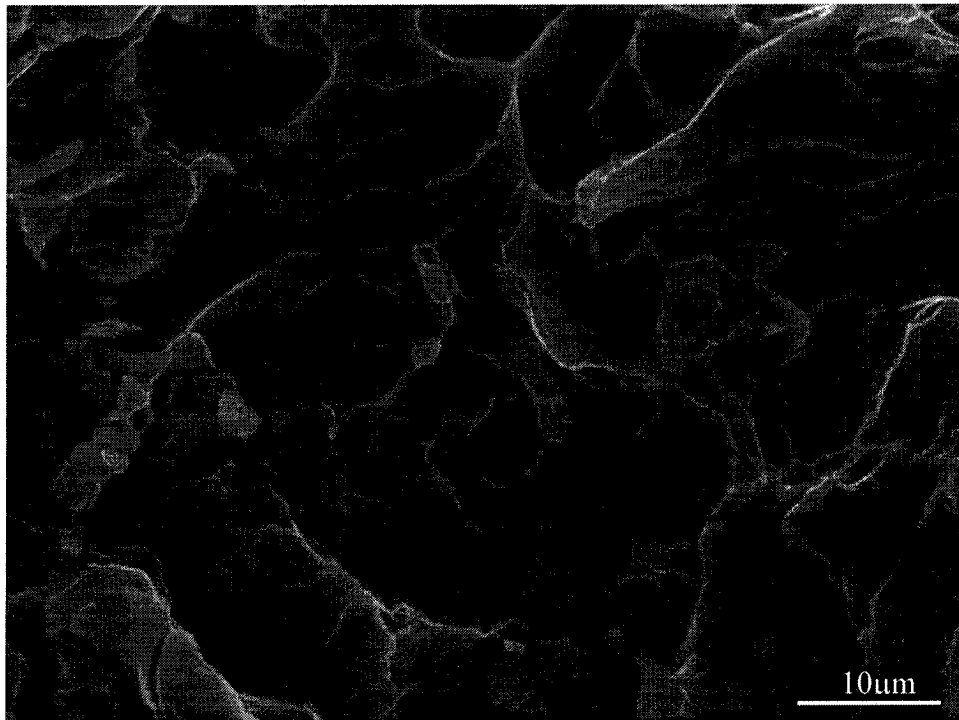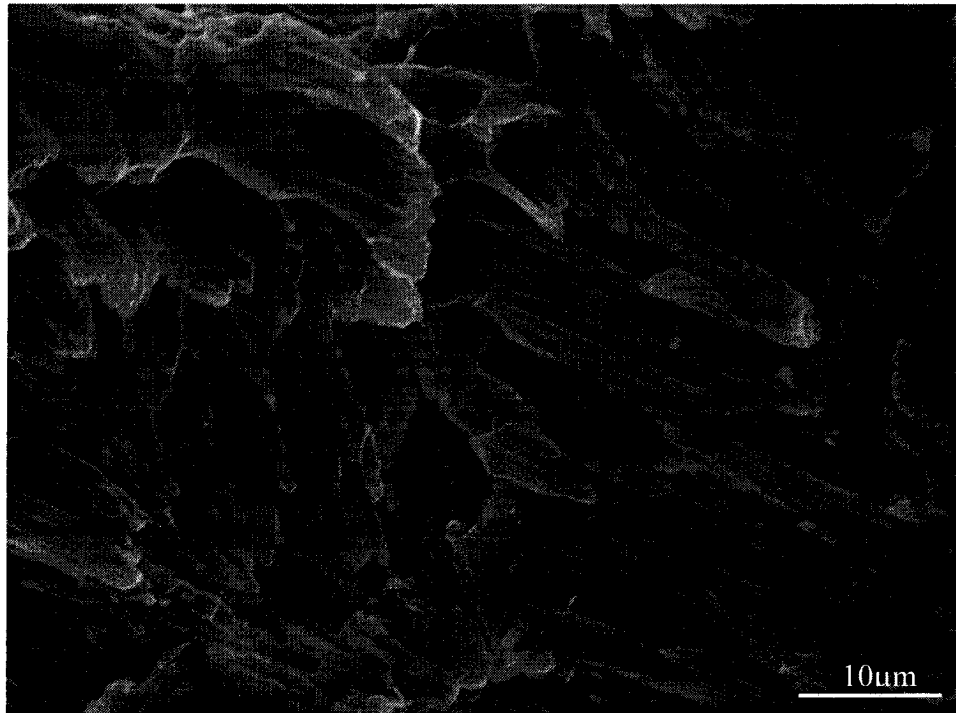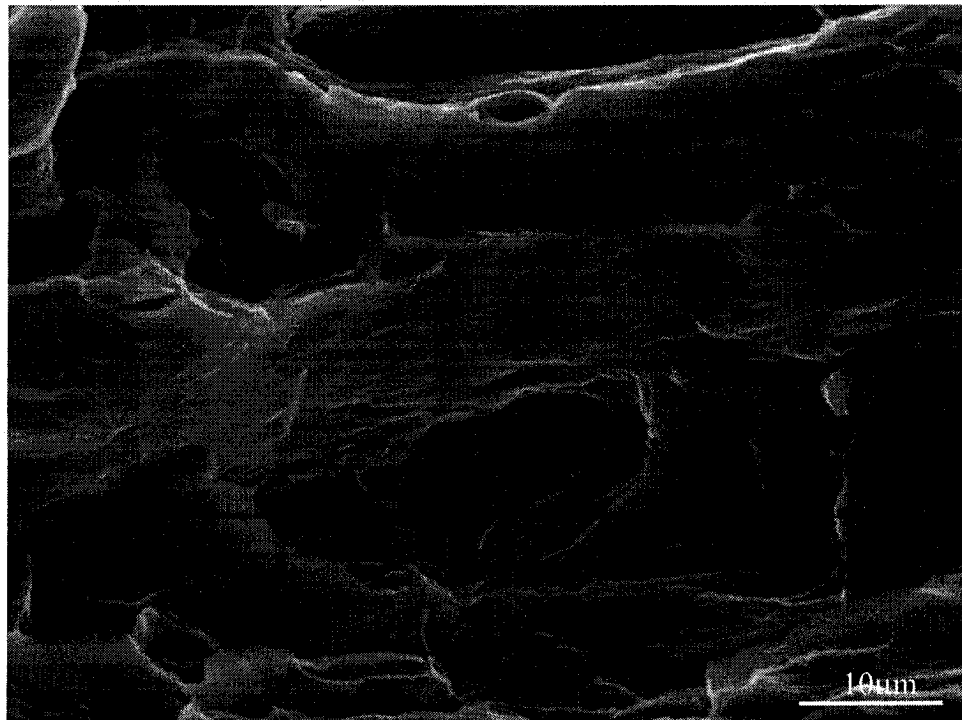AMS605A (X3000)

146

AMS605B (X500)

AMS605B (X3000)

147
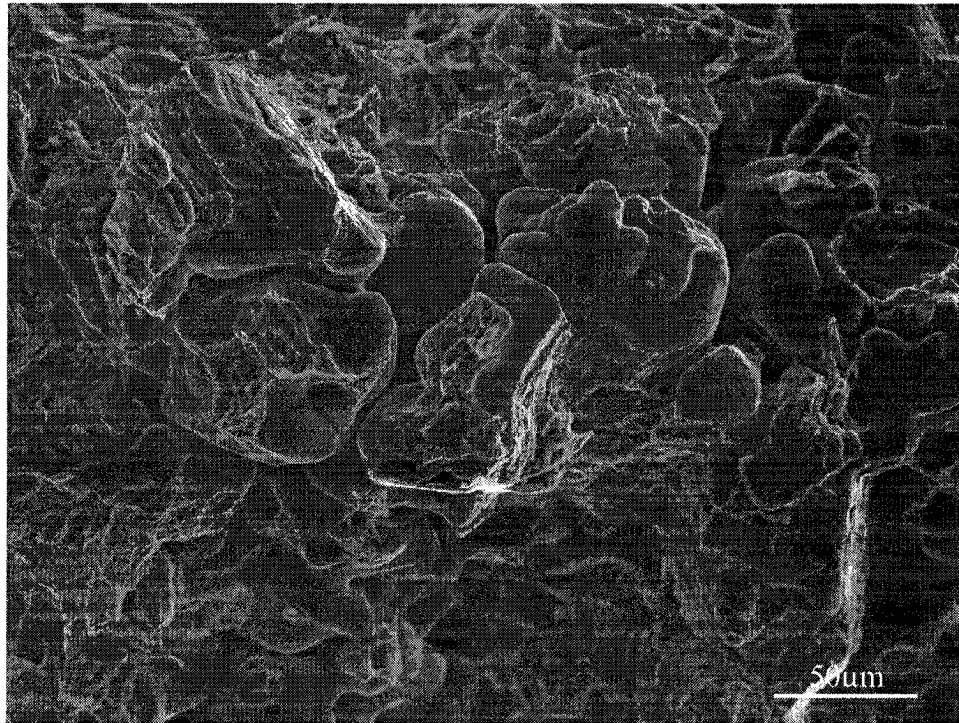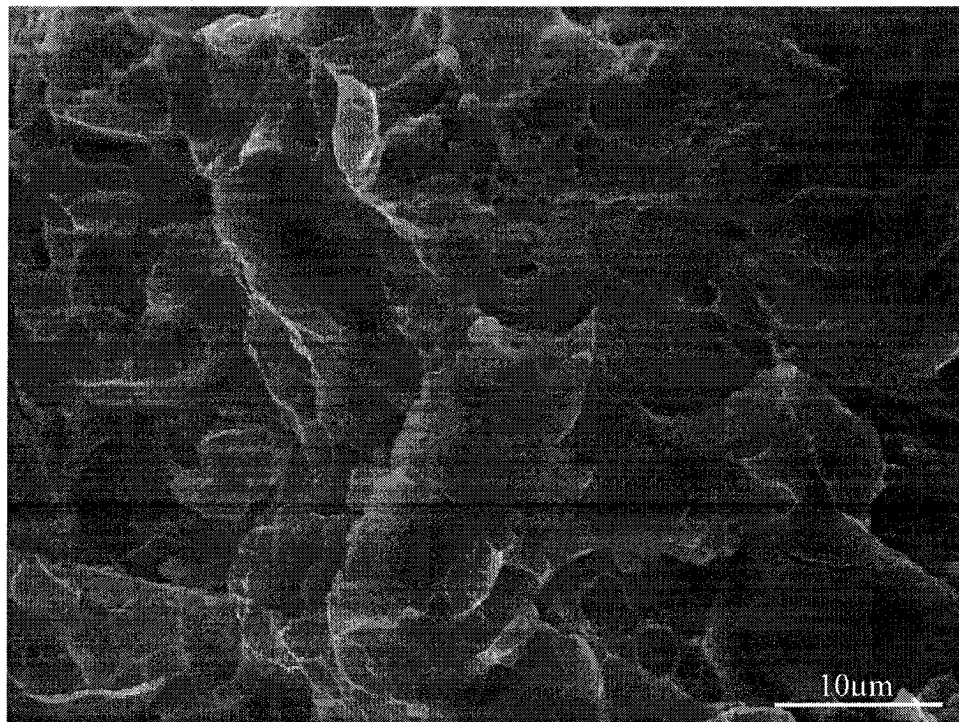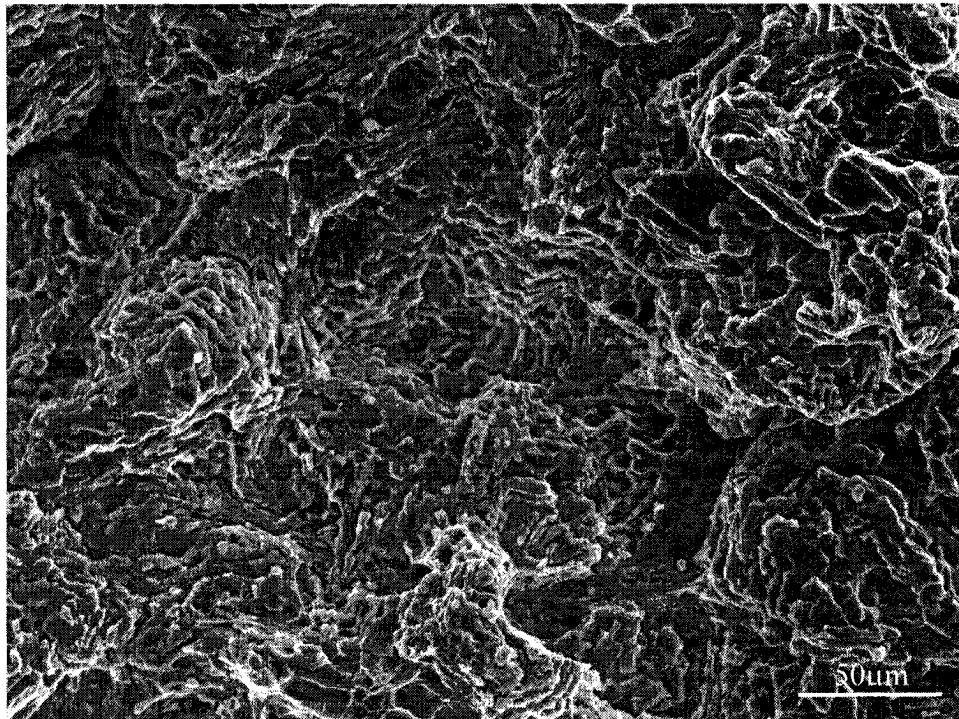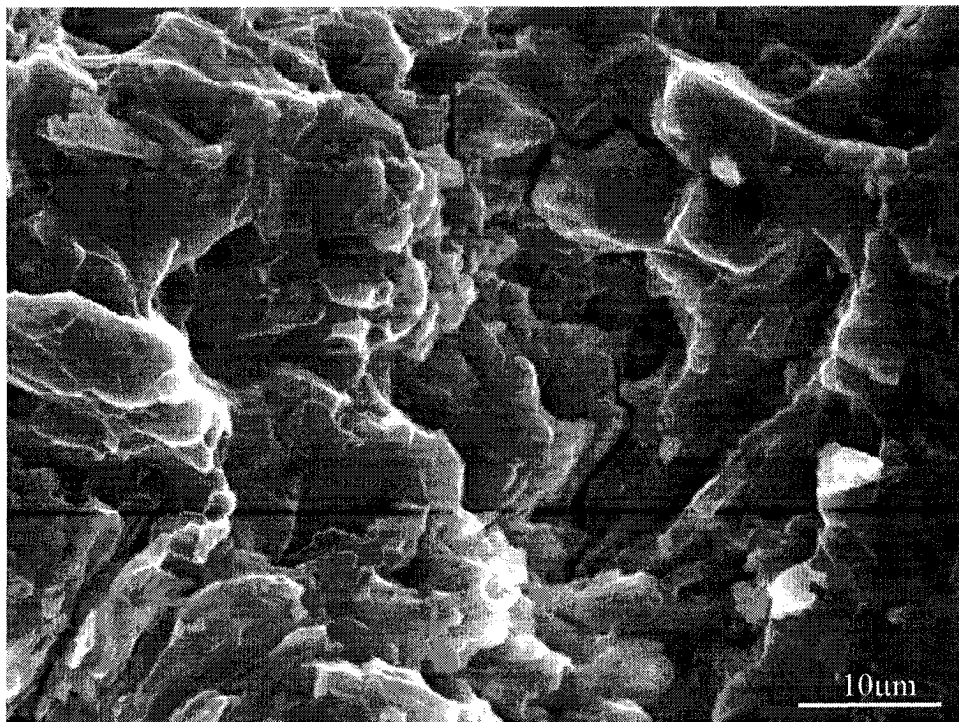
AMS605C (X500)

AMS605C (X3000)

148
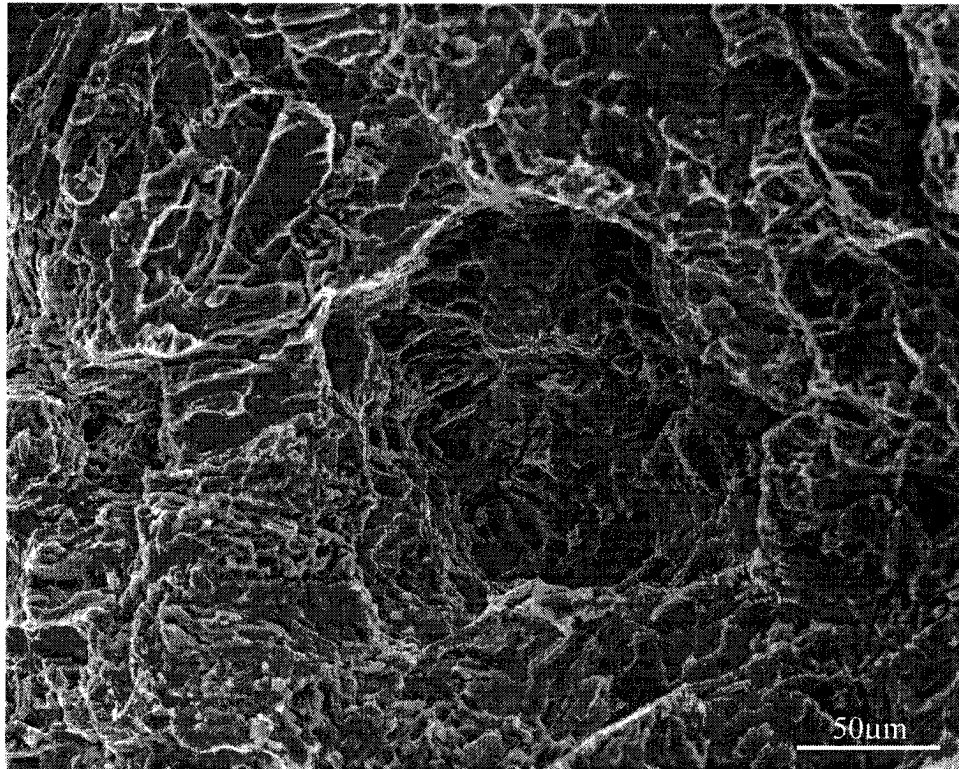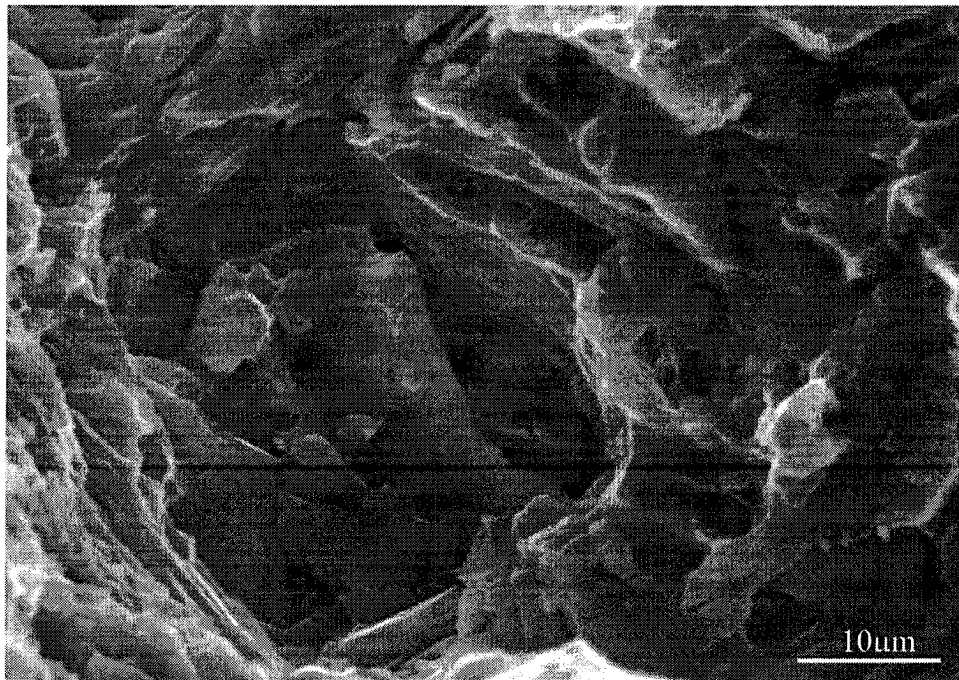
AMS605D (X500)

AMS605D (X3000)

149
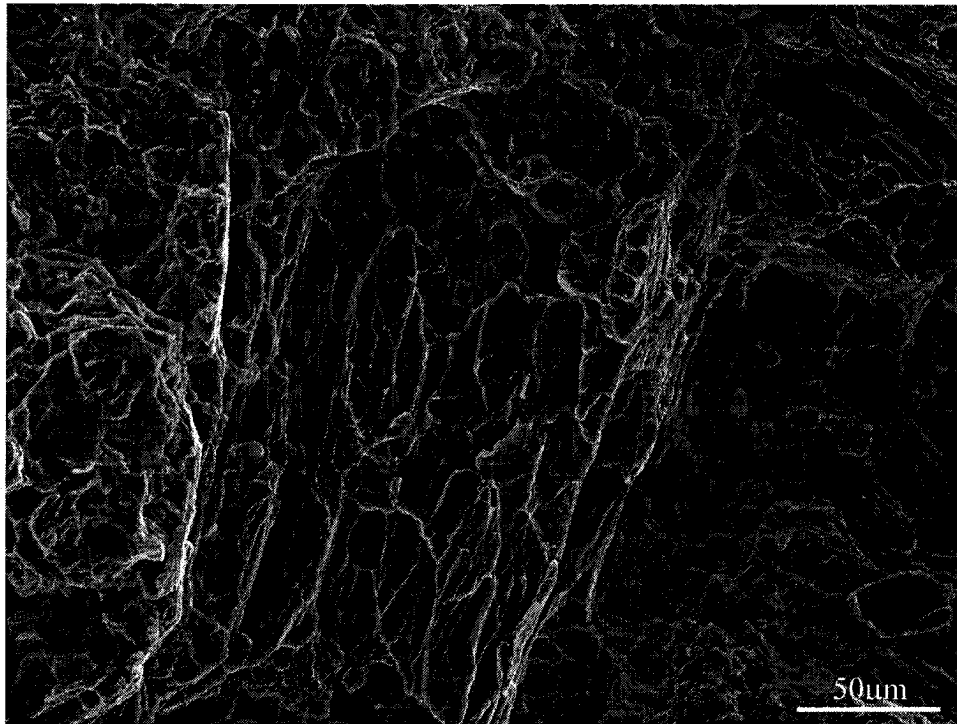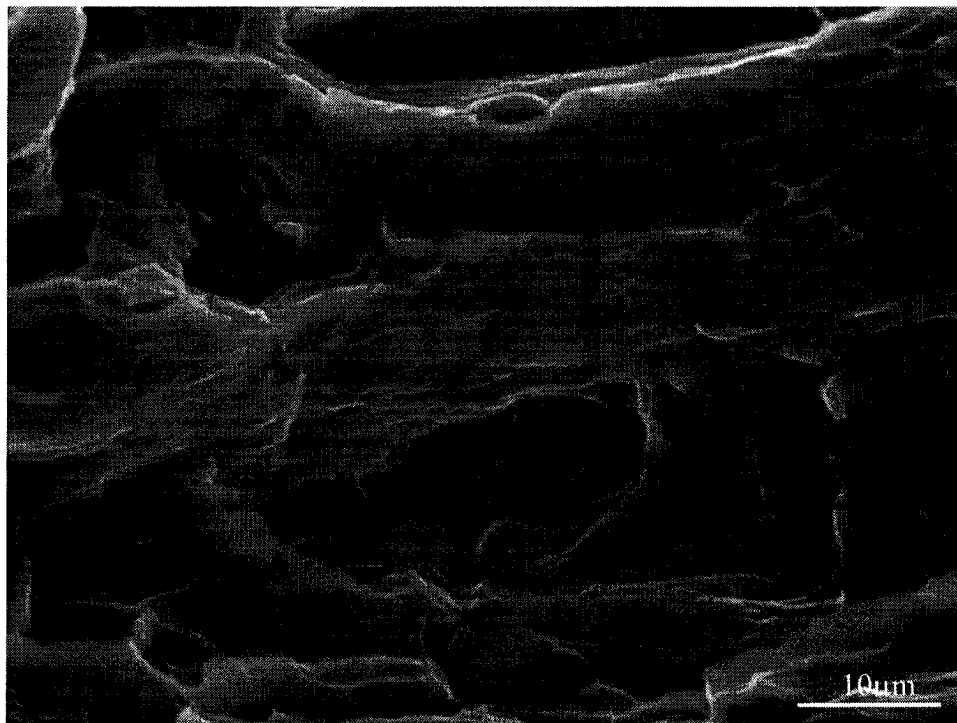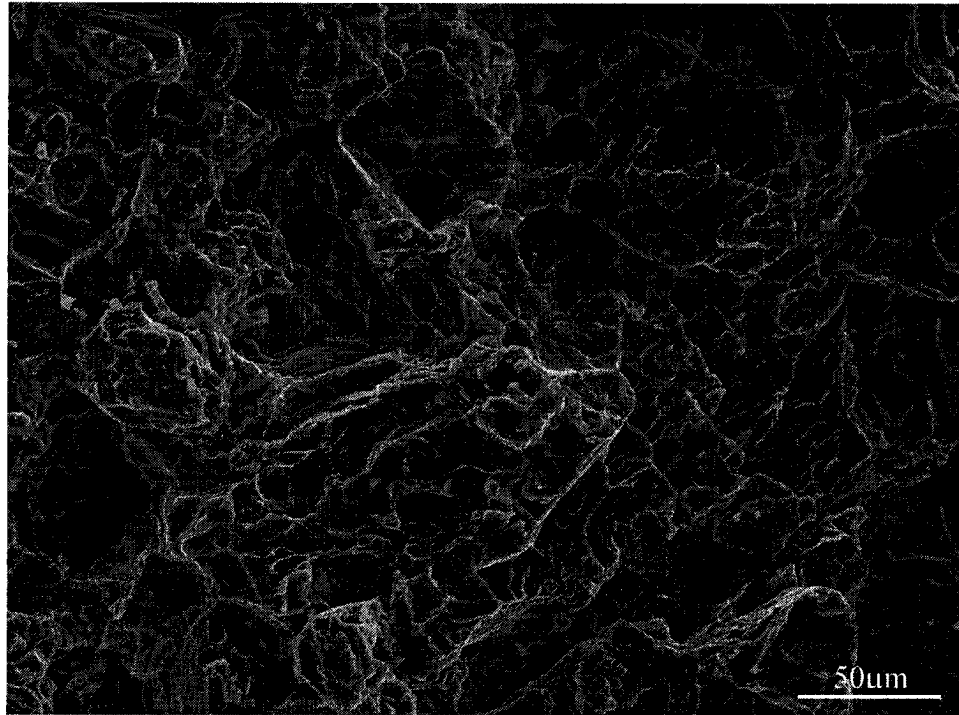
AMS600B (X500)

AMS600B (X3000)

150

AMS605B (X500)

AMS605B (X3000)

151
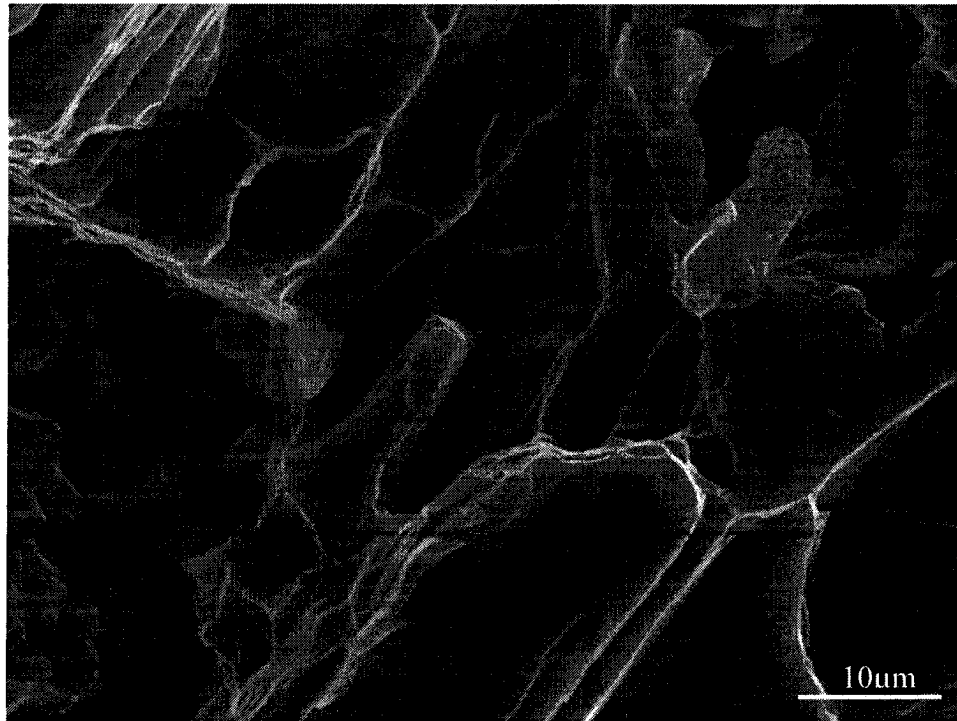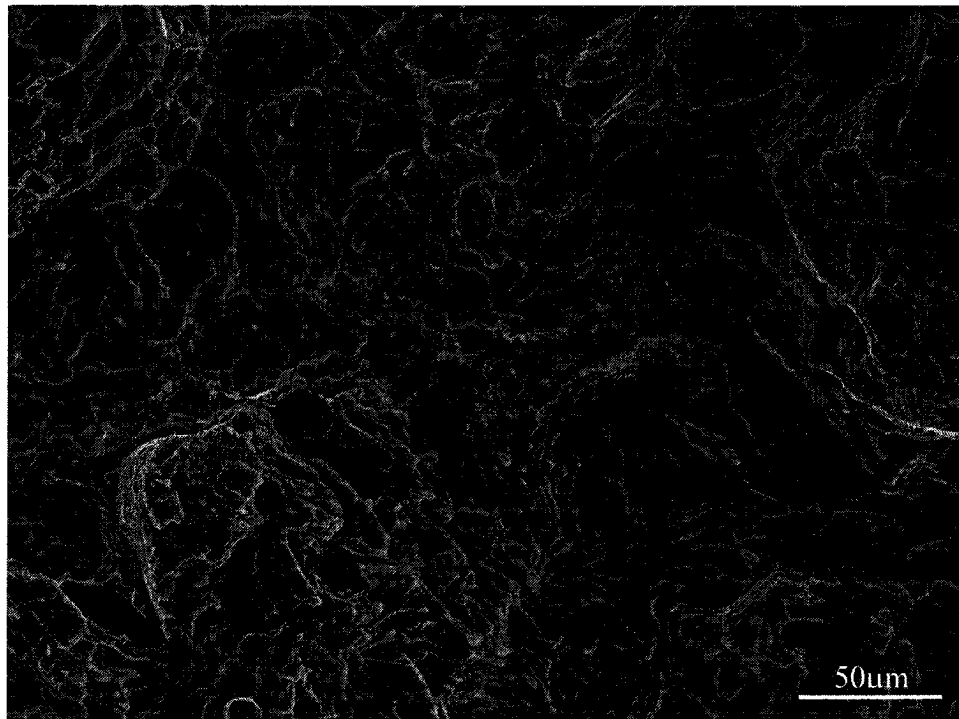
AMS615B (X500)

AMS615B (X3000)

152
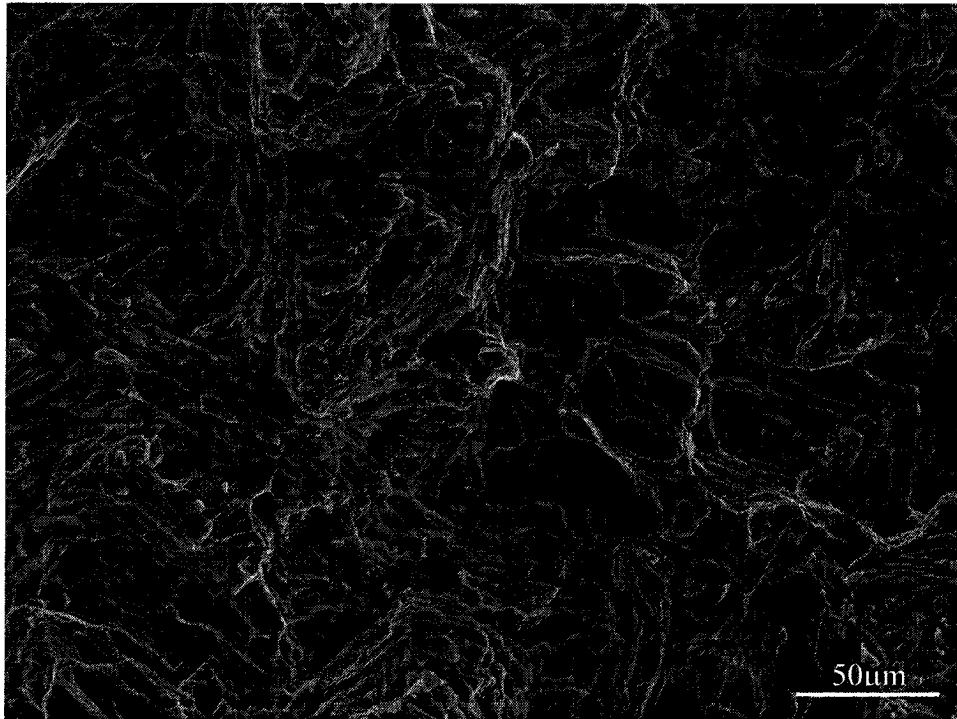
AMS620B (X500)

AMS620B (X3000)

153
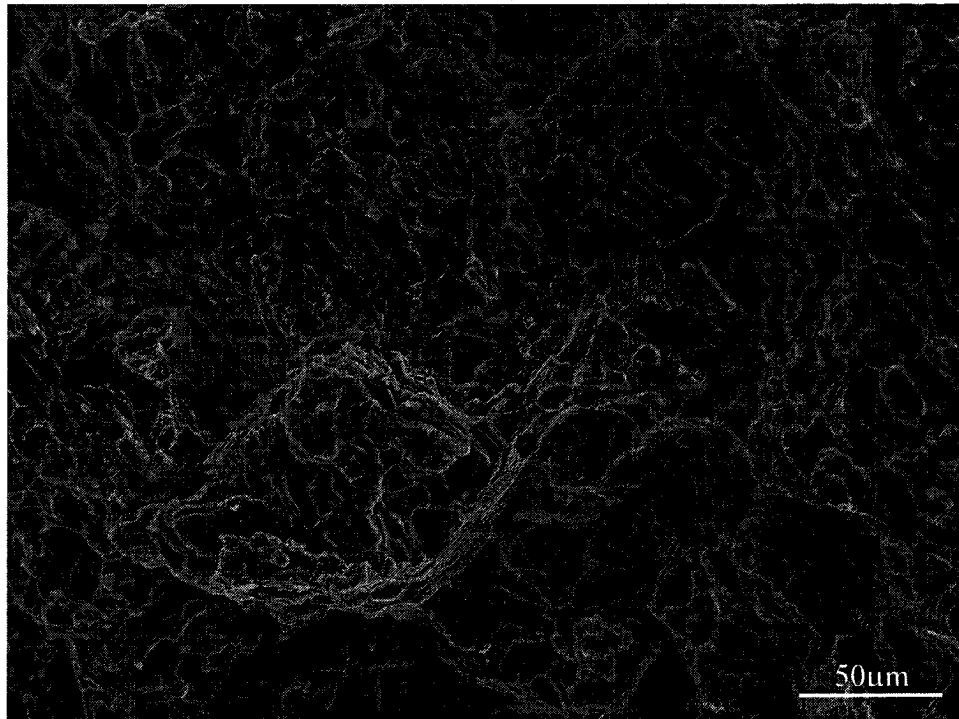
AMS630B (X500)
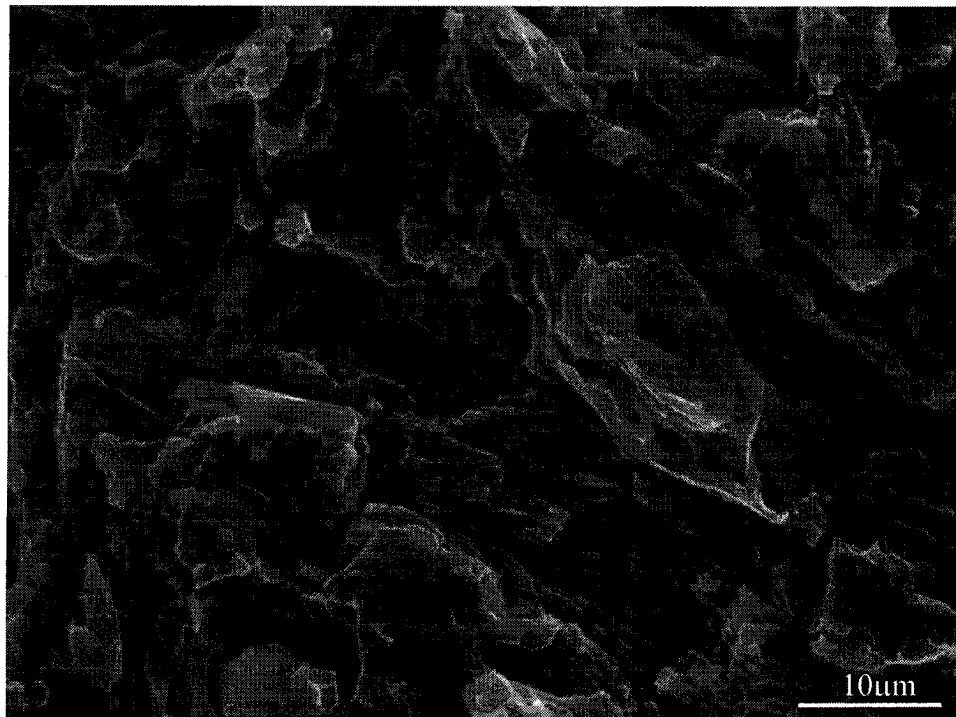

AMS630B (X3000)
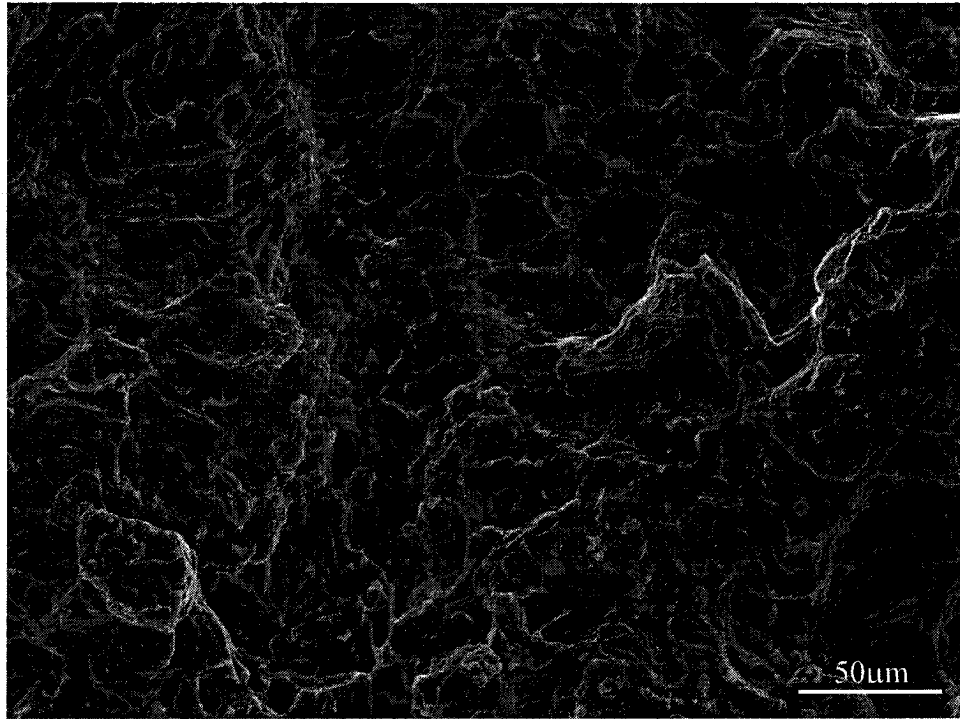

154
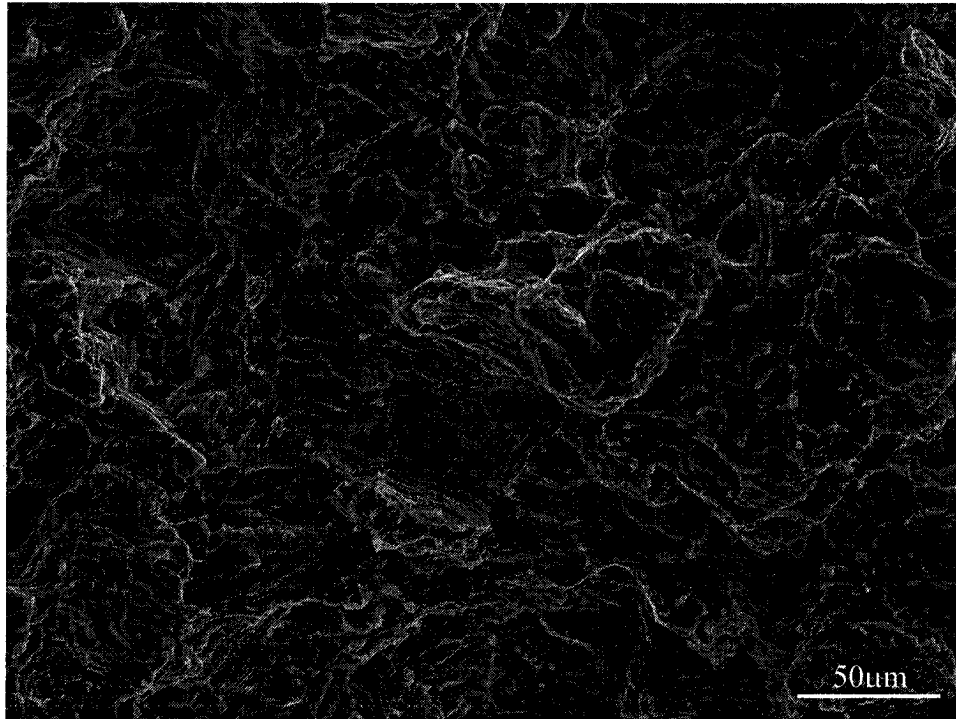
AMS600D (X500)

AMS600D (X3000)

155
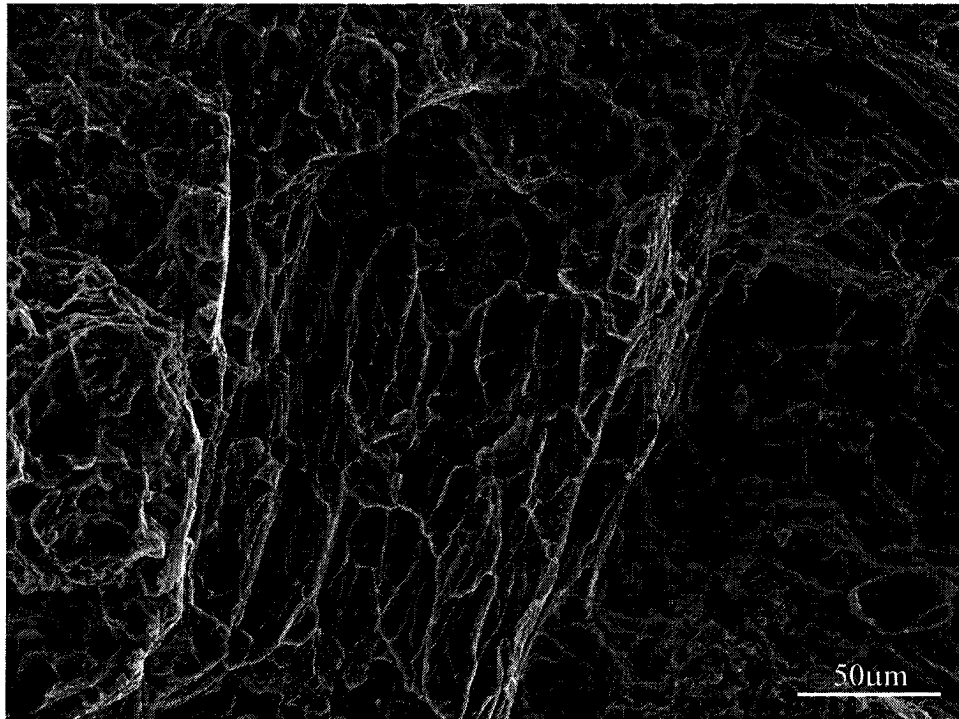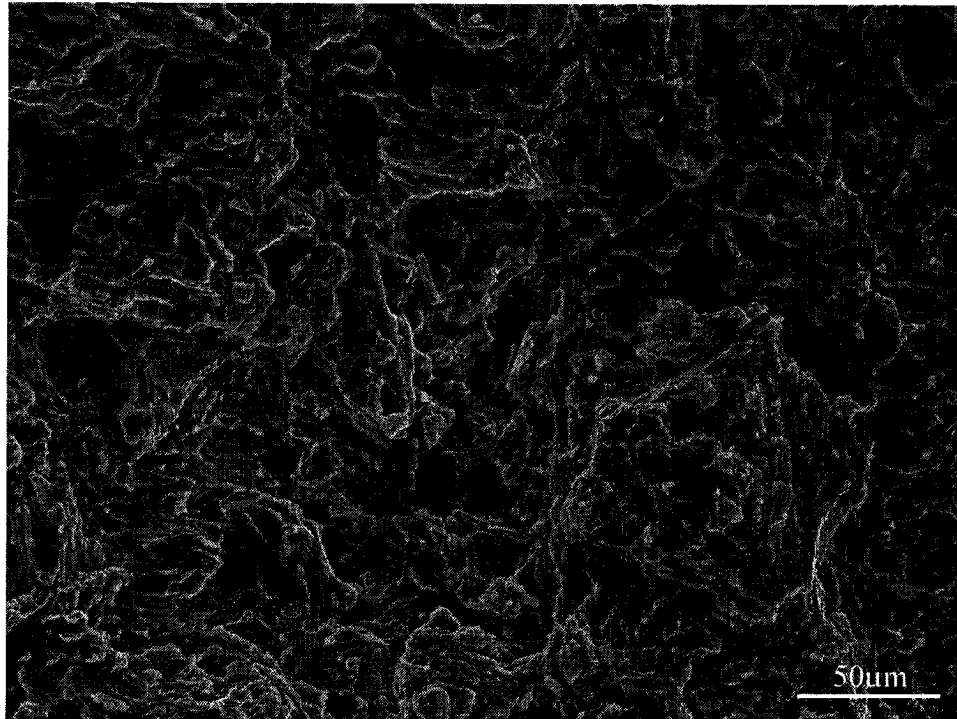
AMS615D (X500)

AMS615D (X3000)

AMS620D (X500)

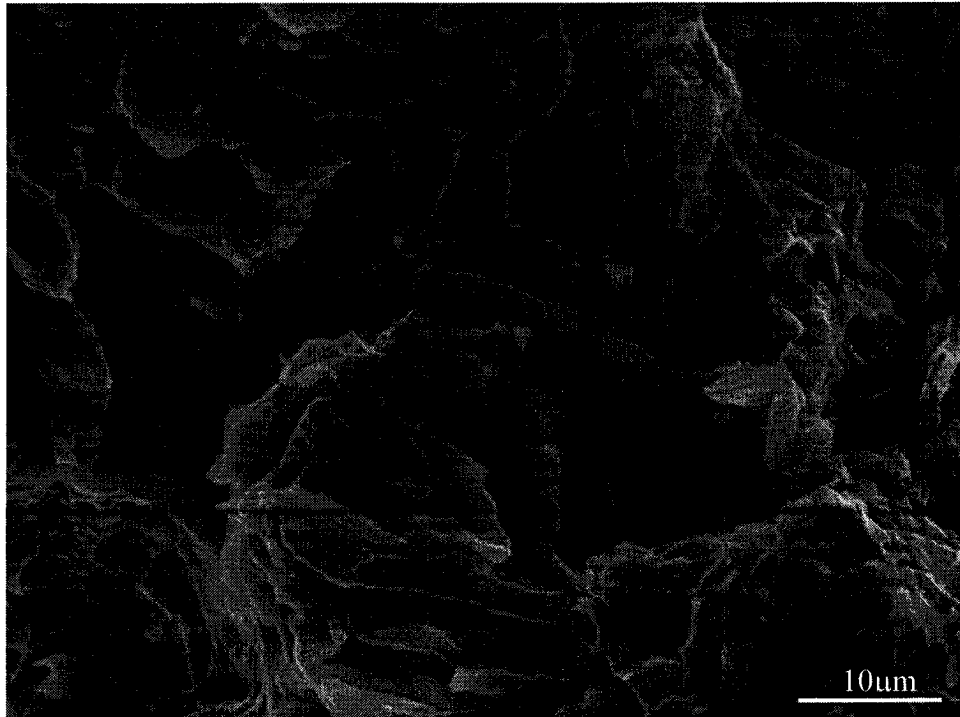AMS620D (X3000)
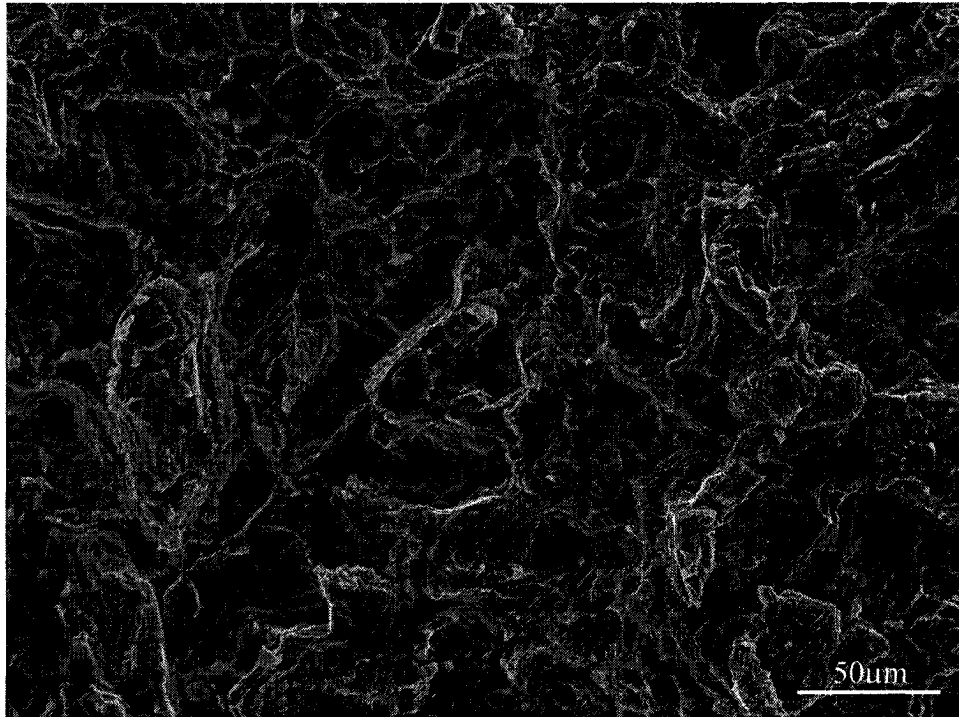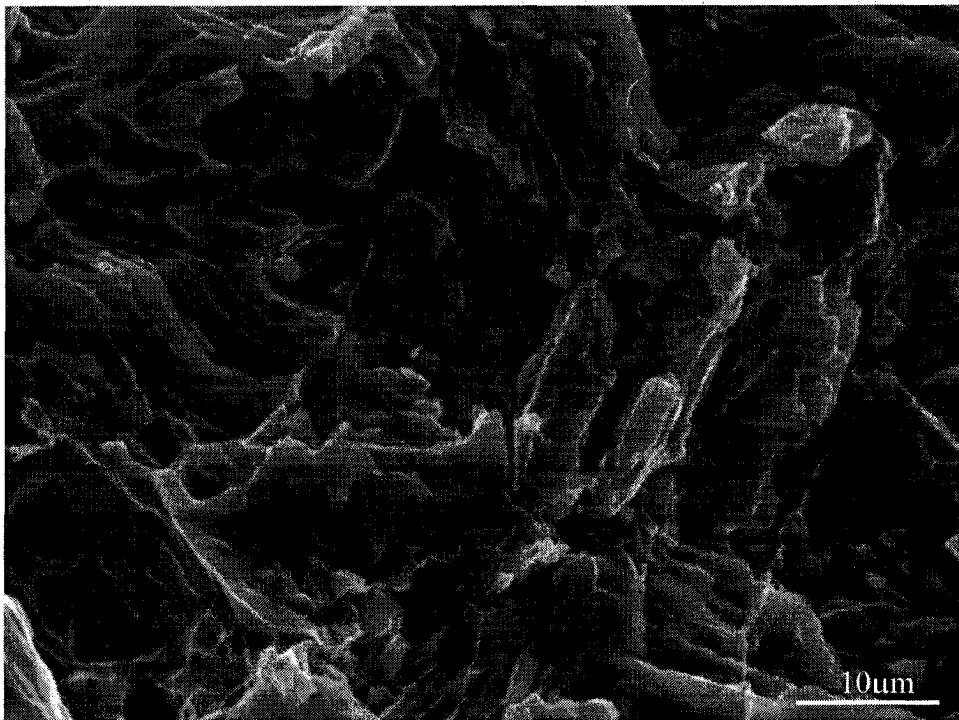

157

AMS630D (X500)

AMS630D (X3000)

158

VITA AUCTORIS

NAME: Shuping Wang

PLACE OF BIRTH: Taiyuan, Shanxi, China

DATE OF BIRTH: March 08, 1966

EDUCATION: University of Windsor, Windsor, ON, Canada

                             2005-2007 M.Sc. in Material Engineering

                             Algonquin College, Ottawa, ON, Canada

                             2002-2003 Diploma in Robotics

                             North University of China, Taiyuan, China

                             1985-1989 B.Sc. in Material Engineering

159